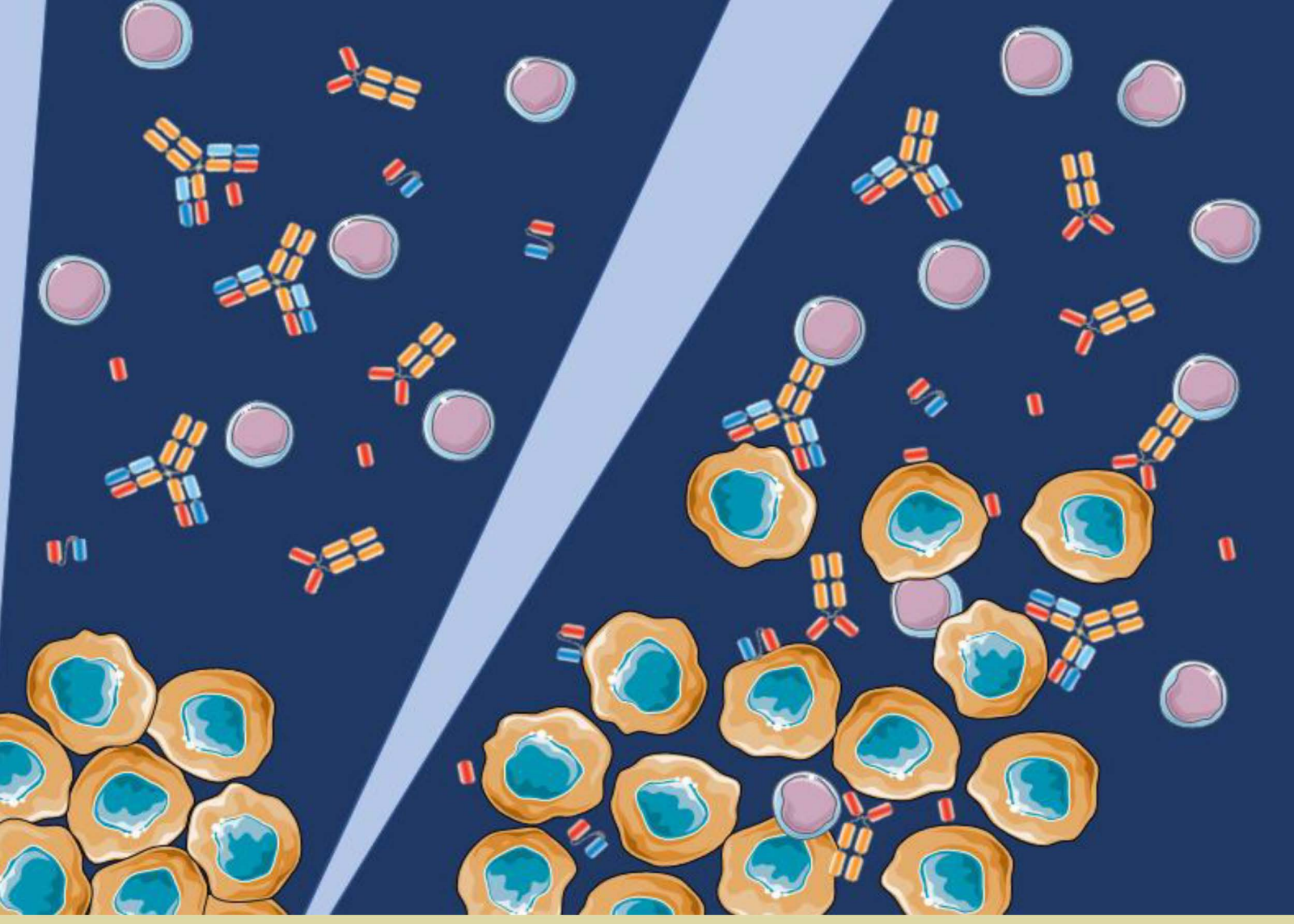

Sofia Pereira Constantino Romano

NOVEL ANTI-NUCLEOLIN ANTIBODIES FOR TARGETED CANCER THERAPY

Tese de doutoramento em Biologia Experimental e Biomedicina, ramo de Biotecnologia e Saúde, orientada pelo Professor Doutor João Nuno Moreira e pelo Professor Doutor João Gonçalves, apresentada ao Instituto de Investigação Interdisciplinar da Universidade de Coimbra.

Agosto 2017

· U C ·

UNIVERSIDADE DE COIMBRA

Sofia Pereira Constantino Romano

NOVEL ANTI-NUCLEOLIN ANTIBODIES FOR TARGETED CANCER THERAPY

PhD thesis presented to the Institute for Interdisciplinary Research of the University of Coimbra (IIIUC) in conformity with the requirements for the degree of Doctor of Philosophy in Biomedicine and Experimental Biology, branch of Biotechnology and Health, under the scientific supervision of Professor João Nuno Moreira (Faculty of Pharmacy and Center for Neuroscience and Cell Biology of the University of Coimbra) and Professor João Gonçalves (Research Institute for Medicines, Faculty of Pharmacy of the University of Lisbon).

Universidade de Coimbra, Agosto de 2017

The work included in this thesis was performed at the Center for Neuroscience and Cell Biology of the University of Coimbra and at the Research Institute for Medicines, Faculty of Pharmacy of the University of Lisbon. This work was funded by FCT – Portuguese Foundation for Science and Technology, by the PhD fellowship SFRH/BD/51680/2011, attributed by the PhD Programme in Experimental Biology and Biomedicine (PDBEB), coordinated by the Center for Neuroscience and Cell Biology of the University of Coimbra. The work was also funded by FCT under the strategic project UID/NEU/04539/2013 and by FEDER funds through Programa Operacional Factores de Competitividade – COMPETE 2020 and under the research project POCI-01-0145-FEDER-007440 .

Agradecimentos

Aos meus orientadores, Professor Doutor João Nuno Moreira e Professor Doutor João Gonçalves, pela oportunidade de participar neste projeto, pelo apoio e acompanhamento ao longo destes anos e por todo o contributo que deram neste meu percurso.

Aos meus colegas de laboratório em Lisboa, os que me acolheram no início e os que foram chegando, Ana, Catarina, Soraia, Pedro, Luís, Ana Catarina, Rita, Cheila, Padma, João, Renato, Paula, Mariana. Obrigada por todo o apoio e amizade durante as longas horas passadas no CPM. Um agradecimento muito especial ao Vasco, pela ajuda nos momentos de maior correria, pelas constantes gargalhadas, pelas discussões e sugestões e pela disponibilidade e paciência de sempre (mesmo em dias de ADCC). Obrigada por teres continuado tão presente mesmo na fase "pós-CPM" e pelos milhares de malabarismos para não me deixares desanimar.

Aos meus colegas de laboratório em Coimbra, em especial ao Nuno, Ana, Ângela e Rui, pela ajuda e sugestões à colega "emigrada", que tão úteis foram para a realização deste projeto.

À Professora Doutora Cecília Rodrigues, pela oportunidade de realizar os ensaios no xCELLigence, e a todo o seu grupo, pela forma como me acolheram e animaram as horas passadas na sua sala de cultura. Um agradecimento especial ao Pedro Borralho e à Sofia, pelo apoio indispensável com o xCELLigence e pela disponibilidade que sempre tiveram para me ajudar e discutir ideias, e ao Pedro Rodrigues, pela boa disposição contagiante, pelas gargalhadas, piadas e pela companhia nos lanches a correr.

Aos meus colegas do BEB, André, António, Catarina, Dominique, Joana, João, Marcelo, Mariline, Patrícia, Sara e Tânia. Pelos bons momentos no meio de todas as discussões de projetos até altas horas durante os cursos do BEB e por todo o apoio

desde essa altura. Um agradecimento especial à Mariline, pelas visitas em Lisboa, e à Tânia, pelas conversas no Skype e pelo apoio constante.

Aos meus amigos que, longe ou perto, estiveram presentes durante estes anos e cuja amizade, apoio e força foram essenciais. Um agradecimento especial à Inês, por continuar disponível para discutir as ideias mais loucas após 10 anos e estar presente em todos os momentos, ao Rui, pela paciência nas incontáveis vezes em que teve de me salvar de uma crise, ao Johnny, pelas palavras no momento certo, e ao Washington e ao Ricardo, pela amizade transatlântica e o carinho de sempre.

À minha família, em especial aos meus pais e irmãos, pelo apoio e paciência infinitos. Pedro, obrigada pelo apoio à irmãzinha em Lisboa e por me deixares usar a tua cozinha como laboratório. Luís, obrigada pela ajuda com as crises no computador. João, obrigada por nunca nunca te esqueceres de perguntar, a cada telefonema, “Sofia, como está a proteína?”.

Table of contents

Abstract

Cancer is nowadays the second leading cause of death and current therapeutic approaches still reveal ineffective in several cases. Therefore, there is a need to develop more efficacious therapeutic agents, especially for subtypes of cancer where targeted therapies are still missing, and, as such, unmet medical needs are evident.

Limited drug penetration into tumors limits the efficacy of therapies targeting cancer cells. One of the strategies to overcome this problem is upon targeting the more accessible tumor vasculature. In this context, nucleolin arises as a target of extreme relevance, as it is expressed at the surface of cancer and angiogenic endothelial cells thus enabling a dual cellular targeting strategy.

Antibodies have been extensively studied and some have been approved for the treatment of different types of tumors. Antibodies act by several mechanisms, from direct cell death to immune-mediated mechanisms (through the Fc region of the antibody). The latter include antibody-dependent cell-mediated cytotoxicity (ADCC), which plays a central role in the clinical efficacy of some antibodies. However, the high molecular weight of these proteins (≈150 kDa) limits effective penetration in solid tumors. Therefore, smaller units for antigen recognition have been developed. Nanobodies or VHHs are the variable domains of the heavy chains from camelid antibodies that lack light chains, presenting small size (≈15 kDa), high affinity to their antigens and reduced immunogenicity in humans. In addition, they are also versatile platforms for the development of different antibody formats.

The main aim of this project was to develop and characterize new nanobody-based antibody formats against nucleolin. These consisted of (i) nanobodies generated by a grafting strategy using a nucleolin-binding sequence and (ii) an anti-nucleolin nanobody-Fc antibody, aiming at exploring immune mechanisms, namely ADCC. In addition, this

work aimed also at exploring the use of nanobodies as bispecific proteins, where nucleolin and tumor necrosis factor alpha (TNF-α) were selected as models of target proteins.

An anti-TNF-α VHH was used as a scaffold for grafting F3 peptide-derived nucleolin-binding sequences onto either complementarity determining region 1 (CDR1) or 3 (CDR3), the two most relevant antigen-binding regions. The grafted sequences consisted on a 10-amino acid sequence, with or without flanking linkers at each end, aiming at improving CDR flexibility. The generated nanobodies revealed binding to both purified nucleolin and cancer and endothelial cells, as well as to the original target, TNF-α. These nanobodies presented cytotoxic effects in the micromolar range against these cells. Grafting of the F3 peptide-derived sequence onto CDR3 enabled improved binding and cytotoxicity relative to grafting of the same sequence onto CDR1. However, the presence of flanking linkers in the grafted sequence did not alter the binding and cytotoxicity patterns.

These results led to the selection of the nanobody presenting the F3 peptide-derived sequence (without linkers) in CDR3 to generate a nanobody-Fc, upon fusion to the Fc region of a human IgG1. This anti-nucleolin nanobody-Fc antibody presented increased cytotoxic effects (in the nanomolar range) and also capacity of triggering a nucleolin-mediated ADCC effect against a cancer cell line.

In conclusion, in this work, new nucleolin-targeting entities with cytotoxic activity against cancer and endothelial cells were developed. In addition, the nanobodies presented bispecific properties, as evidenced by their binding to two different antigens. Notably, the nanobody-Fc antibody presented nucleolin-mediated ADCC capacity, which had not been described for this target yet. Therefore, the antibodies here described might contribute for the development of novel therapies targeting nucleolin.

Keywords: cancer, nucleolin, antibodies, nanobody, nanobody-Fc, antibody-dependent cell-mediated cytotoxicity

Resumo

O cancro é atualmente a segunda principal causa de morte e as abordagens terapêuticas atuais ainda se revelam ineficazes em muitos casos. Assim, há necessidade de desenvolver agentes terapêuticos mais eficazes, principalmente para subtipos de cancro para os quais não existem terapias direcionadas e para os quais são evidentes as necessidades médicas não satisfeitas.

A limitada penetração de fármacos nos tumores compromete a eficácia das terapias direcionadas para as células cancerígenas. Uma das estratégias para ultrapassar este problema é o direcionamento da terapia para a vasculatura tumoral, que se encontra mais acessível. Neste contexto, a nucleolina surge como um alvo de extrema relevância, uma vez que é expressa à superfície de células cancerígenas e células endoteliais angiogénicas, permitindo uma estratégia de direcionamento multicelular.

Os anticorpos têm sido extensivamente estudados e alguns foram aprovados para o tratamento de diferentes tipos de tumores. Os anticorpos atuam através de diversos mecanismos, desde morte celular direta a mecanismos imunitários (através da região Fc do anticorpo). Nestes últimos, inclui-se a citotoxicidade celular dependente de anticorpos (ADCC), que desempenha um papel central na eficácia clínica de alguns destes agentes terapêuticos. No entanto, o elevado peso molecular destas proteínas (≈150 kDa) limita a penetração eficaz em tumores sólidos. Consequentemente, foram desenvolvidas unidades mais pequenas de reconhecimento de antigénio. Os *nanobodies* ou VHH são os domínios variáveis das cadeias pesadas dos anticorpos de camelídeos sem cadeias leves, apresentando tamanho reduzido (≈15 kDa), elevada afinidade para os seus antigénios e imunogenicidade reduzida em humanos. Além

disso, os *nanobodies* são também plataformas versáteis para o desenvolvimento de diferentes formatos de anticorpos.

O principal objetivo deste projeto foi o desenvolvimento e caracterização de novos formatos de anticorpos baseados em *nanobodies* contra a nucleolina. Estes formatos consistiram em (i) *nanobodies* obtidos por uma estratégia de inserção de um peptídeo de 10 de aminoácidos, derivado de um outro (designado por F3) com demonstrada ligação à nucleolina na superfície de células cancerígenas e (ii) um anticorpo *nanobody*-Fc anti-nucleolina, com o objetivo de explorar mecanismos imunitários, nomeadamente ADCC. Além disso, este trabalho teve também o objetivo de explorar o uso de *nanobodies* como proteínas bi-específicas, tendo a nucleolina e o fator de necrose tumoral alfa (TNF-α) sido selecionados como modelos de proteínas alvo.

Um *nanobody* anti-TNF-α foi usado como base para inserção de sequências derivadas do péptido F3 na região determinante de complementaridade 1 (CDR1) ou 3 (CDR3), as duas regiões mais importantes na ligação ao antigénio. As sequências inseridas consistiram na referida sequência de 10 aminoácidos, com ou sem *linkers* em cada extremidade, os quais visavam aumentar a flexibilidade da CDR. Os *nanobodies* gerados apresentaram ligação a nucleolina purificada e a células cancerígenas e endoteliais, assim como ao alvo original, TNF-α. Estes *nanobodies* apresentaram efeitos citotóxicos na ordem dos micromolar contra células cancerígenas e endoteliais. A inserção da sequência derivada do péptido F3 em CDR3, resultou em ligação e citotoxicidade superiores às observadas com a inserção da mesma sequência em CDR1. Contudo, a presença de *linkers* nas extremidades da sequência inserida não alterou os padrões de ligação e citotoxicidade.

Estes resultados levaram à seleção do *nanobody* com a sequência derivada do péptido F3 no CDR3 (sem *linkers*) para gerar um *nanobody*-Fc, após fusão a uma região Fc de uma IgG1 humana. Este anticorpo *nanobody*-Fc anti-nucleolina apresentou efeitos citótoxicos mais pronunciados (na ordem dos nanomolar) e também a

capacidade de promover um efeito de ADCC mediado por nucleolina, contra uma linha celular de cancro.

Em conclusão, neste trabalho foram desenvolvidas entidades direcionadas para a nucleolina com atividade citotóxica contra células cancerígenas e endoteliais. Além disso, os *nanobodies* apresentaram propriedades bi-específicas, como evidenciado pela sua ligação a dois antigénios diferentes. De notar que o anticorpo *nanobody*-Fc apresentou capacidade de ADCC mediada por nucleolina, um efeito que ainda não tinha sido descrito para este alvo. Desta forma, os anticorpos apresentados neste trabalho poderão contribuir para o desenvolvimento de novas terapias direcionadas para a nucleolina expressa em tumores.

Palavras chave: cancro, nucleolina, anticorpos, *nanobody*, *nanobody*-Fc, citotoxicidade celular dependente de anticorpos.

List of abbreviations

ABTS	2,2'-azino-bis(3-ethylbenzothiazoline-6-sulphonic acid
ADCC	antibody-dependent cell-mediated cytotoxicity
AUC	area under the curve
BiTE	bispecific T cell engager
BSA	bovine serum albumin
CAM	chick choriallantoic membrane
CAR	chimeric antigen receptor
CD44E	epithelial isoform of CD44
CDC	complement-dependent cytotoxicity
CDR	complementarity determining regions
CEACAM 6	carcinoembryonic antigen-related cell adhesion molecule 6
CH	constant region of an antibody
CHO	Chinese hamster ovary
CTLA-4	T-lymphocyte antigen 4
CXCR	C-X-C chemokine receptor
DNA	deoxyribonucleic acid
DR5	death receptor 5
EGFR	epidermal growth factor receptor
ELISA	enzyme-linked immunosorbent assay
ER	estrogen receptor
ERK	extracellular signal–regulated kinase
Fab	antigen binding fragment
Fc	fragment crystallizable
FcRn	neonatal Fc receptor
FcγR	Fc-gamma receptor
FR	framework region
HCab	heavy chain antibody
HDGF	hepatoma-derived growth factor

HER2	human epidermal growth factor receptor 2
HGF	hepatocyte growth factor
HGFR	hepatocyte growth factor receptor
HIV	human immunodeficiency virus
IC_{50}	half maximal inhibitory concentration
IFN-γ	interferon gamma
Ig	immunoglobulin
IL	interleukin
IPTG	isopropyl β-D-1-thiogalactopyranoside
LB	lysogeny broth
MHC	major histocompatibility complex
MMP-2	matrix metalloproteinase-2
MOPS	3-(N-Morpholino)propanesulfonic acid
MTT	3-(4,5-Dimethylthiazol-2-yl)-2,5-Diphenyltetrazolium Bromide
NF-κB	nuclear factor kappa B
NK	natural killer
OD	optical density
PBMC	peripheral blood mononuclear cell
PBS	phosphate buffer saline
PD-1	programmed death-1
PDGFβ	platelet-derived growth factor receptor beta
PI3K	phosphoinositide 3-kinase
PLK1	anti-polo-like kinase 1
PR	progesterone receptor
rDNA	ribosomal deoxyribonucleic acid
RNA	ribonucleic acid
RPTPβ/ζ	receptor protein tyrosine phosphatase β/ζ
rRNA	ribosomal ribonucleic acid
SCCHN	squamous cell carcinoma of the head and neck
scFv	single-chain fragment variable
SDS-PAGE	sodium dodecyl sulfate polyacrylamide gel electrophoresis
siRNA	small interfering RNA

SOB	super optimal broth
SOC	super optimal broth with catabolic repressor
TBS	Tris-buffered saline
tmTNF-α	transmembrane tumor necrosis factor alpha
TNF-α	tumor necrosis factor alpha
VEGF	vascular endothelial growth factor
VH	variable heavy chain
VHH	variable region of a heavy chain antibody
VL	variable light chain
WT1	Wilms' tumor 1

List of figures

List of tables

Chapter 1

General Introduction

1.1 CANCER

Cancer is nowadays the second leading cause of death, only slightly surpassed by heart diseases. Estimates relative to 2012 indicate around 14.1 million new cases worldwide and 8.2 million deaths[1]. For several years, therapeutic approaches for the treatment of cancer consisted on surgery, chemotherapy and radiotherapy, but these are not always effective. In addition, chemotherapy and radiotherapy present severe side effects, as they affect not only cancer cells, but also normal tissues. The need for more efficacious therapies and able to surpass this drawback, led to the development of targeted strategies against markers overexpressed in tumors. One example of this kind of therapy is trastuzumab, an anti-human epidermal growth receptor 2 (HER2) antibody, which led to improvements in the long-term outcomes of HER2-overexpressing breast cancer patients[2]. However, the existence of subtypes of cancer that do not overexpress any of the common markers, strongly limits the development of targeted therapies. This is the case of triple-negative breast cancer, which lacks expression of estrogen receptor (ER), progesterone receptor (PR) and HER2[3,4]. Therefore, it becomes important to identify novel therapeutic targets within these subtypes of cancer, where there are recognized unmet medical needs.

1.2 TUMOR MICROENVIRONMENT AND THERAPY

General understanding of tumor development and biology suffered a major shift with the finding that there is a crucial interplay between cancer cells and the surrounding cells and extracellular matrix. Previously regarded as homogenous masses of cancer cells, tumors are nowadays known to be much more complex entities, being supported by an intricate network of other cells and components, the tumor microenvironment, as

endothelial cells, pericytes, fibroblasts and infiltrating immune cells, as well as the associated extracellular matrix, cytokines and chemokines. The continuous cross-talk between cancer cells and the tumor microenvironment favors tumor development, enhancing its proliferation and metastization, as summarized in Figure 1.1[5–7].

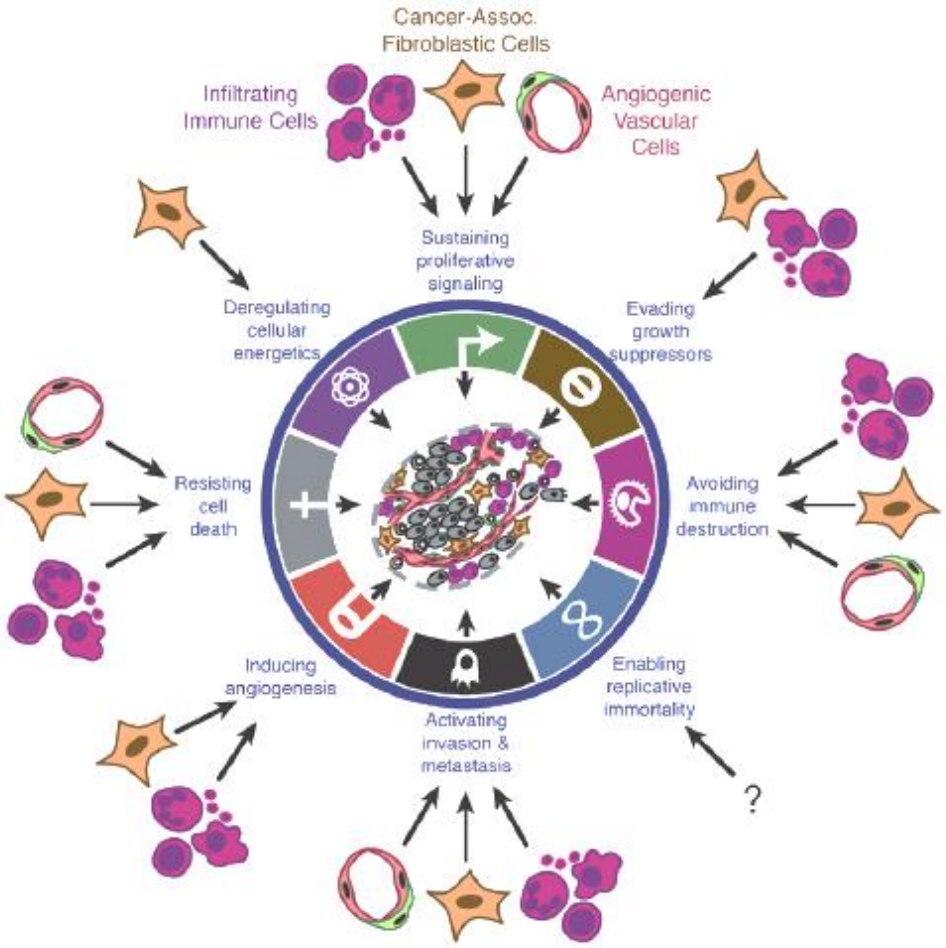

Figure 1.1. The role of microenvironment in tumor development and progression. Tumor-associated immune cells, fibroblasts and endothelial cells play a role in each of the main hallmarks of cancer (indicated by the arrows), enabling its continuous growth and further metastization. Notwithstanding tumors present a variety of properties and characteristics, these eight factors appear as common traits. The role of the stromal cells in these traits, highlights the potential of therapies targeted to the tumor microenvironment (Adapted from ref. 6).

1.2.1 Tumor vasculature

The development of a vasculature to support the tumor has been described as one of the hallmarks of cancer, as it supplies the needed nutrients and oxygen, as well as the elimination of metabolic wastes and carbon dioxide[5].

In their early development, tumors lack blood vessels to adequately provide oxygen to the tumor, which leads to hypoxia. This results in upregulation and secretion of pro-angiogenic molecules by cancer cells, such as vascular endothelial growth factor (VEGF), resulting in the formation of new blood vessels. However, this vasculature is architecturally different from normal blood vessels. Normal vasculature presents an organized structure, with well-defined arterioles, capillaries and venules and regular branching. On the contrary, tumor blood vessels lack a normal basement membrane and are irregularly shaped and dilated, with unorganized branching and leakiness. This results in fluid extravasation into the tumor interstitium and consequent increase of tumor interstitial pressure.

In addition, associated endothelial cells present higher proliferation rates. Actively proliferating cancer cells around the vasculature exert mechanical stress on the vessels, further contributing to the chaotic structure of the vasculature as well as to the increased tumor interstitial pressure. This combination of factors contributing to irregular blood flow, with focal leaks and unevenly distributed, further promotes a hypoxic environment. In addition, existing fenestrations in the tumor blood vessels, play an important role in the invasion and metastization processes[8–11].

1.2.2 Tumor vasculature as a therapeutic target

The tumor microenvironment is now considered an important target for cancer therapy. On one hand, as stromal cells do not present the same proliferative potential as

cancer cells, they are less likely to evolve and become resistant to therapy[9,12]. On the other hand, the increased tumor interstitial pressure, to which the tumor microenvironment contributes, renders drug transport and accumulation in the tumor more difficult. Therefore, anti-angiogenic therapies have been a focus of research and some inhibitors of angiogenesis are currently used, including the anti-VEGF antibody bevacizumab, used as monotherapy (in multiform glioblastoma) or in combination with chemotherapy or cytokine therapy (in colorectal cancer, metastatic breast cancer, non-small-cell lung cancer, and metastatic renal cell carcinoma)[11,13].

Therapies that target both cancer cells and surrounding microenvironment are now envisioned as a way to more effectively achieve a relevant anticancer effect, as remaining cancer cells would not have an appropriate environment to further grow and proliferate[14,15].

1.2.3 Biological relevance of nucleolin

Nucleolin is a 76 kDa protein which was first described as a nucleolar protein in Novikoff hepatoma cells and Chinese hamster ovary (CHO) cells[16,17]. Its expression was later reported to broadly occur in all cells, in a proliferation-dependent manner[18]. Nucleolin is a non-histone phosphoprotein and can represent up to 10% of total nucleolar protein in exponentially growing eukaryotic cells. In the nucleus, its main functions include regulation of rRNA synthesis and ribosome biogenesis. Nucleolin presents a tripartite structure: a N-terminal domain with acidic stretches, involved in several protein-protein interactions, which controls rDNA transcription; a central globular domain, with four RNA-binding domains, involved in pre-RNA processing; and a C-terminal domain, constituted by arginine-glycine-glycine repeats, which interacts with ribosomal proteins.

Nucleolin acts as a shuttling protein between the cytoplasm and the nucleus, promoting the import of ribosomal subunits to the nucleus, where it brings them together with RNA[19–21].

1.2.3.1 Surface nucleolin: targeting opportunity towards tumors of diverse histological origins

In highly proliferating cells, such as metabolically active cancer cells, nucleolin translocates from the nucleus to the cytoplasm and cell membrane, in an energy-dependent process that occurs through the actin cytoskeleton[22]. This translocation also takes place in endothelial cells of angiogenic blood vessels[23]. Therefore, nucleolin arises as a potential target for therapies targeting both cancer cells and the tumor microenvironment, more specifically, the tumor vasculature. Recently, expression of surface nucleolin has also been identified in cancer stem cells from different breast cancer cells lines, correlating with tumorigenic potential[24]. Since cancer stem cells are highly tumorigenic cells, playing a crucial role in metastization and tumor relapse[25,26], these findings further highlight the relevance of nucleolin as a therapeutic target.

Although the role of nucleolin at the cell surface is still not fully understood, different studies have revealed interactions with different proteins and signaling pathways. At the cell surface, nucleolin can bind to and mediate the internalization of a plethora of ligands, in a calcium-dependent mechanism[27]. These include urokinase-type plasminogen activator (involved in cell proliferation and migration during angiogenesis)[28], the human immunodeficiency virus (HIV) inhibitors midkine[29] and pleiotrophin[30] and cell proliferation inhibitor lactoferrin[31]. Upon binding to nucleolin, the complex thus formed is quickly internalized and transported to either the cytoplasm or the nucleus[22,27,31–33]. Nucleolin also binds to endostatin, an endogenous 20 kDa protein with anti-angiogenic and

antitumoral effects that has low toxicity. Shi et al. identified nucleolin as responsible for internalization of endostatin and its transport to the nucleus of endothelial cells, leading to anti-tumoral and anti-angiogenic effects[32,34].

At the cell surface, nucleolin interacts simultaneously with epidermal growth factor receptor (EGFR) and Ras, promoting EGFR phosphorylation and dimerization and contributing to anchorage-independent cell growth in cell lines of diverse histological origin, such as breast, kidney and brain[35,36]. Expression of nucleolin, Ras or EGFR in the MDCK cell line did not alter the colony formation capacity of the cells. However, *in vivo*, the overexpression of these three proteins enabled a higher rate of tumor growth than cells expressing just one or two of those proteins[36]. The potential of these proteins as therapeutic targets has been supported in several studies. Incubation of prostate and colon cancer cell lines with a Ras and a nucleolin inhibitors, enabled increased cell death and inhibition of anchorage-independent cell growth and cell migration than single drug incubations[37]. Incubation of U87-MG glioblastoma cells with the same combination of inhibitors led to higher cell death and reduced cell migration[38]. However, in an ectopic U87-MG model, administration of both inhibitors did not have stronger impact on tumor volume than single drug treatment. Nevertheless, inhibition of cell proliferation and cell death was more pronounced in tumors treated with the drug combination, as evaluated by Ki-67 and caspase 3 staining[38].

In non-Hodgkin's lymphoma, surface nucleolin forms a complex with Fas, a member of the tumor necrosis factor superfamily of apoptosis receptors. The interaction blocks the binding of Fas to its ligand, FasL, resulting in a decrease in the apoptosis level. This suggests that nucleolin plays a role in cells that, although overexpressing Fas, are resistant to its activation[39].

Nucleolin also interacts with heparin-bound growth factors. In prostate cancer cells, it interacts with hepatocyte growth factor (HGF), a regulator of carcinoma growth and invasion that binds to Met receptor. In the absence of this receptor, HGF is still able to activate the extracellular signal–regulated kinase (ERK) and Akt signaling pathway upon

binding to nucleolin[40]. In hepatoma cells, nucleolin interacts with hepatoma-derived growth factor (HDGF), involved in cell proliferation and metastasis. HDGF elicits translocation of nucleolin to the cell surface, where the two proteins interact and, similarly to what was observed with HGF, activate the Akt pathway[41].

In papillary thyroid cancer and glioblastoma, nucleolin activates C-X-C chemokine receptor type 4 (CXCR4) signaling, contributing to cell growth, migration and invasion. Knockdown of nucleolin using small interfering RNA (siRNA) led to decreased ERK and Akt phosphorylation and resulted in impairment of overall cell growth and migration[42–44]. In addition, in glioblastoma, nucleolin interacts with the $\alpha_v\beta_3$ integrin and receptor protein tyrosine phosphatase β/ζ (RPTPβ/ζ), components of the phosphoinositide 3-kinase (PI3K)/Akt pathway[45]. In this study, surface nucleolin was detected only in cells expressing $\alpha_v\beta_3$ integrin and was dependent on integrin phosphorylation upon RPTPβ/ζ activation[45].

Considering the overexpression of nucleolin at the cell surface of both cancer cells and angiogenic blood vessels and its role in several pathways that regulate tumor growth and metastization, several approaches have been explored aiming at targeting nucleolin. These strategies rely on two main goals: using nucleolin as a target protein for the delivery of therapeutic payloads, as well as disrupting nucleolin signaling.

1.2.3.2 Surface nucleolin as a target for intracellular drug delivery

The expression of nucleolin at the surface of a variety of cancer cells and endothelial cells from the tumor vasculature, represents an opportunity for receptor-mediated intracellular drug delivery. This type of strategy usually encompasses the use of a nanoparticle encapsulating the therapeutic payload and functionalized with an internalizing targeting ligand. Alternatively, the drug can also be covalently conjugated

to the nucleolin-binding ligand itself. Among these, the F3 peptide and the AS1411 aptamer are the ones that have been explored the most.

1.2.3.2.1 F3 peptide as targeting ligand for intracellular drug delivery

The nucleolin-binding F3 peptide is a 31-amino acid peptide that has been used as a targeting ligand of nanoparticles containing chemotherapeutic drugs (doxorubicin[46] or cisplatin[47]), photodynamic therapy agents[48] or chemically conjugated to radiotherapeutics[49] (Table 1.1). In this respect, nanoparticles of different nature have been tested in different types of cancer models.

A F3 peptide-targeted cisplatin-loaded hydrogel nanoparticle affected, upon intravenous administration, the tumor vasculature, as suggested by the reduced viability of primary tumor endothelial cells and vascular density of a teratoma model, with a human vasculature. This resulted in decreased tumor progression, relative to treatment with combined administration of free cisplatin and empty targeted nanoparticles. Moreover, in A2780- or SKOV3-derived tumors (cisplatin-sensitive and cisplatin-resistant, respectively) it even enabled reduction of tumor volume, in contrast with the aforementioned controls, resulting in improved survival[47].

F3 peptide-targeted strategies also improved the outcome of photofrin-containing nanoparticles[48] and ^{213}Bi-DTPA-based radiotherapy [49], namely in terms of survival in *in vivo* models of gliosarcoma and peritoneal carcinomatosis, respectively.

The potential of intracellular drug delivery mediated by nucleolin has been further confirmed in different settings. Treatment of mice bearing MDA-MB-435 tumors in the mammary fat pad, with F3 peptide-targeted pH-sensitive liposomes containing doxorubicin enabled a suppression of tumor invasion into adjacent healthy tissues, in contrast to a number of different controls tested, including the non-targeted counterpart[46]. The versatility of the strategy was further demonstrated with the encapsulation of a drug

combination of doxorubicin and the sphingolipid, C6-ceramide (inhibitor of the PI3K pathway)[50]. A killing level of 100% was achieved against both stem-like and non-stem MDA-MB-231 triple-negative breast cancer cells, in contrast with the targeted counterpart containing doxorubicin alone that did not go beyond 90 %[24]. The versatility of the strategy has also been reflected on the nature of the drug to be encapsulated. In fact, F3 peptide containing anti-polo-like kinase 1 (*PLK1*) siRNA decreased viability of both PC-3 prostate cancer cells and HMEC-1 endothelial cells, a model of endothelial cells from angiogenic blood vessels. In addition, upon combination with paclitaxel, a 3-fold reduction of IC_{50} (relative to paclitaxel alone) was obtained[51].

A targeting approach based on fusion toxins, comprised by the F3 peptide and the ribosome-inactivating protein gelonin, has also been developed. Three formats of fusion toxins, differing in the number of F3 peptide sequences used, presented improved cytotoxicity against prostate cancer cell lines, relative to gelonin alone. However, only the multimeric formats enabled improved tumor accumulation and reduced tumor growth in ectopic models of prostate cancer and glioblastoma, respectively. The most potent effects obtained with these formats, relative to the monomeric fusion toxin, could be due to their increased valency or improved exposure of the F3 peptide sequences, enabled by the use of multimers and the linker $(GGSG)_3$ between each F3 peptide sequence[52].

1.2.3.2.2 AS1411 as targeting ligand for intracellular drug delivery

Aptamers are guanine-rich oligonucleotide molecules that form four-stranded structures and present specific protein-binding (aptameric) properties. One of the main issues regarding oligonucleotide-based therapies is their stability in serum and in the presence of cellular nucleases. However, aptamers present increased resistance to nuclease activity, due to their quadruplex structure, making them more suitable for therapeutic purposes.

Table 1.1. F3 peptide-conjugated agents for intracellular drug delivery.

Drug and delivery agent	*In vitro* effects	*In vivo* model	Schedule	*In vivo* effects
CIS-loaded, hydrogel NP[47]	↓ viability of TEC[a]	*BD/T*: C57BL6 mice 10^7 ID8-VEGF cells Ectopic (flank)	*BD*: i.v. 100 mg/kg F3-FITC-NP	High uptake in tumor vessels No significant uptake in liver and kidney
			T: i.v. 100 µg/kg F3-CIS-NP (days 10, 14 and 21)	↓ tumor weight (2.5-fold)[a] ↓ tumor volume (3.5-fold)[a] ↑ regions of hemorrhage and necrosis[a] ↓ tumor islet size[a]
		T: Nude mice 10^7 SKOV3 or A2780 Ectopic (axillary) $2x10^6$ ID8 cells Ectopic (i.p. injection)	i.v. 100 µg/kg F3-CIS-NP (days 10 and 14; ID8 and SKOV3 xenograts also day 21)	↓ tumor volume[a] ID8: ↑ survival[a]
		T: Teratoma model Non-obese SCID mice 10^6 undifferentiated H9 embryonic stem cells Ectopic (axillary) 10^5 HEY1 cells within teratoma	i.v. F3-Cis-Np (75 µg/kg CIS) (days 10, 14, 17 and 21)	↓ tumor progression [a] ↓ tumor weight [a] ↓ tumor blood vessels[a]
Photofrin-loaded PEG-PLGA NP [48]	↓ viability of MDA-MB-435 (90%) (10 µM, 4 h)	Fisher 344 rats 10^5 Rat 9L cells Orthotopic	*I*: i.v., 200 mg NP/kg	↑ half-life (3-fold) ↑ contrast-to-noise ratio (2-fold)
			T: i.v. of F3-targeted Photofrin/iron oxide–encapsulated NP with light activation 1 h later	↑ survival (2.5-fold)

Table 1.1. *(Continuation)*

Drug and delivery agent	*In vitro* effects	*In vivo* model	Schedule	*In vivo* effects
^{213}Bi-DTPA-[F3]$_2$ [49]	↓ clonogenic capacity ID50 - 23.9 to 119 kBq/mL (EMT6, MIAPACA, CMT93, OVCAR3 and MDA-MB-435)	SCID mice 10^7 MDA-MB435 (peritoneal carcinomatosis model) Orthotopic (i.p.)	*BD*: i.p. 3.7 MBq ^{68}Ga-DTPA-[F3]$_2$ *T*: i.p., 1.85 MBq ^{213}Bi-DTPA-[F3]$_2$, between days 4 and 14 (tumor prevention) or between days 16 and 26 (tumor reduction)	Accumulation in tumor (32%) and kidney ↑ survival (80% or 62.5%, respectively) smaller number of tumor nodules
Anti-*PLK1* siRNA-loaded pH-sensitive LP[51]	↓ viability (2 µM siRNA, 80 h)[b] PC3: 57% HMEC: 39.4%	-	-	-
DOX-loaded pH-sensitive LP [24,46]	IC_{50} (24 h), untargeted and targeted: MDA-MB-435S: 87.33 and 3.95 µM HMEC-1: 3.57 and 0.195 µM ↓ vessel formation (27.5%)	Balb/c mice MDA-MB-435S Orthotopic	*BD*: i.v., 0.5 lmol phospholipid/mouse *T*: i.v., 5 mg DXR/kg, every week for 5 weeks	↑ accumulation in tumors (57-fold) ↓ accumulation in spleen and liver ↓ viable rim area ↑ cell death in tumor periphery ↑ tumor necrosis ↓ vascular density ↓ invasion to adjacent tissue
F3-Gel, 2F3-Gel and 3F3-Gel fusion toxins (comprising 1 to 3 repeats of F3 peptide sequence, respectively) [52]	↓ viability, IC_{50} (48 h), untargeted and targeted (monomeric, dimeric and trimeric F3): LNCaP: 4100, 470, 63 and 88 nM PC3: 4200, 360, 99 and 94 nM DU145: 3100, 310, 73 and 100 nM	*BD*: Athymic mice $2x10^8$ LNCaP Ectopic (left flank) *T*: Athymic mice $2x10^8$ U87 MG Ectopic (left flank)	*BD*: i.v., 8 mg/kg Gel *T*: i.v., 8 mg/kg Gel (days 9, 12 and 15)	↑ accumulation in tumors (3.6- and 3.1-fold for 2F3-Gel and 3F3-Gel, respectively) ↓ tumor volume (44% or 39% for 2F3-Gel and 3F3-Gel, respectively)

BD, biodistribution studies; ^{213}Bi-DTPA, alpha emitter ^{213}Bi, conjugated to diethylenetriaminepentaacetic acid; CIS, cisplatin; DOX, doxorubicin; Gel, gelonin; *I*, imaging studies; LP, liposome; NP, nanoparticle; *T*, therapeutic studies. Administration: i.p., intraperitoneal; i.v., intravenous. Cells: 9L, rat gliosarcoma; A2780, HEY-1, OVCAR3 and SKOV3, human ovarian cancer; CMT93, murine colon cancer; DU145, LNCaP and PC3, human prostate cancer; EMT6, MDA-MB-231, human breast cancer; HMEC-1 and TEC, human tumor endothelial cells; ID8, murine ovarian tumor; MIAPACA, human pancreatic cancer; U87 MG, human glioblastoma. Unless otherwise indicated, the percentages indicated are in comparison to the control without the F3 peptide. [a]relative to CIS+F3-NP; [b]relative to untreated cells

The AS1411 aptamer has been used to target nanoparticles of different nature, containing either siRNA[53] or small drugs[54–58] towards nucleolin-overexpressing cells (Table 1.2). Similar to what has been described for the F3 peptide, AS1411-based strategies led to improved cytotoxicity against nucleolin-overexpressing cell lines relative to non-targeted counterparts[59–61]. Similar effects to the ones reported for F3 peptide-targeted approaches were also observed, namely a marked tumor growth inhibition and improved survival, depending on the tumor model. Of notice in this set of studies is the absence of reported effects on the tumor vasculature.

AS1411 has also revealed to have antiproliferative activity on its own (Table 1.3). At the molecular level, in breast cancer cells, it enabled destabilization of *bcl-2* mRNA and downregulated expression levels of miR-21, miR-221, miR-222 and miR-103, usually associated with tumor aggressiveness and resistance to antineoplastic therapy[62,63]. Furthermore, inhibition of nuclear factor kappa B (NF-κB) activation was observed following incubation with human prostate, breast and lung cancer cell lines[64]. The pharmacological activity, both *in vitro* and i*n vivo*, that the AS1411 aptamer has revealed against tumors of diverse histological origin, including leukemia[65,66], supported a phase II clinical trial in patients with acute myeloid leukemia, in combination with cytarabine (NCT00512083). An improved anti-leukemic activity, with acceptable safety profile and improved overall survival, was observed. However, a phase IIb clinical trial to determine duration of response and survival (NCT01034410) was terminated. Since then, no reports on new clinical trials have been disclosed.

Notably, the positive outcome of both F3 peptide- and AS1411-targeted platforms were observed in tumor models from different histological origins, supporting the relevance of nucleolin as a target in a wide range of tumors.

Table 1.2. AS1411-conjugated agents for intracellular drug delivery.

Drug and delivery agent	*In vitro* effects	*In vivo* model	Schedule	*In vivo* effects
PTX-loaded PEG-PLGA NP[54]	↓ viability of C6 $IC_{50,}$ 96 h: untargeted - 0.08 ug/mL targeted - 0.03 ug/mL	Nude mice $2x10^6$ C6 cells Ectopic (right anterior limb)	*BD*: i.v., 3 mg/kg PTX *T*: i.v., 3 mg/kg PTX, (days 6, 8, 10, 12, 14, 16, 18)	↑ accumulation in the tumor ↓ tumor volume and weight
		Wistar rats $3x10^7$ C6 cells Orthotopic	i.v., 3 mg/kg PTX, (days 4, 6, 8, 10, 12 and 14)	↑ survival (22%)
DOX-loaded nanorod[55]	↓ viability of MCF-7 (50%) (40 µM, 48 h)	-	-	-
PTX-loaded, PLGA-lecithin-PEG NP[67]	↓ viability of MCF-7 and GI-1	-	-	-
DTX-loaded, TGN-conjugated PEG-PCL NP[59]	-	Balb/c mice $5x10^5$ C6 cells Orthotopic	*I*: i.v. *T*: i.v., 6 mg/kg DTX (every 3 days, 3 times)	↑ ratio tumor/brain accumulation ↑ survival (increase of 47% or 28% for AS1411/TGN- or AS1411-targeted NP)
PTX-loaded protein NP[56]	↓ viability of MCF-7	-	-	-

Table 1.2. *(Continuation)*

Drug and delivery agent	*In vitro* effects	*In vivo* model	Administration	*In vivo* effects
NMM-loaded gold NP[58]	↓ viability of Hela (30%) (10 nM NP, 24 h)	-	-	-
Anti-BRAF siRNA-loaded, MAL-activated PEG-DOPE liposomes[53]	↓ viability of A375	Balb/c nude mice 2x10^6 A357 cells Ectopic (right flank)	*BD*: i.v., 1.2 mg Cy5.5-siRNA /kg *T*: i.v., 1.2 mg/kg siRNA, 3 consecutive days	Accumulation in tumor and kidneys gene silencing in tumor tissues ↓ tumor cell number tumor necrosis
DOX- or AZD8055-loaded gold NP[57]	↓ viability of MCF-7, OMM1.3, Mel202 (72 h) DOX: 49.4, 58.1 and 38.5% AZD8055:17.9, 21.6 and 34.5%	-	-	-
PTX-loaded, pH-sensitive micelles[68]	↓ viability of SKOV3 IC_{50} (pH 7.4, 48 h): untargeted, 0.832 µM; targeted, 0,552 µM IC_{50} (pH 5.8, 48 h): untargeted, 0.298 µM; targeted, 0.108 µM	-	-	-
DOX-loaded, MAL-PEG-LP[69]	↓ viability of MCF-7/ADR	Nude mice 5x10^6 MCF-7/ADR cells Ectopic (left flank)	i.v. 0.2 mg/kg (DOX), every 4 days, 4 times (tumor site heated at 42°C)	↑ accumulation in tumor ↓ tumor volume
DOX-loaded, redox-responsive HPAEG[70]	↓ viability of MCF-7 IC_{50} (48 h): non-targeted - 2.30 µg/mL; targeted - 1.33 µg/mL	-	-	-

Table 1.2. *(Continuation)*

Drug and delivery agent	*In vitro* effects	*In vivo* model	Administration	*In vivo* effects
Gemcitabine-loaded PEG-PLGA NP[71]	↓ viability of A549 IC_{50} (48 h): untargeted - 28.9 µg/ml targeted - 4.9 µg/ml	-	-	-
DTX-loaded polymeric NP [72]	↓ viability of LNCaP IC_{50} (48 h): untargeted - 0.251 µg/mL targeted - 0.085 µg/mL	Balb/c mice $2x10^7$ LNCaP cells Ectopic (right flank)	iv. 10 mg/kg of DTX, every other day, for 2 weeks	↓ tumor weight (35%)
DOX-loaded, PEP polymersome[60]	↓ viability of MCF-7 IC_{50} (48 h): control aptamer: 369.4 ng/mL targeted: 210.9 ng/mL	Mice bearing MCF-7 tumors	*BD*: i.v. 2 mg/kg of ICG Cellular uptake: i.v. 5 mg/kg DOX *T*: i.v. 5 mg/kg DOX (days 0, 3 and 6)	↑ accumulation in the tumor (1.75-fold)[a] ↑ cellular uptake (2 fold) [a] ↓ tumor volume (45%) [a] ↑ tumor growth inhibition (43%) [a] ↑ apoptotic area [a] ↓ cell proliferation [a]
DTX-loaded, PLGA-TPGS NP[73,74]	↓ viability, IC_{50} (48h), untargeted and targeted: MCF-7: 6.88 and 1.69 µg/mL HeLa: 3.07 and 0.47 µg/mL	SCID mice $2x10^6$ MCF-7 cells Ectopic (back) TA2 mice (spontaneous breast cancer) SCID mice $2x10^6$ HeLa cells Ectopic (back)	*BD*: i.v. 1 mg/kg IR-780 *T*: i.v. 10 mg/kg DOX (days 0, 4, 8, 12, 16) *T*: i.v. 10 mg/kg DOX (days 0, 4, 8, 12, 16) *T*: i.v. 10 mg/kg DOX (days 0, 4, 8, 12, 16, 20)	↑ accumulation in the tumor ↓ tumor volume ↑ survival (22%) ↑ survival (24%)
PTX-loaded, PGG NP[61]	↓ viability, IC_{50} (48h), untargeted and targeted: U87 MG: 0.73 and 0.21 µM	Balb/c mice $5 x10^5$ U87 MG cells Orthotopic (right striatum)	*I:* i.v. DiR-labeled AS1411-PGG-PTX (10 µg DiR) *T*: i.v 10 mg/kg PTX (days 3, 6, 9, 12)	↑ accumulation in the brain ↑ penetration in glioma tissue ↑ survival (1.1 fold)

Table 1.2. *(Continuation)*

Drug and delivery agent	*In vitro* effects	*In vivo* model	Administration	*In vivo* effects
CPT-loaded, pegylated PAMAM[75]	↓ viability, IC_{50} (48h), untargeted and targeted: HT29: 5.75 and 2.07 µg/mL C26: 2.67 and 0.67 µg/mL	Balb/c mice $3x10^5$ C26 cells Ectopic (right flank)	i.v. 3 mg/kg CPT (twice a week, for 3 weeks)	↓ tumor volume ↑ survival
let-7 microRNA gene-loaded EV[76]	-	Balb/c mice $3x10^6$ MDA-MB-231 cells Ectopic (right flank)	*I:* i.v., 50 µg EV *T*: i.v. 150 µg let-7, every other day, until day 25	↑ accumulation in the tumor ↓ tumor volume (29%)
DOX/SPION-loaded, PLGA NP[77]	↓ viability, IC_{50} (48h), untargeted and targeted: C26: 1.76 and 0.37 µg/mL	Balb/c mice $3x10^5$ C26 cells Ectopic (right flank)	i.v. 10 mg NP/kg	*BD*: ↑ accumulation in the tumor *T*: ↑ survival (1.2-fold) ↑ tumor growth delay (1.4-fold)

BD, biodistribution studies; CPT, camptothecin; DOPE, dioleoylphosphatidylethanolamine; DOX, doxorubicin; DTX, docetaxel; EV, extracellular vesicles; HPAEG, hyperbranched poly(2-((2-(acryloyloxy)ethyl)disulfanyl)ethyl 4-cyano-4-(((propylthio)carbonothioyl)-thio)-pentanoate-co-poly(ethylene glycol) methacrylate); *I*, imaging studies; MAL, maleimide; NMM, N-methylmesoporphyrin IX; NP, nanoparticle; PAA, polyacrylamide; PAMAM, Polyamidoamine dendrimer PEG, polyethyleneglycol; PEP, poly[methoxy-poly(ethylene glycol)/ethyl-p-aminobenzoate phosphazene; PCL, polycrapolactone, PGG, poly(L-γ-glutamylglutamine) PLGA, poly(d,l-lactide-co-glycolide); PTX, paclitaxel; SPION, superparamagnetic iron oxide nanoparticles; *T*, therapeutic studes; TGN, blood brain barrier-targeting peptide; TPGS, D-α-tocopheryl polyethylene glycol 1000 succinate. Administration: i.p., intraperitoneal; i.v., intravenous. Cell lines: A375, human melanoma; A549, human lung cancer; C26, murine colon cancer; C6, rat glioma; HeLa, human cervix cancer; HT29, human colorectal cancer; LNCaP, human prostate cancer; MDA-MB-231 and MCF-7, human breast cancer; OMM1.3 and Mel202, human melanoma; SKOV3, human ovarian cancer; U87 MG, human glioblastoma. Unless otherwise indicated, the percentages are in comparison to the control without the AS1411. [a]relative to nanoparticles with control aptamer

1.2.3.3 Nucleolin as a target for pseudopeptides and antibody formats

Although the effectiveness of AS1411 in clinical trials remains unconfirmed, the promising results obtained in several models of nucleolin-overexpression tumors, paved the way to the development of other entities aiming at disrupting nucleolin signaling, namely pseudopeptides and antibody formats (Table 1.3).

1.2.3.3.1 Nucleolin as a target for pseudopeptides

The nucleolin-binding pseudopeptide HB-19 has a pentavalent structure composed by the tripeptide lysine-proline-arginine (with a reduced bond between the lysine and proline residues) coupled to an 9-amino acid template. The reduced bond between lysine and proline provides resistance to serum proteases[78]. Upon binding to nucleolin, this pseudopeptide is translocated to the cytoplasm, but not to the nucleus, leading to a reduction in the nucleolin levels, both at the cell surface and in the cytoplasm[79].

HB-19 decreased the colony formation capacity of several cell lines, the proliferation and migration of VEGF-stimulated HUVEC, and enabled anti-angiogenic effects in a chick choriallantoic membrane (CAM) assay, reducing blood vessel length by 50%. Importantly, these effects translated into antitumoral and anti-angiogenic effects in *in vivo* breast cancer models, without evidences of toxicity in normal tissues[79]. HB-19 activity relied on the decrease of both the percentage of cells in the S phase of the cell cycle and ERK1/2 phosphorylation[79]. The activity of HB-19 has been further demonstrated against rhabdoid tumor-derived cells, upon reducing the tumorigenic potential as well as the expression of different genes involved in tumorigenesis and angiogenesis like Wilms' tumor 1 (WT1), matrix metalloproteinase-2 (MMP-2), epithelial isoform of CD44 (CD44E) and VEGF. In TIII melanoma cells, it reduced the expression of MMP-2, MMP-9 and tumor necrosis factor α (TNF-α)[80].

Among the different analogs generated from the original HB-19, the one codenamed N6L, proved to be particularly promising[81]. N6L consists of six repeats of lysine-2-aminoisobutyric acid-glycine, with the pseudotripeptide lysine-proline-arginine (reduced peptide bond between lysine and proline) grafted onto the lysine residues. In contrast with HB-19, which was translocated to the cytoplasm upon binding to nucleolin, N6L was translocated to the nucleolus[81]. Interestingly, N6L enabled distinct inhibitory mechanisms depending on the tumor cell type, as 90% cell growth inhibition for the most sensitive cell lines. In leukemia and lymphoma cell lines, it not only inhibited cell growth, but also promoted a level of cell death that varied between 35 and 70%[82]. Other N6L effects were also dependent on the cell type. In cell lines from breast, prostate and cervical cancer, N6L treatment restored contact inhibition, whereas inhibition of spreading and migration was observed in cells lines from colon carcinoma and breast cancer, respectively[82].

In consonance with the impact of N6L on cancer cell growth and death, studies approaching its effects at the molecular level reported alterations on apoptotic pathways and cell cycle. In MDA-MB-231 breast cancer cells, N6L led to caspase-dependent apoptosis[81] and in glioblastoma cells it decreased the levels of cyclins D1 and B2, promoting increased number of cells in G1 phase and cell cycle inhibition[83]. In addition, in these glioblastoma cells, treatment with N6L promoted autophagy, as evaluated by the expression of the autophagic markers p62, LC3I and LC3II[83].

Similar to other nucleolin-targeting strategies, N6L also affected angiogenic endothelial cells. HUVEC cells incubated with N6L presented decreased adhesion, proliferation and migration, consistent with the observed decreased expression of MMP-2 (involved in the degradation of the extracellular matrix and therefore in migration) and activation of several kinases (Src, FAK, Akt and ERK1/2) that regulate cell adhesion and proliferation[84]. Also consistent with its anti-proliferative effects, N6L increased the percentage of cells in G1 phase[85]. These effects translated into angiogenesis inhibition, evaluated by CAM assay[81].

Importantly, in endothelial cells N6L also decreased secretion or expression of Ang-2 (after a 5 h or 72 h incubation, respectively), a protein that prevents vessel normalization, and increased expression of platelet-derived growth factor receptor beta (PDGFβ), involved in pericyte recruitment, which helps maintain the vasculature structure[85]. In fact, *in vitro* assays showed improved pericyte migration upon incubation with N6L. These results supported an effect of N6L on both cancer cells and tumor vasculature, which was confirmed *in vivo*. In both xenograft and syngeneic models, N6L enabled antitumoral and anti-angiogenic properties with no associated toxicity[81,83,85]. In a syngeneic model of pancreatic cancer, treatment with N6L not only affected tumor volume and metastasis, but also promoted normalization of the tumor vasculature, by increasing pericyte coverage (which prevents vascularization) and reducing hypoxic area (evaluated by pimonidazole and carbonic anhydrase 9 staining).[85] In line with the *in vitro* results, N6L-treated mice presented a 68% reduction of Ang-2 levels in the plasma, as well as decreased expression in the tumor. The tumor vasculature normalization resulted in improved perfusion and doxorubicin delivery, with a 3.5-fold increase of the tumor drug level. The positive impact of vasculature normalization was further confirmed in pancreatic tumors. N6L combined with gemcitabine, the standard of care in this setting, enabled significant tumor growth inhibition relative to single treatments[85].

Due to these promising results, N6L was evaluated in a phase I/IIa clinical trial on advanced solid tumors (NCT01711398), the report of which is not known yet.

1.2.3.3.2 Nucleolin as a target for antibodies

Antibody-based constructs against nucleolin have also been explored, such as NCL3, a rabbit nucleolin-binding full-length antibody, whose effects were mainly seen at the tumor vasculature level, accompanied by downregulation of Bcl-2 expression[86].

Anticancer activity has been also observed with an anti-nucleolin single-chain variable fragment, 4LB5 (scFv, an antibody format generated by fusion of the variable domains of a heavy chain and a light chain, as explained in section 1.3.2.2 and depicted in Figure 1.4). It affected cancer proliferation, both *in vitro* and *in vivo*, without evidence of side effects. Activity was supported by downregulation of miR-21, miR-221 and miR-222 and increased apoptosis[87]. Fusion of 4LB5 to human pancreatic RNase, which becomes toxic upon internalization, resulted in a significant reduction of colony formation and tumor growth inhibition, relative to 4LB5 alone. Although tumors from mice treated with this fusion construct presented reduced cellularity than the ones treated with 4LB5, proliferation was increased. These results suggested that this construct acted mainly through cytotoxic effect, rather than a cytostatic one[88].

The generation of anti-nucleolin full-length antibodies has also been reported. These antibodies reduced the viability of leukemic MV4-11 cells, from 30-80% of untreated cells. Moreover, some of the antibodies presented increased cytotoxic activity in the presence of human serum (source of complement), relative to the control condition using heat inactivated human serum, suggesting a complement-dependent cytotoxicity (CDC; section 1.3.2) effect[89].

Overall, the studies herein presented confirm the relevance of nucleolin as a therapeutic target for several tumors. However, despite the different strategies that have been developed, antibody-based approaches focused on the recruitment of the immune system, particularly antibody-dependent cell-mediated cytotoxicity (ADCC; section 1.3.2.1) remain largely unexplored.

Table 1.3. Nucleolin-binding agents with impact on cancer and/or endothelial cells.

Name and format	*In vitro* effects	*In vivo* model	Schedule	*In vivo* effects
AS1411 (aptamer)	↓ viability of cell lines of 14 histological origins, most with reduced viability of at least 30% (for 6.3 µM)	Nude mice DU145 Ectopic Nude mice A549 SKMES	i.p. 5 mg/kg (days 1, 2, 3, 5, 7 and 9) i.v. 5-40 mg/kg (days 1-5, daily)	↓ tumor growth A549: ↓ tumor size SKMES: ↓ tumor volume
HB-19 (PP)[79,80,90]	↓ colony formation (5 µM) MDA-MB-231, MDA-MB-435 PC-3, U87 MG, B16 and G401: ↓ proliferation and migration of VEGF-stimulated HUVEC	Antiangiogenic effects: Swiss mice Matrigel plug model Antitumoral effects: nude mice Right flank (MDA-MB-231) or mammary fat pad (MDA-MB-435) MT/ret+/- transgenic mice (C57BL/6 background) Spontaneous melanoma model Nude mice $4x10^6$ HB-19-treated G401 cells Ectopic (back),	1 µM HB-19 i.p., sc., or peritumoral, 5 mg/kg, 3 times per week i.p., 5 injections/week during week 1-3 and 2 injections/week during week 4-42. 50, 100, and 200 µg for the first, second and the rest of the weeks, respectively.	↓ blood vessel density ↓ tumor weight (95% and 57%, respectively) delayed onset of cutaneous tumors and nodules ↓ tumorigenicity (50%)

Table 1.3. *(Continuation)*

Name and format	*In vitro* effects	*In vivo* model	Schedule	*In vivo* effects
		Nude mice Ectopic (right flank, MDA-MB-231 or PC3)	i.p. 1g/kg 5 times/week	↓ tumor volume (90% in MDA-MB-231, 40% in PC3)
		Balb/c and C57BL/6 mice $5x10^6$ A20 cells $5x10^5$ T29 cells	i.p. 8g/kg 5 times/week	↑ survival (2-fold in A20 and 6-fold in T29)
	GI_{50} (72 h): 2.7 - >40 µM Panel of 22 cell lines from different origins, (lowest and highest values corresponding to HUVEC and Renca, respectively)	Balb/c nude mice $1.5x10^5$U87-LUC cells Orthotopic	i.p.10 mg/kg, 5 days/week from day 1 post-cell inoculation for 4 weeks.	↑ survival (50%)
	↓ HUVEC proliferation			↓ tumor volume (43.4%) ↓ cell proliferation ↑ apoptosis ↓ liver metastasis area (67%) ↓ vessel density (42%) ↓ vessel branching (62%) ↑ perfusion of tumor vasculature (>2-fold) ↑ pericyte coverage (~70%) ↓ hypoxic area (>50%)
N6L (PP)[81,83,85]	↓ HUVEC adhesion (40%), proliferation and migration (61%) for 50 µM		i.p. 10 mg/kg, 3 days/week, for 3 weeks	
	↓ MIA PaCa2 and mPDAC migration (~70%, for 50 µM)			
	↓ mPDAC invasion	FVB/n syngeneic mice 10^3 mPDAC cells Orthotopic	i.p. 2 mg/kg N6L 3 days/week, for 1 week, followed by i.v. 100 mg/kg of gemcitabine 2 days/week and i.p. 2 mg/kg N6L 3 days/week, for 2 weeks	↓ tumor volume (75%)[a]
	↑ HBVP migration			
		RIP-Tag2 transgenic mice	10 mg/kg, 3 days/week (from 12 to 16 weeks of age)	↓ tumor growth (40%) ↑ apoptosis (90%) ↓ vessel density ↓ vessel branching ↑ perfusion of tumor vasculature

Table 1.3. *(Continuation)*

Name and format	*In vitro* effects	*In vivo* model	Administration	*In vivo* effects
NCL3 (rabbit IgG)[86]	↓ HUVEC capillary-like tube formation (10 µg/mL) ↓ HUVEC viability (>50%), modest effect in C8161	Balb/c nude mice Matrigel plug model BALB/c nude mice $2x10^6$ MDA-MB-435 cells Orthotopic	200 µg NCL3, daily, for 7 days. i.v. 400 µg NCL3, every 3 days	↓ blood vessel density No reduction in tumor growth ↓ blood vessel density Normalization of the tumor vasculature
4LB5 (human scFv)[87]	↓ viability IC_{50} (72 h): MDA-MB-231: 30 nM T47D: 20 nM BT549: 58 nM MDA-MB-436: 50 nM PLC-PRF: 3 nM	NOD-SCID mice $2x10^6$ Luc^+MDA-MB-231 cells Orthotopic	i.p. 2 mg/kg, twice a week	↓ tumor volume ↓ cellularity ↓ cell proliferation
4LB5-HP-RNase (human scFv fused to human pancreatic RNase)[88]	↓ viability IC_{50} (72 h): MDA-MB-231: 25 nM BT549: 12.5 nM MDA-MB-436: 50 nM MCF-7: 25 nM ↓ colony formation of MDA-MB-231, BT549 and MDA-MB-436[b]	NOD-SCID mice $2x10^6$ Luc^+MDA-MB-231 cells Orthotopic	i.p. 2mg/kg, twice a week	↓ tumor volume[b] ↓ cellularity[b] ↑ cell proliferation[b]

scFv, single chain fragment variable; Administration: i.p., intraperitoneal; i.v., intravenous. Cell lines: B16, mouse melanoma; A20, murine lymphoma; BT549, MDA-MB-231, MDA-MB-436 and T47D, human breast cancer; C8161, human melanoma; HBVP, human brain vascular pericytes; HUVEC, human umbilical vein endothelial cells; MIA PaCa2, human pancreatic cancer; mPDAC, murine pancreatic cancer; PC-3, human prostate cancer; PLC-PRF, human hepatoma; T29, human lymphoma; U87, human glioblastoma. Unless otherwise indicated, the percentages indicated are in comparison to untreated cells/PBS-treated mice. [a]relative to single treatments; [b]relative to treatment with 4LB5

1.3 CANCER AND THE IMMUNE SYSTEM

Immune evasion is as a key factor in tumor development[91], as evidenced by the high tumor take rate, following xenotransplantation of mouse strains with deficiencies in cells and factors of the immune system, such as T cells, B cells and interferon gamma (IFN-γ).

The current theory of cancer immunosurveillance and immune-editing states that the immune system is in dynamic interaction to avoid tumor development. Escaping its tight regulation and promoting an immunosuppressive environment constitute major steps in tumor development. Therefore, research on anticancer therapy has been focusing on counteracting this immunological shutdown and restoring some of the immune system activity.

1.3.1 Cancer immunotherapy

Immunomodulatory therapy and adoptive transfer of immune factors are currently the main cancer immunotherapeutic strategies[92–94]. Immunomodulatory therapy aims at breaking the immune tolerance that characterizes the tumor microenvironment, by activating T cells or by blocking key players on the regulation of the magnitude of the T-cell response. One of these players is T-lymphocyte antigen 4 (CTLA-4) of helper T cells, which inhibits cytotoxic T cells[92–94]. Ipilimumab, an anti-CTLA-4 antibody, was the first drug to enable improved overall survival in patients with advanced melanoma, as well as single-agent activity in other malignancies. However, toxicity associated with ipilimumab is not insignificant and many patients do not respond to therapy[95,96]. Preclinical and early clinical studies targeting the programmed death-1 receptor (PD-1), another T cell co-inhibitory receptor, have shown even better response rates and lower toxicity than ipilimumab. However, despite its clinical benefit, there were still 55-67% non-

responders[97]. The lack of known biomarkers to predict the efficacy of these antibodies remains a drawback in these therapies[96].

Adoptive transfer of immune effectors is based on the *ex vivo* generation of large numbers of T cells or monoclonal antibodies that trigger immune responses, which are then administered to the patient.

Adoptive transfer of T cells in combination with IL2 has shown promising results in metastatic melanoma, with objective response rates of 50%, and is currently being tested also for prostate cancer. An alternative to this strategy is the use of engineered T cells that express chimeric antigen receptors (CARs), which consist on single-chain constructs fused to a T-cell receptor signaling domain. This results in a targeted activation of T cell signaling, which could have the additional advantage of leading to immunological memory. However, CAR-based therapies still present high toxicity to healthy tissues[92–94].

1.3.2 Structural features of monoclonal antibodies

Antibodies, also known as immunoglobulins (Ig), are proteins produced by B cells of the adaptive immune system in response to antigen detection. In mammals, antibodies are grouped in five isotypes (IgA, IgD, IgE, IgG and IgM), each presenting a specific structure and role in immunological processes. The most common of these, IgG, accounts for up to 80% of the antibodies in normal serum and is usually one of the components of recombinant proteins for therapeutic purposes for several diseases, including many types of cancer[98].

A typical antibody (Figure 1.2) is a Y-shaped molecule that presents two main regions, the antigen binding fragments (Fab) and the fragment crystallizable (Fc) region. Each Fab presents two variable domains (variable heavy chain, VH, and variable light

chain, VL), along with a constant region (CH1). Both VH and VL domains present three complementarity determining regions (CDR1, CDR2 and CDR3), which are responsible for the binding to the antigen, with CDR1 and CDR3 usually presenting the highest binding extent[99,100]. These domains also present four framework regions (FR) that act as scaffolds that support the loops of the CDRs. The remaining constant domains of the antibody, CH2 and CH3, constitute the fragment crystallizable (Fc). The Fc fragment is responsible for the prolonged serum half-life typical of monoclonal antibodies, upon binding with the neonatal Fc receptor (FcRn), further transporting it within and across cells, thus preventing degradation[101]. In addition, it also plays a central role in mediating different types of cell death, such as antibody-dependent cell-mediated cytotoxicity (ADCC) and complement-mediated cytotoxicity (CDC).

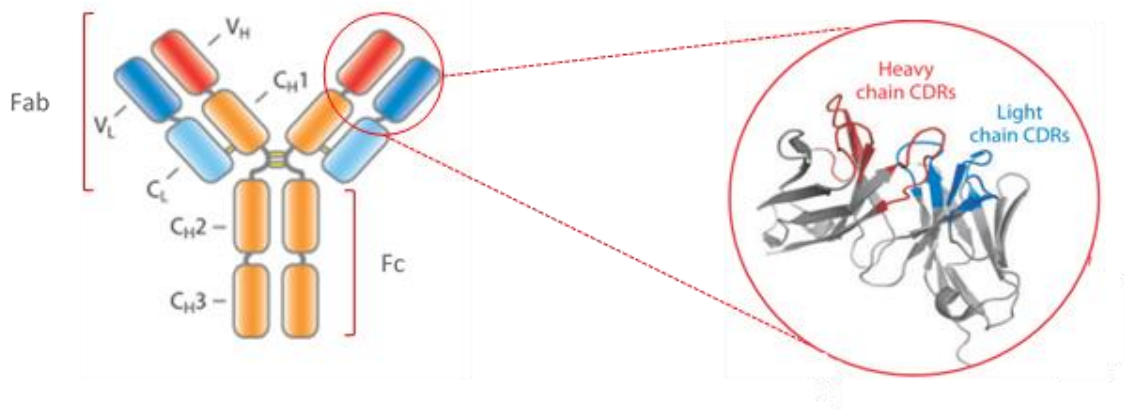

Figure 1.2. Structure of a canonical IgG1 antibody. IgGs are homodimeric proteins, with both constant (C) and variable (V) domains that organize into light (L) and heavy (H) chains. IgGs present two main regions: the antigen-binding fragments (Fab), which bind to the antibody target with high affinity and specificity, and the fragment crystallizable (Fc) region, responsible for triggering immune responses upon binding of the antibody to the target. The specificity of the antibody to the different target, derives from highly variable sequences of loops in the Fabs, the complementary-determining regions (CDRs), which are present both in the light and the heavy chains. (Adapted from ref. 125)

The two Fabs are linked to the Fc region by the hinge region, a flexible linker that impacts on the flexibility of the molecule: the upper hinge portion determines the Fab-

Fab flexibility, and therefore the angle between the Fab arms; the lower hinge portion influences the position of the Fab arms relative to the Fc region, thus being responsible for the Fab-Fc flexibility. The flexibility conferred by the hinge region is believed to play a role on the antibody's capacity to trigger immune functions, as Fab orientation relative to the Fc can alter the accessibility of the latter to C1q (first component of the complement cascade) and FcγR (IgG Fc receptor)[102].

Differences in the amino acid composition and structure of the hinge region are the main characteristics for grouping IgGs in four subclasses (from IgG1 to IgG4). IgG3 presents the longest hinge, thus being the subclass with the highest flexible hinge region between Fabs and Fc region. The flexibility of the hinge region decreases, subsequently, in the following order: IgG1, IgG4 and IgG2. Based on this feature, IgG1 and IgG3 are more prone to trigger immune functions, presenting the former the strongest ADCC activity, and the latter the strongest CDC capacity. However, other factors, besides the hinge region flexibility, rule the effectiveness and extent of responses of this nature. ADCC responses are affected by the antibody affinity and the antigen density, as well as by immunoglobulin expression by the target cells, whereas CDC effects are regulated by the presence of membrane-bound complement inhibitory proteins[103–106].

In terms of serum stability, IgG3 is the least stable, with a serum half-life of 7 days. The other subclasses present half-lives of about 21 days, which make them more adequate for therapeutic applications. Therefore, IgG2 or IgG4 are the preferential choices when immune responses arising from the release of pro-inflammatory cytokines are undesirable, as in inflammatory and autoimmune disorders. For diseases in which immune functions have a beneficial effect, such as cancer and viral diseases, IgG1 is the subclass of preference[102].

Antibodies can exert their effects by several mechanisms, ranging from inducing direct cell death to the recruitment of components of the immune system. Antibody binding to its target can alter signal transduction pathways that are involved in cell proliferation and survival, thus switching off the overall proliferative capacity of these

cells. Trastuzumab, bevacizumab and cetuximab are examples of antibodies that present this kind of mechanism and act on the signaling pathways associated with the activation of HER2, VEGF and EGFR, respectively. Conversely, antibodies can act as receptor agonists and be used to trigger signaling cascades that lead to cell cycle arrest and apoptosis, as is the case of apomab, which binds the death receptor 5 (DR5).

In addition to these target-specific effects, antibodies can act by recruiting effectors of the immune system, either cells or complement factors, leading to ADCC or CDC mechanisms, respectively[107–110] (Figure 1.3).

1.3.2.1 Antibody-dependent cell-mediated cytotoxicity

ADCC is triggered by the simultaneous binding of an antibody to its target cell, through the Fab domains, and to cells of the immune system (mainly NK cells, but also T cells), through the Fc region. This double binding initiates a signaling pathway in the effector cells of the immune system that culminates in the release of several toxins into target cells the antibody is bound to, thus leading to cell death. Perforin, granzyme A and granzyme B are the main granule factors involved in this process[111].

The importance of this cell death mechanism, enabling a more favorable therapeutic outcome, has been demonstrated in several studies involving polymorphisms in the IgG1 Fc receptors-coding *FcγRIIA* and *FcγRIIIA* genes. These receptors present different expression patterns depending on the type of immune cells. FcγRIIa and FcγRIIIa/CD16a are low-affinity activating receptors for IgG1 Fc and are expressed by subpopulations of NK cells, macrophages or T cells. Some polymorphisms in these genes augment the affinity of the IgG1 Fc region towards the receptor and correlate with better clinical responses, when compared with the responses in the cohort without the polymorphisms.

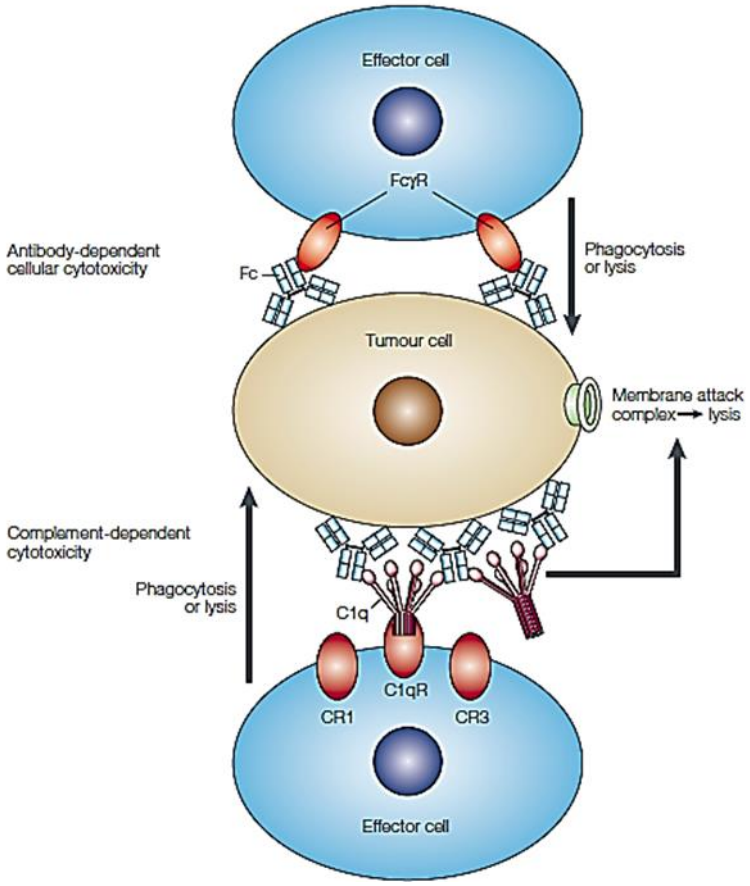

Figure 1.3. Antibody-mediated immune responses. The binding of the antibody to its target can trigger two main immune responses: antibody-dependent cell-mediated cytotoxicity (ADCC) and complement-mediated cytotoxicity (CDC). In ADCC, the antibody binds to the target and then to Fc receptors at the surface of effector cells of the immune system (predominantly, NK cells), which results in the release of cytolytic molecules from the effectors cells and death of the target cell. In CDC, the antibody binds to the target and the to the C1q protein of the complement cascade. This activates the cascade, which culminates in the formation of a membrane attack complex at the surface of the target cells and leads to cell death. Alternatively, the C1q can bind to effectors cells that kill the target cell by phagocytsis or lysis. (Adapted from ref. 110)

For example, non-Hodgkin lymphoma patients presenting a mutation at position 158 of FcγRIIIa (where phenylalanine was replaced by valine), have been associated with complete response to rituximab, subsequent to a stronger binding to the corresponding Fc region [112,113]. Also, in a cohort of patients with metastatic colorectal cancer, progression free survival was higher in patients with FcγRIIa-131H/H and

FcγRIIIa-158V/V genotypes, regardless of the *KRAS* status[114]. In another setting, treatment efficacy with trastuzumab was increased in patients with metastatic HER2-positive breast cancer presenting V/V or H/H genotype, which correlated with higher *ex-vivo* ADCC activity of peripheral blood mononuclear cells (PBMCs)[115,116]. In this respect, there are experimental evidences suggesting a stronger ADCC component underlying trastuzumab mechanism of action than the single interference at the level of the HER2-associated intracellular signaling pathway. In fact, in patients with HER2+ metastatic breast tumors, with complete or partial remission, upon treatment with preoperative trastuzumab, tumor infiltration of lymphoid cells was identified along with *ex-vivo* ADCC activity of PMBCs. In these patients, neither HER2 downmodulation nor changes in proliferation (as evaluated by Ki-67 staining) were observed during therapy[117]. Enhanced ADCC responses were observed upon incubation of cetuximab with a squamous cell carcinoma of the head and neck (SCCHN) cell line, along with patient-derived NK cells, being also predictive of increased progression-free survival, and further supporting the relevance of ADCC in antibody therapy[118].

1.3.2.2 Antibody fragments and associated molecular size versatility

Although antibodies are an important component in the treatment of several types of cancer and other diseases, they present some characteristics that limit their therapeutic efficacy. For example, in the case of the treatment of solid tumors, the main disadvantage arises from their high molecular weight (about 150 kDa), which limits tumor penetration[119]. For diseases in which the target are cells from the immune system (such as in autoimmune disorders), the presence of the Fc region becomes a disadvantage, as it activates cells expressing Fc receptors, leading to massive cytokine release and

toxicity. As a result, efforts have been made to take advantage of the binding capacity of the antibodies, while removing associated components that could be detrimental in specific settings, thus maximizing treatment efficacy. With this goal in mind, a plethora of antibody fragments has been generated (Figure 1.4).

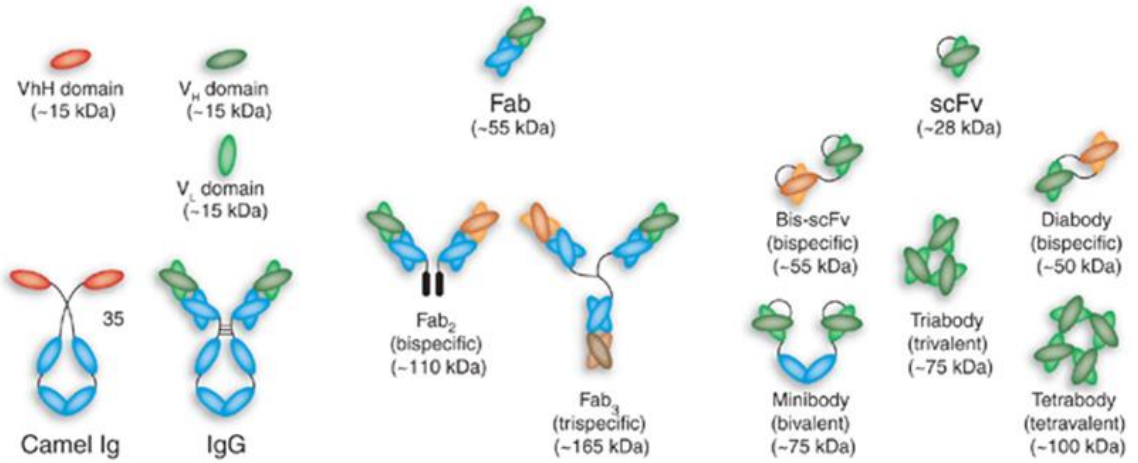

Figure 1.4. Schematic representation of antibody formats. Both canonical (IgG) and non-canonical (camel Ig) immunoglobulins are depicted, as well as the different antibody formats that can be generated. These formats include not only fragments that are obtained from the full IgG, such as single domains and Fabs, but also formats that can be originated by combining different fragments. This combination allows the generation of antibody formats with multivalency and/or multispecificity. For each format, approximate size in kilodaltons is indicated. (Adapted from ref. 120)

Research on antibody fragment was initially focused on the use of single Fabs, as they can be obtained by proteolytic cleavage of the antibody using papain. This enables a ~50 kDa antibody format, subsequent to the absence of the Fc region. The development of recombinant technologies provided a way to further explore different formats, such as scFv, in which the VH and VL domains are joined by a linker that confers stability to the resulting protein. Production of smaller functional fragments (VH or VL) proved ineffective, as these fragments do not fold properly, are water insoluble and

aggregate due to the exposure of hydrophobic amino acids within the VH/VL interface. Therefore, scFv was the smallest functional fragment that could be successfully used[101,120].

However, in 1993 Hamers and colleagues identified camel antibodies in which the light chains and CH1 domain were absent[121], resulting in an antigen binding region composed by a single VH in each arm. These smaller antibodies (~100 kDa) had nonetheless an extensive antigen-binding repertoire and retained high affinity to the antigen[122]. The discovery of these naturally-occurring non-canonical antibodies, named heavy chain antibodies (HCabs), evidenced that different antibody formats could be obtained in a stable and effective form. This has further paved the way to the development of a new class of antibody fragments, including camelid VHs, named variable region of a heavy chain antibody (VHHs) or nanobodies.

In addition to their small size, VHHs display long surface loops that enable them to reach target antigens that are not usually recognized. In HCabs, the CDR3 is usually longer than the human VH CDR3, which might account for the VHH effectiveness in target binding, even in the absence of the VL[99,100].

Nanobodies also present some advantages in terms of manufacturing. They can be expressed in high yields (higher than 50 mg/L) in simple systems such as *Escherichia coli*, with low aggregation propensity, in contrast to scFv. In addition, camelid VHs have been shown to present high similarity to the human VH3 family and therefore have low immunogenicity in humans. An important difference between the human and the camelid VHs is the occurrence of three amino acid substitutions in framework 2 that make the surface more hydrophilic. In camelid VHH, G44, L45, W47 replace the amino acids E44, R45 and G47, occurring in human VH[123,124]. This difference is important to improve water solubility and prevent aggregation. In addition, a disulfide bond between CDR1 and CDR3 stabilizes the protein[123,125] (Figure 1.5). Humanization of camelid VHH can be used to further reduce immunogenicity[126].

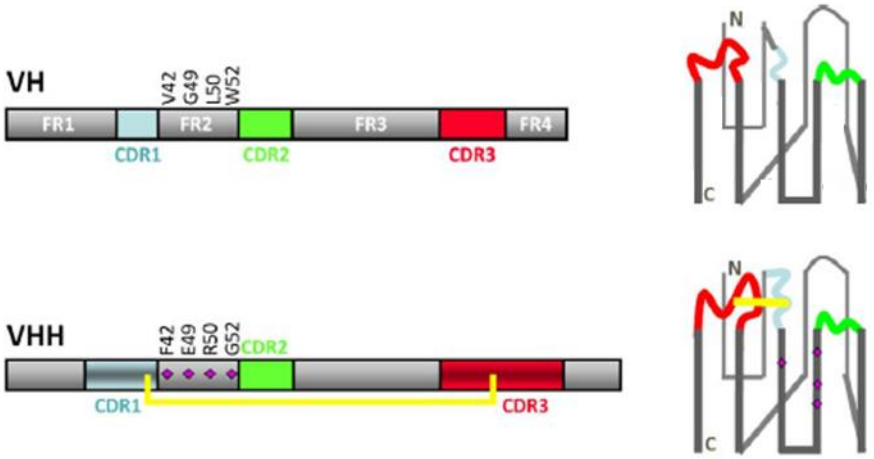

Figure 1.5. Comparison of human and camelid VH domain. The CDRs of the VHH are longer than the VH counterparts, especially the CDR3, which accounts for the high affinity of the small domains. Four substitutions in the framework two (FR2) render the VHH more hydrophylic and thus contribute to its solubility, which contributes to an easier purification of this kind of fragment. The presence of a disulfide bond between CDR1 and CDR3 (indicated in yellow) stabilize the VHH in the absence of the VL that is present in canonical IgGs. (Adapted from ref.124)

One of the main advantages of nanobodies arises from their versatility to originate diverse protein formats. They can be engineered to originate bifunctional molecules (upon linking or genetically fusing them to a molecule with the desired function), multimerized or altered to present bispecificity or even trispecificity, and their blood half-life can be adapted according to the application[127]. Overall, nanobodies are the smallest binding unit, presenting high affinity that can be modified to different sizes, valencies and mechanisms of action, thus constituting ideal building blocks.

1.3.2.3 Nanobodies in cancer therapy

EGFR has been one of the main focus of nanobody development for cancer therapy. Roovers et al. developed a panel of anti-EGFR nanobodies that, within the nanomolar/low micromolar range, enabled a significant decrease of the growth of EGFR-

overexpressing cancer cells[128]. However, nanobodies have a size below the kidney filtration size limit, which results in high blood clearance rate. Therefore, new strategies have been developed to overcome this limitation. One of them consisted on the fusion of nanobodies to an albumin-binding unit, as this protein has a half-life of approximately 20 days, similar to that of a full-length antibody. This strategy proved efficient as it increased blood half-life of an albumin-binding anti-EGFR nanobody and subsequent 25-fold increase of tumor accumulation (along with a 8-fold decrease accumulation in the kidney), relative to the counterpart without the albumin component[129]. Other approaches included multimerization of nanobodies (with three to five nanobody units), which not only increased the molecular weight and improved pharmacokinetics, but also increased valency, and thus avidity[130]. In an ectopic A431 squamous carcinoma model, intraperitoneal administration of trivalent anti-EGFR nanobodies resulted in significant tumor growth inhibition[128]. In the same animal model, a biparatopic version of one of these trivalent nanobodies, in which two nanobodies with specificity towards different epitopes of the same target are cloned, enabled significant tumor growth inhibition[131]. The versatility of nanobodies, and particularly anti-EGFR nanobodies, has been further evidenced as targeting ligands of nanoparticles containing chemotherapeutic drugs[132] [133].

Nanobodies have also been developed against other cancer targets, following different constructions. An anti-carcinoembryonic antigen-related cell adhesion molecule 6 (CEACAM6) nanobody was tested alone or fused to a Fc region, with both antibody formats inhibiting prostate cancer cell proliferation and tubule formation by HUVEC[134]. in an ectopic U87-MG glioblastoma murine model, intraperitoneal administration of anti-hepatocyte growth factor receptor (HGFR) nanobodies, fused to an albumin-binding sequence, decreased tumor volume and increased survival [135]. A bivalent anti-CXCR7 nanobody, also fused to the albumin-binding sequence, reduced angiogenesis and tumor growth in an ectopic 22A hepatoma model[136]. Tang et al. developed an anti-mesothelin single domain antibody fused to an Fc region, resulting in a protein with *in*

vitro ADCC and CDC activity, which caused a 70% decrease in the volume of epidermoid tumors relative to non-treated controls[137].

Following the idea of tumor microenvironment targeting, anti-VEGF nanobodies have also been developed and inhibited VEGF-induced HUVEC proliferation *in vitro*[138,139]. In addition, nanobodies targeting receptors overexpressed in angiogenic endothelial cells, such as VEGFR[140] and CD105[141], inhibited endothelial tube formation.

1.3.2.4 Bispecific antibodies formats in cancer therapy

Bispecific antibodies can be divided into two general groups: those that retarget effector cells of the immune system to tumor cells and those that target two tumor antigens. In the first case, the antibody binds a tumor antigen and a T cell receptor, usually CD3. The construct is often a bispecific T cell engager (BiTE), comprised by two scFV fragments that form a bridge between the T cells and the tumor cells, leading to the release of cytotoxic granules and consequently cell death, in a MHC-I-independent manner[142,143].

The second type of bispecific antibody aims at a dual blockade of tumor-associated signaling pathways. Tumors frequently find a way to evade the anti-tumorigenic effects of a therapy, upon switching the preferential survival mechanism. As such, simultaneous targeting of two different pathways with the same therapeutic entity is envisioned as a promising way to decrease the extent of drug resistance and increase overall efficacy. Antibodies targeting tumor MET and EGFR[144], Dll4 and VEGF[145], Ang-2 and VEGF[146], EGFR and VEGFR2[147], or HER2 and HER3[148] are examples of bispecific proteins, currently in phase I and phase II clinical trials[142]. Importantly, some of these structures target simultaneously different cellular components of the tumor, as cancer cells and

tumor vasculature. This kind of strategy has used both full-length antibodies and antibody fragments, from Fab to scFv and VHHs.

1.4 OBJECTIVES

Nucleolin targeting has been explored using different strategies, from ligand-mediated delivery of cytotoxic payloads, to disruption of cell proliferation signaling with pseudopeptides and antibodies. Overall results show promising effects on affecting cancer cell growth as well as the endothelial compartment of the tumor, while presenting low toxicity.

Antibodies are an increasingly explored therapeutic field. Their high specificity and affinity, combined with the different mechanisms by which they can act, have turned them an important tool in cancer therapy. Nowadays, their potential is being further explored by taking advantage of the capacity to generate different formats with a wide variety of properties, for instance, in terms of size, valency, multispecificity and cell death mechanisms.

The main objective of this work was to develop two types of nanobody-based platforms targeted to nucleolin, developed for the first time developed against this target, to the author's best knowledge. The first one consisted on the engraftment of nucleolin-binding sequences onto nanobodies, to take advantage of their potential as building units to generate other types of constructs. The second platform consisted on anti-nucleolin nanobody-Fc antibody, in order to explore potential immune mechanisms, namely ADCC, which had not been previously reported against this target. These proteins were characterized in terms of cellular association, cytotoxicity and ADCC capacity using cancer and endothelial cells. Additionally, the potential of using nanobodies as bispecific

molecules was also explored. In this respect, nanobodies targeting nucleolin and TNF-α were used as a model.

Chapter 2

Development and characterization of nucleolin-targeting nanobodies

2.1 INTRODUCTION

Nanobodies arise as a promising approach to develop targeted therapeutic strategies. They are the smallest binding unit of antibodies, while retaining high affinity and favoring tumor penetration. In contrast to scFv, they are not prone to aggregation and can be produced with high yields, presenting high physicochemical stability[149,150]. In addition, nanobodies can also originate a variety of constructs, enabling antitumor responses or targeted delivery of drug payloads[127,151]. Based on these features, nanobodies have been tested, either alone, against VEGFR2[140] or EGFR[128,129], or as targeting ligands, for example, of nanoparticles[132,133], Pseudomonas exotoxin A[152] or of a photosensitizer[153], to generate anticancer therapies with increased efficacy.

Nanobodies have been also explored in the context of bispecific targeting. In a conventional antibody, bispecificity is usually achieved by fusing two nanobodies against each target of interest[142]. Therefore, the current method for nanobody-based development of bispecific entities results in formats with twice the molecular weight. So far, no strategies to endow nanobodies with bispecificity without compromising their size have been reported. This issue was addressed in this work, by conferring different specificities to CDR1 and CDR3, towards different targets as nucleolin and tumor necrosis factor α (TNF-α).

Nucleolin is considered a promising target for cancer therapy, due to its overexpression at the cell surface in two different cellular subpopulations in solid tumors, as the cancer cells and endothelial cells of the vasculature[23,27]. In fact, overexpression in endothelial cells enables a facilitated access of any therapeutic molecule, and namely nanoparticles, to a solid tumor, following intravenous administration. Importantly, the target overexpression at the tumor level constitutes an important factor to decrease the extent of severe side effects[154]. Therefore, a variety of agents targeting nucleolin have been developed, including targeted nanoparticles, aptamers and pseudopeptides. *In vivo*

studies testing several of these nucleolin-targeting approaches supported increased therapeutic efficacy[87,155,156].

TNF-α is a cytokine expressed as a 26 kDa transmembrane protein (tmTNF-α), which localizes at the cell surface of monocytes, macrophages and activated T cells. Upon proteolytic cleavage, the 17-kDa soluble TNF-α, a cytokine involved in inflammatory processes, is originated[157,158]. However, in some breast cancer tissues and breast cancer cell lines it has been reported that expressed tmTNF- α is not processed into its mature form, but rather remains at the cell surface. This renders cancer cells resistant to soluble TNF-α and thus prone to survive[159,160]. Targeting this transmembrane TNF-α with an antibody specific to the extracellular portion of the cytokine led to decreased tumor volume and inhibited tumor growth rate by 70%, in an orthotopic MDA-MB-231 mouse model of triple-negative breast cancer. This was accompanied by a decrease of lymph node metastasis[161]. These results reinforce tmTNF-α as a potential target for anticancer therapy.

Based on the therapeutic potential of nanobodies, along with vascular tumor targeting, the aim of the work herein presented was to engineer nucleolin-binding nanobodies upon grafting of the nucleolin-binding F3 peptide-derived 10-amino acid sequence, onto CDR1 or CDR3 of an anti-human TNF-α VHH. Based on this strategy, the generation of bispecific nanobodies (anti-nucleolin and anti- anti-human TNF-α) was also assessed.

2.2 MATERIALS AND METHODS

2.2.1 Reagents

Human recombinant nucleolin was from Abnova (Taiwan) and human recombinant TNF-α was from Thermo Scientific (USA). F3 peptide

(KDEPQRRSARLSAKPAPPKPEPKPKKAPAKK) was custom synthesized by Genecust (Luxemburg). Infliximab was from Janssen Biologics BV (The Netherlands). All other chemicals were of analytical grade purity.

2.2.2 Cell lines

MDA-MB-435S (ATCC® HTB-129™, USA), MDA-MB-231 (ATCC® HTB-26™, USA) and 4T1 (ATCC® CRL-2539™, USA) cell lineswere cultured in RPMI-1640 (Lonza, Switzerland), supplemented with 10% (v/v) heat-inactivated FBS (HyClone, USA), 2 mM of L-glutamine (Lonza, Switzerland) and 1% (v/v) Pen/Strep/Fungiezone solution (HyClone, USA), and maintained at 37°C in a humidified atmosphere of 5% CO_2. HMEC-1 cells line was a generous gift by the Centers for Disease Control and Prevention (USA) and was maintained in the same conditions as the other cell lines, being the culture medium further supplemented with 10 µg/L mouse epidermal growth factor and 1 µg/L hydrocortisone (Sigma, USA).

2.2.3 Development of anti-nucleolin nanobodies

An anti-human TNF-α VHH (Ablynx, Belgium)[162], here referred to as parental VHH, was used as a scaffold for the development of nanobodies targeting nucleolin. Parental VHH is presented in Figure 2.1A (DNA and protein sequences are presented in Appendix, Figure 1), and incorporates: (i) a N-terminal peptide leader sequence, which targets the protein to the cell periplasm, minimizing the formation of inclusion bodies and thus allowing high yields of protein after purification; (ii) a histidine (His) tag for affinity

purification; and (iii) a hemmaglutinin (HA) tag for protein detection by western blot, enzyme-linked immunosorbent assay (ELISA) and flow cytometry.

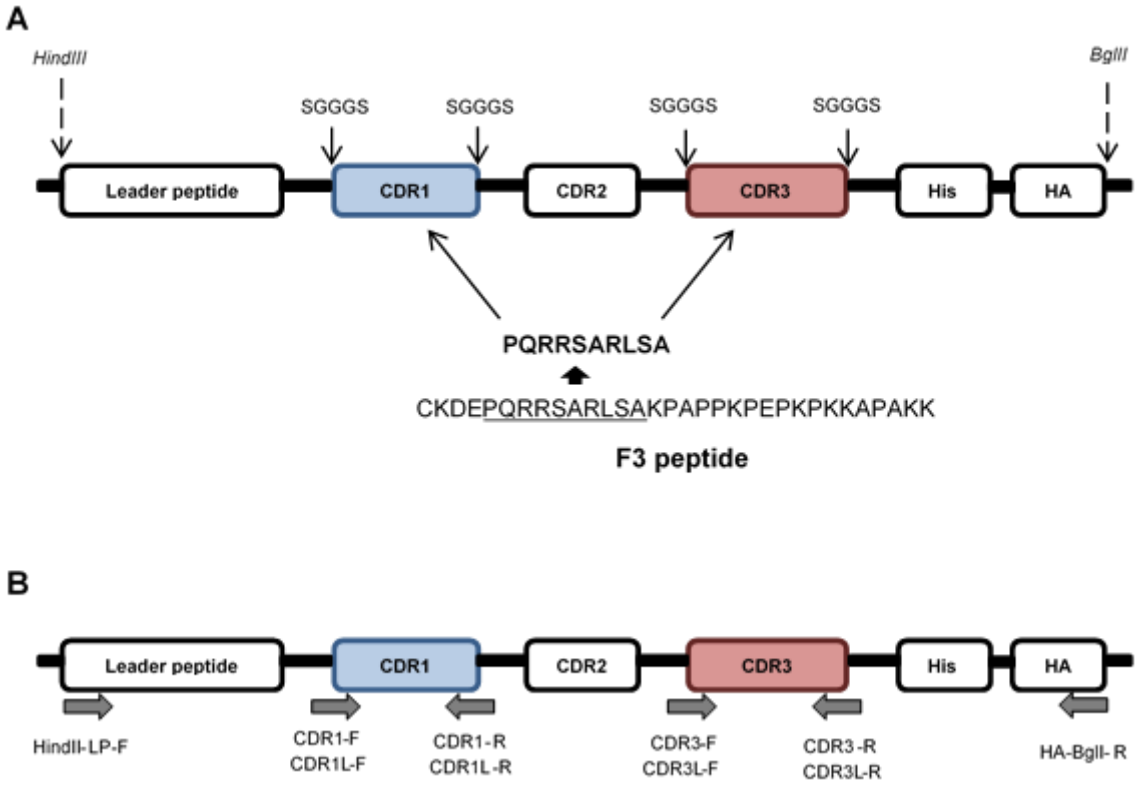

Figure 2.1 Schematic representation of the VHH cloning. (A) Sites of insertion of the F3 peptide-derived nucleolin-binding sequence, the linker SGGGS and restriction sites of the enzymes used for cloning. (B) Primers used in the PCR reactions.

To generate a nucleolin-binding nanobody, CDR1 or CDR3 domains were grafted with the nucleolin binding F3 peptide-derived 10-amino acid sequence (Figure 2.1A), giving rise to two different nanobodies (αNCL-CDR1 VHH and αNCL-CDR3 VHH; Appendix 1, Table 1). In addition, a variant of this sequence, flanked by the linker SGGGS at both ends, was also grafted onto each CDR, originating the nanobodies αNCL-CDR1-L VHH and αNCL-CDR3-L VHH. First, to amplify by PCR the 10-amino acid sequence with which end of the framework regions around CDR1 or CDR3, primer HindIII-LP-F was used in combination with primer CDR1-R, CDR1L-R, CDR3-R or

CDR3L-R and primer BglII-HA-R was used in combination with primer CDR1-F, CDR1L-F, CDR3-F or CDR3L-F, as indicated in Figure 2.1B (primer sequences are listed in Appendix 1, Table 3). PCR reactions were carried out with Phusion DNA Polymerase (Thermo Scientific, USA), under the conditions described in Appendix 1, Table 1. PCR products were visualized on a 1.5% (w/v) agarose gel with 10% (v/v) ethidium bromide (Electran, BDH, UK) to confirm proper amplification, using ChemicDoc XRS System with Quantity One software (Bio-Rad, USA), and recovered with the NzyGelPure kit (Nzytech, Portugal). Purified DNA was quantified with NanoDrop 1000 Spectrophotometer (ThermoScientific, USA). A second PCR was carried out to overlap the two sequences obtained. PCR conditions were the same as for the first PCR, however primers were only added after 10 cycles. Upon recovery, the DNA was digested with HindIII and BglII (Thermo Scientific, USA) and inserted onto a pT7 vector, a bacterial T7 promoter-based vector, used for protein expression in *E. coli*. T4 DNA Ligase (Thermo Scientific, USA) was used for the ligation reaction of 40 ng of digested pT7 and 12 ng of digested VHH DNA, at 22°C for 2 h, followed by enzyme inactivation at 70°C for 5 min. Two microliters of the resulting mixture were added, on ice, to 40 µl of JM109 *E. coli* electrocompetent cells, followed by electroporation on a Gene Pulser II Electroporation System (Bio-Rad, USA), at 200 Ω, 25 µFD, 1.8 kV. Super optimal broth with catabolic repressor (SOC) medium (2% w/v tryptone, 0.5% w/v yeast extract, 0.05 w/v NaCl, 2.5 mM KCl, 10 mM $MgCl_2$, 20 mM glucose, pH 7.0) was immediately added to the cells and the mixture was transferred to a tube and incubated for 1 h at 37°C, under mechanical stirring at 220 rpm. Bacteria were then plated on solid high salt lysogeny broth (LB) medium (1% w/v tryptone, 0.5% w/v yeast extract, 1% w/v NaCl, 1.5% w/v agar) with ampicillin (100 mg/L), the resistance marker of the pT7 vector. After overnight incubation at 37°C, colony screening was performed.

2.2.4 Colony screening

For screening of positive clones, colonies were harvested and transferred to 20 µl of sterile water and 5 µl of this suspension was used in a PCR reaction with Green Master Mix (Nzytech, Portugal), as indicated in Appendix 1, Table 2. The remaining suspension was stored at 4°C until further use. One colony without the digested VHH DNA sequence was used as control. PCR reactions were then visualized on a 2% (w/v) agarose gel, as described in section 2.2.2. Colonies for which there was a strong band were selected for a small-scale test of protein expression. Bacteria were grown overnight in LB medium (1% w/v tryptone, 0.5% w/v yeast extract, 1% w/v NaCl, 1.5% w/v agar) with ampicillin (100 mg/L) and plasmid DNA was recovered by miniprep, with the Zyppy Plasmid Miniprep Kit (Zymo Research, USA). Bl21 (DE3) *E. coli* electrocompetent cells were transformed with 100 ng of recovered DNA, following the same protocol as previously described for transformation of JM109 *E. Coli* bacteria (section 2.2.3).

2.2.5 Preparation of electrocompetent cells

Bacteria from a -80°C stock were inoculated in super optimal broth (SOB) medium (2% w/v tryptone, 0.5% w/v yeast extract, 0.05 w/v mM NaCl, 2.5 mM KCl, 10 mM $MgCl_2$, pH 7.0) and grown overnight at 37°C, with mechanical stirring at 220 rpm. Afterwards, a 1/100 dilution was prepared with SOB medium and the culture was grown until an optical density (OD) value of 0.5, at 600 nm. The culture was then chilled on ice and centrifuged (4,000 x g, 4°C, 45 min). Supernatant was discarded and the pellet was ressuspended in an ice-cold solution of 10% (v/v) glycerol. Centrifugation and ressuspension steps were repeated and after a final centrifugation, supernatant was discarded and bacteria ressuspended in the residual volume. Forty-microliters aliquots were quickly frozen in

liquid nitrogen and then stored at -80°C. Transformation efficiency of the cells was evaluated by transforming with pUC18 and counting the colony forming units.

2.2.6 Small-scale test of protein expression

Positive clones identified in the screening by PCR were grown overnight in LB medium with ampicillin, after which 50 µl inoculated in 5 mL of super broth (SB) medium (3% w/v tryptone, 2% w/v yeast extract, 1% w/v 3-(N-Morpholino)propanesulfonic acid, MOPS, 10 mM $MgCl_2$, pH 7.0) with ampicillin and then grown at 37°C, with mechanical stirring at 220 rpm, until reaching an optical density between 0.7 and 0.9, at 600 nm. Expression was induced with 1 mM of isopropyl β-D-1-thiogalactopyranoside (IPTG, Thermo Scientific, USA) at 30°C, with mechanical stirring at 220 rpm, for 5 h. Bacteria were then harvested by centrifugation (10,000 x g, 4°C, 10 min), ressuspended in 400 µl of phosphate buffer saline (PBS, 137 mM NaCl, 2.7 mM KCl, 10 mM Na2HPO4, 1.8 mM KH2PO4, pH 7.4) with EDTA-free protease inhibitor cocktail (Roche, Switzerland) and further lysed in a ultrasonic bath, for 30 min. Following centrifugation, the soluble fraction from each clone was used to evaluate protein expression by ELISA and protein integrity by Western Blot.

2.2.7 Detection of protein expression by ELISA

Soluble fraction (100 µl) of the expressed proteins was plated on a Costar 96-well plate (Thermo Scientific, USA) and incubated at 37°C for 1 h, after which unbound protein was removed upon washing with PBS. Nonspecific binding sites were blocked

with 3% (w/v) bovine serum albumin (BSA, Sigma, USA) in PBS, for 1 h at 37°C. After five washing steps with PBS, 100 µl of anti-HA-peroxidase antibody (clone 3F10 from Roche, Switzerland, diluted at 1:1000 in 1% BSA in PBS) were added and incubated for 1 h at 37°C. Following five additional washing steps, 100 µl of 0.06% (v/v) of H_2O_2 in 0.4 mM 2,2'-azino-bis(3-ethylbenzothiazoline-6-sulphonic acid) (ABTS, Merck Millipore, USA) solution were added to the wells. Absorbance (405 nm/495 nm) was measured after 5-15 min on Tecan Infinite 200 microplate reader (Tecan Trading AG, Switzerland).

2.2.8 Western Blot

For western blot analysis, protein samples were diluted in Laemmli buffer (62.5 mM Tris, pH 6.8, 2% (w/v) SDS, 4% (v/v) glycerol, 0.001% (w/v) bromophenol blue, 6 % (v/v) β-mercaptoethanol) and denaturated at 95°C, for 10 min. Diluted protein samples and PageRuler prestained protein ladder (Thermo Scientific, USA) were then loaded in a 1.5 mm 15% (w/v) polyacrylamide gel and separated by sodium dodecyl sulfate polyacrylamide gel electrophoresis (SDS-PAGE), using a Tris-glycine buffer (25 mM Tris, 192 mM glycine, 0.1% w/v SDS, pH 8.3). Once separated, the proteins were transferred onto a nitrocellulose membrane (GE Healthcare, UK) using Tris-glycine buffer with 20% (v/v) methanol. Non-specific binding sites in the membrane were then blocked with a blocking buffer consisting of 5% (w/v) non-fat milk in Tris-buffered saline (TBS, 50 mM Tris, 150 mM NaCl, pH 7.5) with 0.1% (v/v) tween 20 for 1 h, at room temperature, in a shaker. After blocking, incubation with rat anti-HA-peroxidase antibody (clone 3F10, Roche, Switzerland, diluted 1:4000 in blocking buffer) was performed, in the same conditions used in the blocking step. The membrane was washed five times for 10 min with TBS with 0.1% (v/v) tween 20 and incubated with Immobilon Western Enhanced

Chemiluminescent HRP substrate (Merck Millipore, USA) for 5 min. Chemiluminescent signals were detected on a film.

2.2.9 Sequencing

Clones presenting the highest values of expression, as evaluated by ELISA, and which were detected by Western Blot, were further sequenced at Macrogen, Inc (The Netherlands). Clones with the correct sequence (Appendix 1) were selected for larger scale expression and subsequent assays.

2.2.10 Expression and purification of nanobodies

An overnight-grown culture containing the VHH of interest was diluted to 1:100 in SB medium with ampicillin (100 mg/L), which was then grown at 37°C, 220 rpm, until reaching an OD between 0.7 and 0.9, at 600 nm. Protein expression was induced with 1 mM of IPTG, for 16 h, 140 rpm. The culture was then centrifuged, ressuspended in binding buffer (50 mM phosphate buffer, 300 mM NaCl, 40 mM imidazole, pH 7.0) with complete, EDTA-free protease inhibitor cocktail and sonicated (20 min per liter of culture, pulsed), keeping the tubes on ice. After sonication and centrifugation (10,000 x g, 45 min, 4°C), protein was purified from the soluble fraction by affinity chromatography using HiTrap Chelating HP columns, eluted in 300 mM imidazole at a flow rate of 1 ml/min using a peristaltic pump P-1 (GE Healthcare, UK). At each step of the purification, a fraction of the eluted solution was recovered for SDS-PAGE analysis, in order to assess protein purity. Parental VHH, which was also used in the subsequent assays, was

purified with a buffer of 50 mM HEPES, 1 M NaCl, 5 mM CaCl2, pH 7.5, as described by Morais et al.[163]

After confirmation of protein purity in Coomassie-stained SDS-PAGE gel (15% (w/v) polyacrylamide), protein was desalted by gel chromatography (using PD-10 desalting columns, GE Healthcare, UK) and concentrated by centrifugal filtration (Amicon Ultra-4 Centrifugal Filter Unit with Ultracel-10 membrane, Merck Millipore, USA).

Protein purity and integrity was confirmed by SDS-PAGE followed by Coomassie staining. Proteins were quantified using by Bradford assay and using NanoDrop 1000 spectrophotometer (ThermoScientific, USA).

2.2.11 SDS-PAGE electrophoresis and Coomassie staining

SDS-PAGE electrophoresis was performed as described in section 2.2.7, but using 1 mm 15% (w/v) polyacrilamide gels. After protein separation, the gel was incubated with a staining solution of 0.1% w/v Coomassie blue brilliant G (Sigma, USA), 25% v/v methanol, 5% v/v acetic acid. The staining solution was then removed, a washing step with distilled water was performed and the gel destained with a solution of 20% (v/v) methanol and 20% (v/v) acetic acid, at room temperature, in a shaker with gentle rotation. The destaining procedure was repeated until background staining was removed.

2.2.12 Nanobody binding to human nucleolin and human TNF-α

Ninety-six-well (Corning Costar, USA) were coated with 100 ng of human nucleolin or 200 ng of human TNF-α in carbonate buffer (50 mM sodium carbonate buffer, pH 9.6),

at 4°C, overnight. Nonspecific binding sites were then blocked with 3% (w/v) BSA in PBS for 1 h, 37°C, washed once with PBS and incubated with 120 pmol of each nanobody (diluted in 1% (w/v) BSA in PBS) for 1 h, at 37°C. After five washing steps, 100 µl of anti-HA-peroxidase antibody (clone 3F10, Roche, diluted 1:1000 in 1% w/v BSA in PBS) was added and incubated for 1 h at 37°C. Following five additional washing steps, 100 µl of 0.06% (v/v) of H_2O_2 in 0.4 mM ABTS (Merck Millipore, USA) solution were added to the wells. Absorbance (405 nm/495 nm) was measured after 5-15 min on Model 680 microplate reader (Bio-Rad, USA).

2.2.13 Nanobody binding to cancer and endothelial cells

One hundred thousand cancer or endothelial cells, previously treated with dissociation buffer (Merck Millipore, USA), were incubated with 10, 100 or 1000 nM of VHH proteins, for 45 min at 4°C. Upon washing, a second incubation with anti-HA-FITC antibody (Y-11 sc-805, Santa Cruz Biotechnology, USA), at room temperature for 30 min was performed. Cells were again washed and then fixed and analyzed by flow cytometry.

To confirm the involvement of surface nucleolin and TNF-α in binding of the nanobodies, competitive inhibition assays were performed. Cells were pre-incubated with 75 µM of F3 peptide or 1 µM of infliximab, at 4°C for 30 min, followed by incubation with 1000 nM VHH fragments, at 4°C for 45 min.

Sample acquisition and analysis were performed using Guava easyCyte 5HT and the InCyte software module (Merck Millipore, USA).

2.2.14 Nanobody cytotoxicity against cancer and endothelial cells

Different cell densities of cancer or endothelial cell lines were seeded in 96-well plates (5000 MDA-MB-435S or MDA-MB-231 cells, 3000 4T1 cells or 7500 HMEC-1 cells, per well). After 24 h, cell culture medium was exchanged for fresh one, and cells were incubated with serial dilutions of VHH proteins (from 0.5 to 8 µM, each condition performed in duplicate) for a total of 72 h. Cell viability was then determined with 3-(4,5-Dimethylthiazol-2-yl)-2,5-Diphenyltetrazolium Bromide (MTT) assay[164]. Following removal of cell culture medium, cells were washed with PBS and further incubated with 0.5 mg/ml MTT solution in cell culture medium without serum for up to 4 h at 37°C, in a humidified atmosphere of 5% CO_2. Following removal of the MTT solution, the resulting crystals were solubilized with 100 µl of DMSO. Absorbance at 595 nm was then measured in a microplate reader (Model 680, Bio-Rad, USA). Percentage of cell viability was calculated as following:

$$\%\ \text{cell viability} = \frac{\text{ODuntreated cells} - \text{ODtreated cells}}{\text{ODuntreated cells}} \text{x}100$$

2.2.15 Statistical analysis

Analysis of variance (one-way ANOVA) was performed to analyze differences among the proteins in terms of binding and cytotoxicity. Post hoc analysis was carried out using Tukey test. In the competition binding assay, differences between binding without pre-incubation and with pre-incubation (with F3 peptide or infliximab) were analyzed by Student's t-test. Analyses were performed with a level of significance of 5%.

2.3 RESULTS

2.3.1 Anti-nucleolin nanobody expression and purification

Four anti-nucleolin nanobodies were developed upon grafting a F3 peptide-derived 10-amino acid sequence, onto either CDR1 or CDR3 of a parental anti-human TNF-α VHH, with or without flanking linkers (SGGGS) at each end of the grafted CDR. The incorporation of these flanking linkers aimed at conferring higher conformational flexibility to the CDR loop, thus improving antigen binding and recognition[165,166]. For each of the generated constructs, some clones were selected to evaluate protein expression (by ELISA) and integrity (by Western Blot), as exemplified in Figure 2.2 for three clones grafted onto CDR1 (αNCL-CDR1-L) or two clones grafted onto CDR3 (αNCL-CDR3), with or without linkers, respectively. Clones 1 and 3 of αNCL-CDR1-L and clone 2 of αNCL-CDR3 presented an OD at 495 nm ($OD_{405/495}$) higher than 1 (Figure 2.2A) and an expected molecular weight of approximately 18 kDa (Figure 2.2B). The same evaluation was performed for the other two constructs (αNCL-CDR1 and αNCL-CDR3-L). Only the clones presenting high levels of expression and the correct DNA sequence were further expressed.

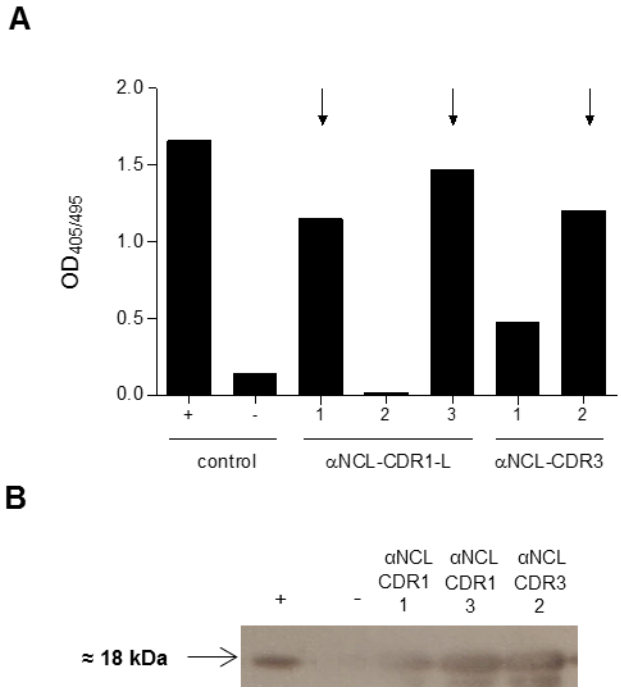

Figure 2.2 Selection of clones for nanobody expression. Expression of nanobodies was evaluated for several clones of each construct by (A) ELISA and (B) Western Blot, using the soluble fractions obtained after a small-scale protein expression test, as exemplified in the figure for three clones grafted onto CDR1 (αNCL-CDR1-L) or two clones grafted onto CDR3 (αNCL-CDR3), with or without linkers, respectively. A clone already known to express a VHH, either with (+) or without (-) induction of expression with IPTG, was used as a positive or negative control, respectively. Arrows in (A), indicate the clones selected for Western Blot analyses.

Expression conditions were optimized for the new generated nanobodies upon assessment by SDS-PAGE, followed by Coomassie staining, as exemplified in Figure 2.3 for αNCL-CDR1-L VHH and αNCL-CDR3-L VHH, expressed at 16°C and 20°C. For both nanobodies, expression at 16°C resulted in the highest expression of protein in the soluble form (Figure 2.3A), along with low levels of insoluble protein (Figure 2.3B). Thus, this temperature was therefore used for further protein expression.

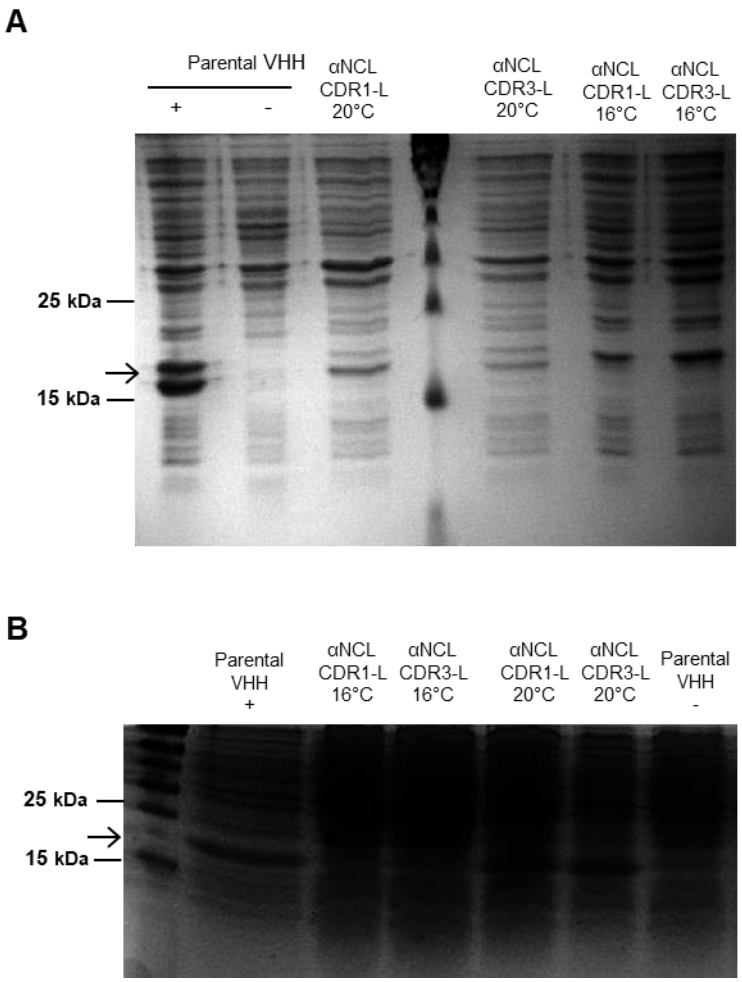

Figure 2.3 Optimization of temperature conditions for nanobody expression. Representative images of the Coomassie-stained SDS-PAGE gels of samples from (A) soluble and (B) insoluble fractions after expression of αNCL-CDR1-L VHH and αNCL-CDR3-L VHH nanobodies, at 16 °C and 20 °C, are presented. As a control, expression of the parental VHH was also performed at 20°C, either with (+) or without (-) induction with IPTG. Arrows indicate the bands corresponding to the nanobodies.

Purification conditions of the nanobodies were also optimized, namely regarding the imidazole concentration in the washing buffer. In this respect, two sequential washing steps were performed, first with 100 mM and then with 120 mM imidazole, with the aim to efficiently remove contaminating proteins, as exemplified in Figure 2.4A (bands corresponding to the nanobodies indicated by the arrows). The washing step with 100 mM imidazole enabled only partial removal of the contaminants (Figure 2.4A, lanes 3),

as these were also present in the second washing fraction (Figure 2.4A, lanes 4). However, elution of the nanobodies after this second washing step, enabled a fraction with high purity (Figure 2.4A, lanes 5). Although the washing steps with 100 or 120 mM imidazole led to some loss of the nanobodies (Figure 2.4A, lanes 3 and 4), the highest concentration of imidazole was selected for purification, as it enabled the production of highly pure nanobodies (Figure 2.4B).

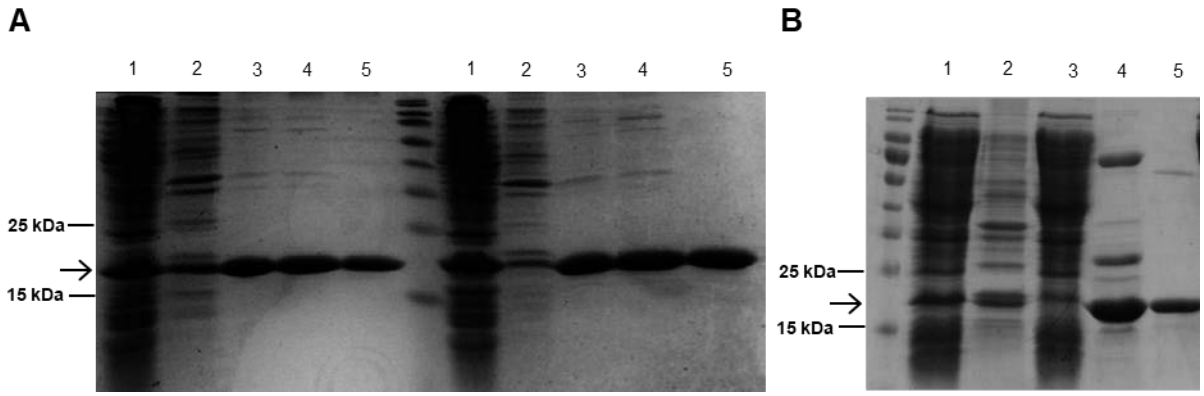

Figure 2.4. Optimization of imidazole concentration for nanobody purification. Representative images of Coomassie-stained SGS-PAGE gels, of fractions collected during protein purification. (A) Fractions resulting from the purification of two proteins for optimization of the conditions (αNCL-CDR1 VHH and αNCL-CDR3 VHH): soluble fraction (1), insoluble fraction (2), washing step with 100 mM imidazole (3) or 120 mM imidazole (4) and eluted fraction (5). (B) Representative gel of the fractions obtained from nanobody purification with the optimized protocol: soluble fraction (1), insoluble fraction (2), eluent from soluble fraction (3), washing step (4) and eluted protein (5). Arrows indicate the bands corresponding to the nanobodies.

Temperature of expression and purification yields for each nanobody are summarized in Table 2.1. αNCL-CDR1 VHH and αNCL-CDR1-L VHH were produced in lower amounts when compared to αNCL-CDR3 VHH and αNCL-CDR3-L VHH, with approximately 50% yield. Both the expression conditions and purification yields were different from the ones of the parental VHH, which was obtained with 8- or 4-fold increased yield when compared with CDR1- and CDR3-grafted VHHs, respectively.

Table 2.1. Temperature of expression and purification yields of the generated nanobodies.

VHH	MW (kDa)	T (°C)	Yield (mg/L culture)
αNCL-CDR1	18.3	16	5
αNCL-CDR1-L	19.0	16	5
αNCL-CDR3	18.2	16	10
αNCL-CDR3-L	19.0	16	10
Parental VHH	18.8	20	40

2.3.2 Anti-nucleolin nanobody binding to human nucleolin and human TNF-α

All the new generated anti-nucleolin VHH fragments bound to nucleolin, regardless of the CDR grafted, with the αNCL-CDR3 VHH and αNCL-CDR3-L VHH presenting the highest extent. The nucleolin-binding VHHs grafted onto CDR1 or CDR3 presented a 2- or 3-fold increased binding to nucleolin, respectively, relative to the parental VHH, without the F3 peptide-derived sequence. This supported the involvement of the F3 peptide-derived sequence on the observed binding of the anti-nucleolin VHH constructs (Figure 2.5A).

The anti-nucleolin VHHs presented an extent of binding to human TNF-α, which was approximately 40% lower than the one observed for the parental VHH (Figure 2.5B). The binding of the parental VHH to human TNF-α was justified by a grafting strategy to generate the anti-nucleolin nanobodies that relied on a parental VHH that had been developed against human TNF-α. This result suggested that bispecific properties can be achieved in the same VHH with two specific CDRs.

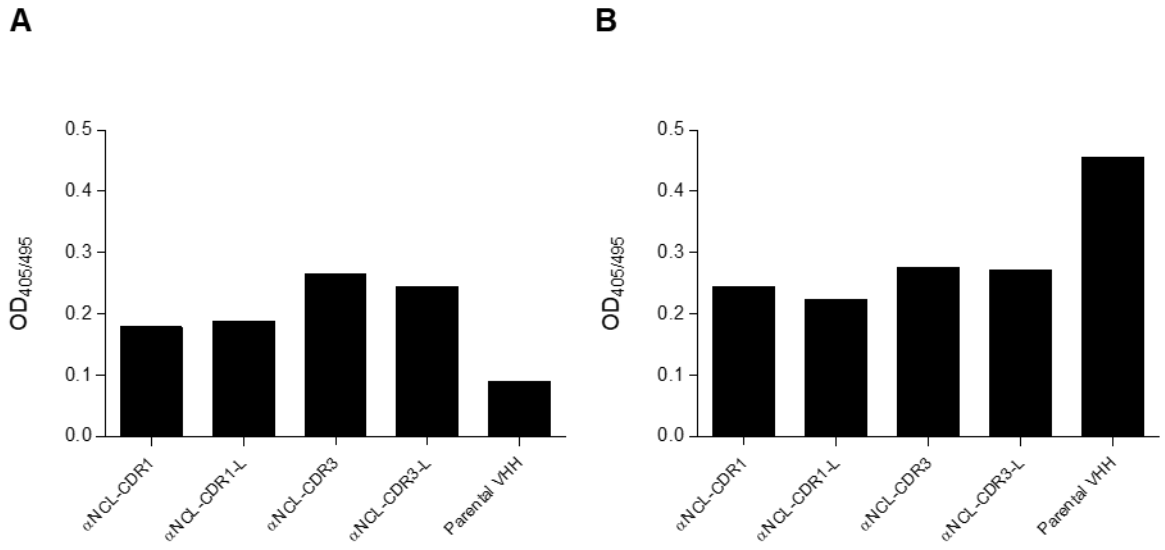

Figure 2.5. Binding of different nanobody constructs to human nucleolin and human TNF-α. Binding of nanobodies grafted with a nucleolin-binding peptide sequence, either onto CDR1 or CDR3, with or without flanking linkers, at the end of the grafted CDR, and the corresponding parental VHH to (A) human nucleolin and (B) human TNF-α, following 1 h incubation at 37°C. Results are from a representative experiment.

2.3.3 Anti-nucleolin nanobody binding to cancer and endothelial cells

The binding capacity of anti-nucleolin nanobodies was further assessed with cancer cells (MDA-MB-435S, MDA-MB-231 and 4T1)[46,167] and a model of angiogenic endothelial cells (HMEC-1)[168]. In terms of TNF-α expression at the cell surface, MDA-MB-231 cells have been reported to present high levels of the membrane protein[161].

As nucleolin mediates internalization of several ligands in an energy-dependent mechanism[27], incubation of the cells with the nanobodies was performed at 4°C, a non-internalizing condition, thus enabling the HA tag detection by the anti-HA-FITC antibody through flow cytometry.

For all cell lines, a concentration-dependent binding of all constructs was observed (Figures 2.6A-2.6D). In the case of MDA-MB-435S cells, a significant difference on the binding, at 100 nM, of αNCL-CDR3 ($p<0.01$) or αNCL-CDR3-L ($p<0.001$) relative to αNCL-CDR1 and αNCL-CDR1-L or to the parental VHH ($p<0.001$), was observed. This trend, favoring a higher binding extent of the construct grafted onto CDR3, relative to CDR1, was further confirmed at 1000 nM of incubated protein ($p<0.001$). At this protein concentration, a significant difference between the binding of α-NCL-CDR1 VHH or α-NCL-CDR1-L VHH and the parental VHH ($p<0.001$) was also observed. At the highest concentration tested, CDR1- and CDR3-grafted VHHs bound a percentage of cells of approximately 40% and 80%, respectively, whereas the parental VHH bound to less than 10% of the cells (Figure 2.6A).

The profile of binding of anti-nucleolin VHH constructs to 4T1 mouse cancer cell line, relative to the parental VHH ($p<0.01$ for CDR3-grafted VHHs, at 100 nM and $p<0.001$ for all anti-nucleolin VHHs, at 1000 nM), was similar to the one reported for MDA-MB-435S (Figure 2.6B). The difference in terms of binding arising from peptide grafting either onto CDR1 or CDR3, was not so evident as for MDA-MB-435S and a decrease on the overall extent of binding of anti-nucleolin VHH was observed, of up to 4-fold, depending on the protein concentration.

In the MDA-MB-231 cell line, a similar concentration-dependent binding was observed for both anti-nucleolin VHHs and parental VHH, with 20-30% of the cells being targeted by the incubated nanobodies, at the highest concentration tested. The extent of binding was higher for αNCL-CDR3 VHH and αNCL-CDR3-L VHH relative to αNCL-CDR1 VHH and αNCL-CDR1-L VHH, but a statistical difference was not observed (Figure 2.6C).

The binding profile with the angiogenic HMEC-1 endothelial cells was similar to the one generated with the MDA-MB-231 cells. For the highest nanobody concentration tested, the extent of binding of parental VHH was lower than the one of anti-nucleolin

nanobodies (Figure 2.6D). For all tested cell lines, the presence of SGGGS sequences flanking the F3 peptide-derived sequence did not alter the anti-nucleolin VHHs binding.

Competition assays were further performed, by pre-incubating the cells with either F3 peptide or infliximab, to confirm that the binding previously observed was either nucleolin- or TNF-α-mediated, respectively. Pre-incubation of each one of the previous cell lines tested with the F3 peptide, reduced the extent of binding of the anti-nucleolin VHHs of at least 50% in MDA-MB-435S, MDA-MB-231 and 4T1 cells (Figures 2.6E-2.6G). The extent of binding reduction of αNCL-CDR3 VHH and αNCL-CDR3-L VHH with MDA-MD-435S cells, was higher than the one observed with pre-incubation with infliximab (Figure 2.6E). With the MDA-MB-231 cells, competitive inhibition with infliximab resulted in a reduction of binding for all anti-nucleolin VHHs, in similar levels to the ones observed when competitive inhibition was performed with the F3 peptide (Figure 2.6G). In contrast, binding of anti-nucleolin VHHs to 4T1 cells was not altered in the presence of infliximab (Figure 2.6F). In HMEC-1 cells no significant differences were observed, although there was a general decrease in binding for all the constructs upon pre-incubation with either F3 peptide or infliximab (Figure 2.6H).

Overall, these results suggested that binding of the novel anti-nucleolin VHHs was nucleolin-mediated, for all the cell lines tested. While in the 4T1 cells, binding was exclusively mediated by nucleolin, in the other cells lines (especially in MDA-MB-231) the involvement of TNF-α was also suggested, pointing out their capacity to act as bispecific constructs against tmTNF-α-expressing cells.

2.3.4 Cytotoxicity of anti-nucleolin nanobodies against cancer and endothelial cells

The cytotoxicity of the developed nucleolin-binding nanobodies was further assessed against the previously used cancer and angiogenic endothelial cells.

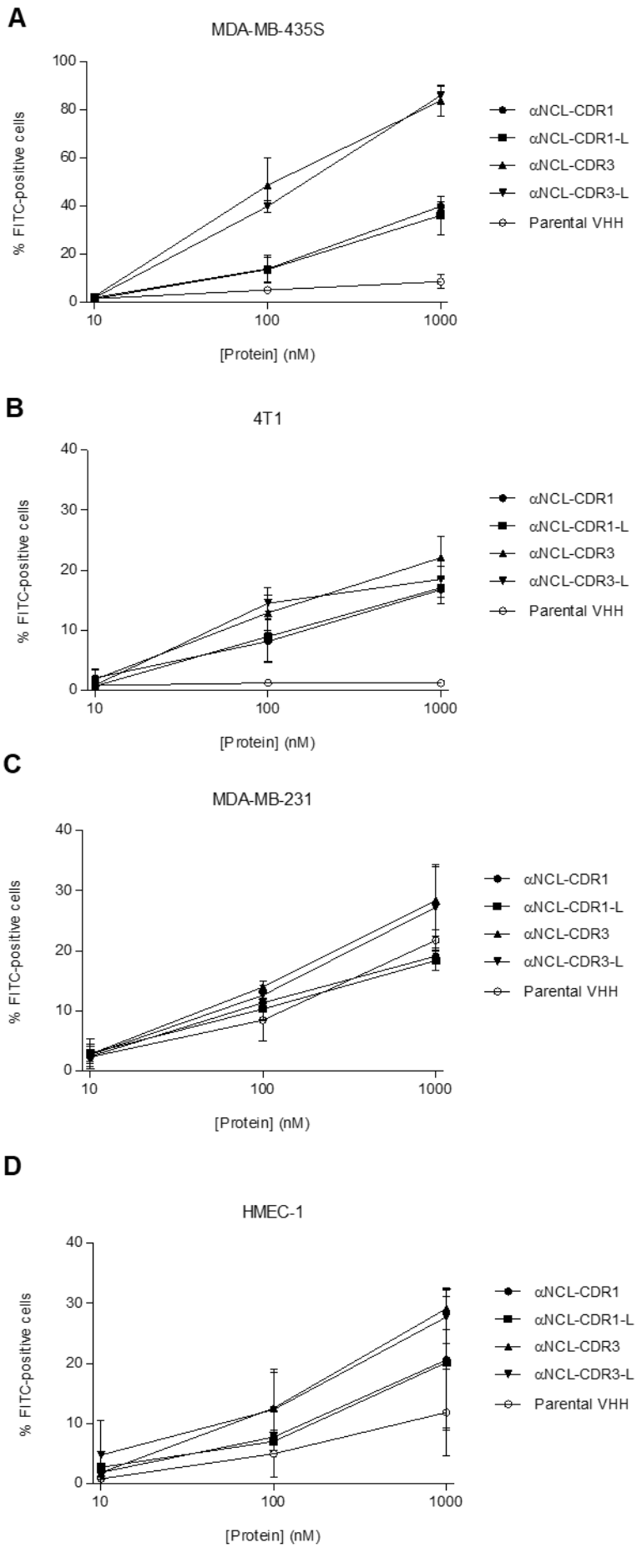
A
MDA-MB-435S
% FITC-positive cells
[Protein] (nM)
αNCL-CDR1
αNCL-CDR1-L
αNCL-CDR3
αNCL-CDR3-L
Parental VHH
B
4T1
C
MDA-MB-231
D
HMEC-1

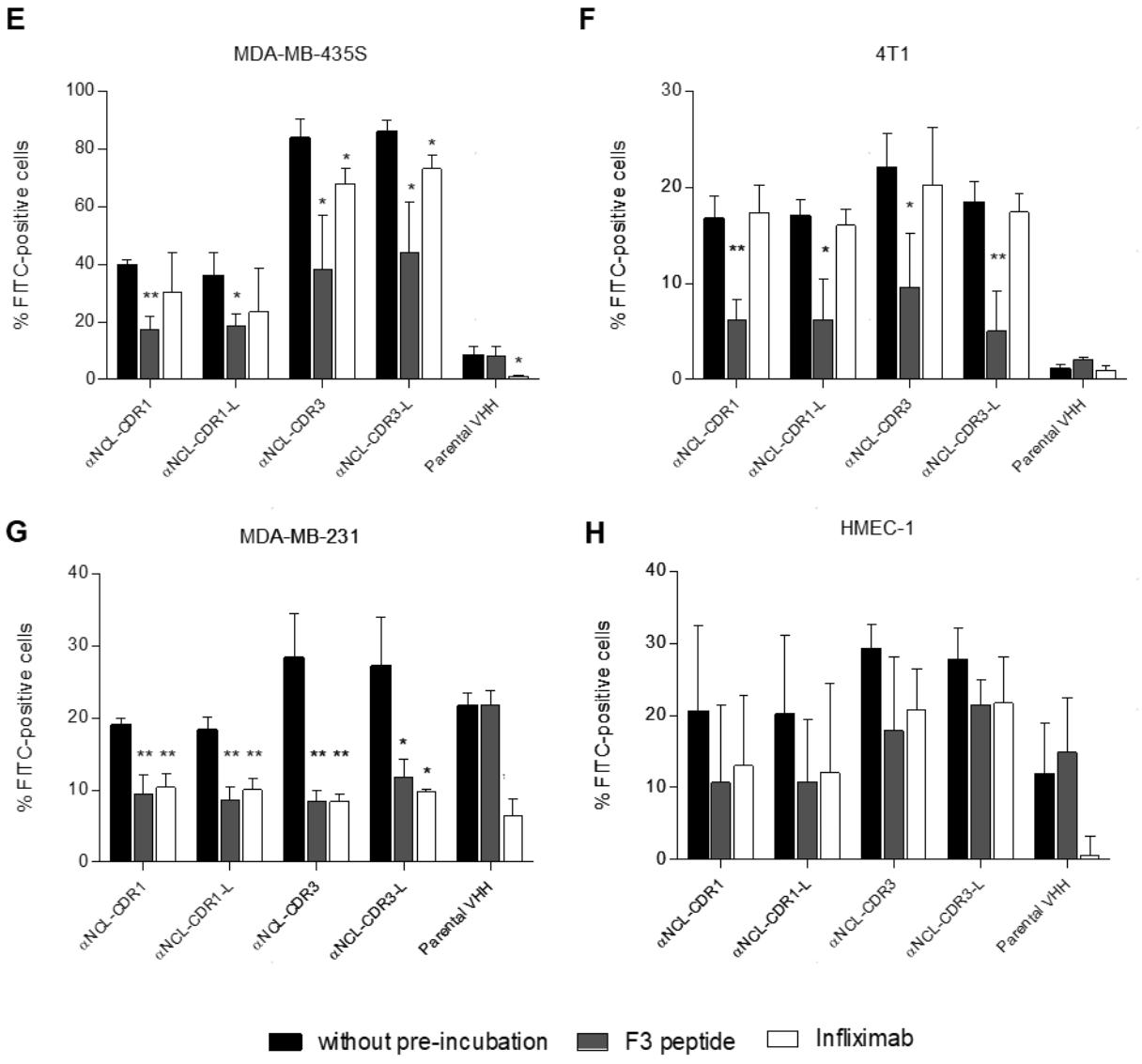

Figure 2.6. Binding of different nanobody constructs to cancer and endothelial cells. One hundred thousand of (A) MDA-MB-435S, (B) 4T1, (C) MDA-MB-231 or (D) HMEC-1 cell lines were incubated with nanobodies grafted with a nucleolin-binding peptide sequence either onto CDR1 or CDR3, with or without flanking linkers at the end of the grafted CDR, for 45 min at 4°C.The corresponding parental VHH was also included. Binding was assessed with a final incubation with anti-HA-FITC antibody and further assessment by flow cytometry. Competitive inhibition assays were also performed for each cell line (E-H), upon pre-incubation of the cells with 75 µM F3 peptide (grey bars) or 1 µM infliximab (white bars), for 30 min at 4°C. A control without competitive inhibition was included. Data represent the mean ± SD of three independent experiments, performed in duplicate. Differences in binding among the nanobodies tested were evaluated by one-way ANOVA followed by Tukey's test. Differences in binding, with or without pre-incubation with F3 peptide/infliximab, were evaluated by Student's t-test (* $p<0.05$, ** $p<0.01$, *** $p<0.001$).

All anti-nucleolin VHH fragments presented cytotoxic effects in the micromolar range against all the cancer cells tested, in a concentration-dependent manner (Figure 2.7).

In the case of MDA-MB-435S cells, differences relative to the parental VHH became evident at 4 μM, with cell viability reduced to 60% ($p<0.001$ for αNCL-CDR1; $p<0.01$ for αNCL-CDR1-L) or 30% ($p<0.001$) by the proteins grafted onto CDR1 or CDR3, respectively (corresponding to 1.5- or 2.5-fold decrease of cell viability, respectively). CDR3-grafted proteins presented a 2-fold decreased of cell viability compared to CDR1-grated proteins ($p<0.001$). At 8 μM, differences of activity among anti-nucleolin VHH fragments were dissipated, resulting in less than 20% of viable cells and reaching a 1.5-fold decrease of cell viability relative to the parental VHH ($p<0.001$), (Figure 2.7A).

The extent of decrease of cell viability achieved with αNCL-CDR3 VHH and αNCL-CDR3-L VHH against 4T1 cancer cells, was similar to the one observed against the MDA-MB-435S cells, throughout the concentrations tested (at 4 μM, $p<0.05$ and $p<0.01$ for αNCL-CDR3 and αNCL-CDR3-L, respectively, and at 8 μM, $p<0.001$ for all anti-nucleolin VHHs, relative to the parental VHH). Results suggested, once again, that grafting onto CDR3 improved the cytotoxicity efficacy (decrease of cell viability) of anti-nucleolin VHHs. However, parental VHH did not affect the cell viability of 4T1 cells (Figure 2.7B), in contrast with the decrease of cell viability down to 45% observed with MDA-MB-435S cancer cells.

Improved cytotoxicity against MDA-MB-231 cancer cells was only evident for αNCL-CDR3 VHH and αNCL-CDR3-L VHH, as compared with αNCL-CDR1 VHH and αNCL-CDR1-L VHH or the parental VHH, throughout the range between 4 ($p<0.05$, compared to CDR1-grafted VHHs) and 8 μM ($p<0.01$ or $p<0.001$, respectively, compared to αNCL-CDR1 VHH; $p<0.001$ compared to αNCL-CDR1-L VHH; $p<0.01$ or $p<0.001$, respectively, compared to parental VHH). CDR1- and CDR3-grafted anti-nucleolin VHHs presented a decrease of cell viability that was 60% and 40% (at 4 μM) or 55% and

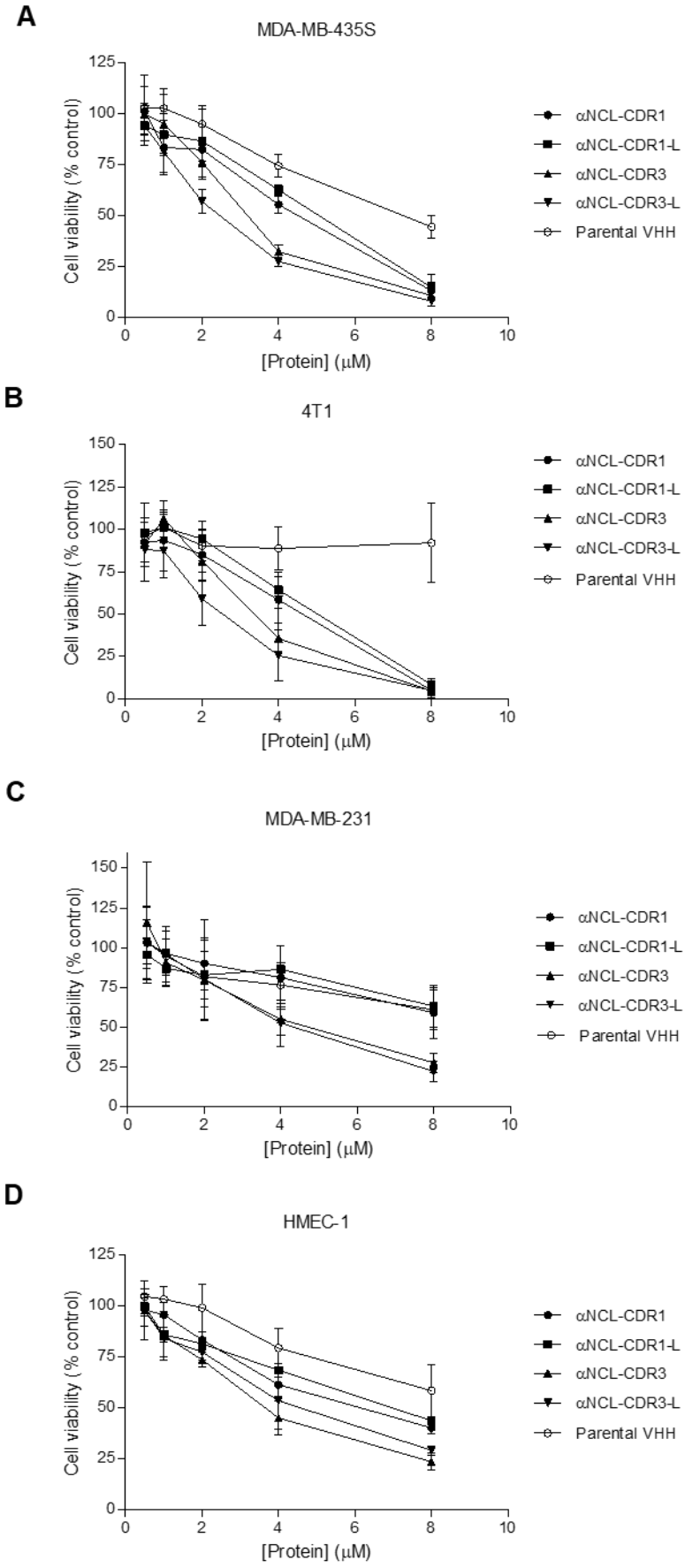
A
MDA-MB-435S
Cell viability (% control)
[Protein] (μM)
αNCL-CDR1
αNCL-CDR1-L
αNCL-CDR3
αNCL-CDR3-L
Parental VHH
B
4T1
Cell viability (% control)
[Protein] (μM)
αNCL-CDR1
αNCL-CDR1-L
αNCL-CDR3
αNCL-CDR3-L
Parental VHH
C
MDA-MB-231
Cell viability (% control)
[Protein] (μM)
αNCL-CDR1
αNCL-CDR1-L
αNCL-CDR3
αNCL-CDR3-L
Parental VHH
D
HMEC-1
Cell viability (% control)
[Protein] (μM)
αNCL-CDR1
αNCL-CDR1-L
αNCL-CDR3
αNCL-CDR3-L
Parental VHH

Figure 2.7. Cytotoxicity of different nanobodies against cancer or endothelial cells. Different nanobodies constructs, grafted with a nucleolin-binding peptide sequence either onto CDR1 or CDR3, with or without flanking linkers at the end of the grafted CDR, were incubated with cells, either neoplastic, as (A) MDA-MB-435S, (B) 4T1 and (C) MDA-MB-231 or the (D) angiogenic endothelial HMEC-1 cells, at concentrations up to 8 μM, for 72 h. The parental VHH, without the targeting component to nucleolin, was included as a control. In the end of the incubation, cytotoxicity was assessed by the MTT assay. Data represent the mean ± SD of at least three independent experiments, performed in duplicate. Differences in cytotoxicity among the tested nanobodies were evaluated by one-way ANOVA followed by Tukey's test (* $p<0.05$, ** $p<0.01$, *** $p<0.001$).

20% (at 8 μM) lower, respectively, than the one observed against MDA-MB-435S cancer cells. Parental VHH also reduced cell viability, down to 60% (Figure 2.7C).

In HMEC-1 cells, αNCL-CDR3 VHH and αNCL-CDR3-L VHH resulted in cell viability values of approximately 50% at 4 μM, corresponding to a 2.6- ($p<0.01$) and a 2.2-fold ($p<0.05$) decrease of cell viability, respectively, compared to the parental VHH. At this concentration, αNCL-CDR3 VHH also presented a 1.7-fold decrease of cell viability when compared to αNCL-CDR1-L VHH ($p<0.05$). At 8 μM, αNCL-CDR1 VHH also presented higher cytotoxicity than parental VHH, with a 1.4-fold decreased cell viability ($p<0.05$), whereas αNCL-CDR3 VHH and αNCL-CDR3-L VHH decreased cell viability down to approximately 70%, corresponding to a 1.7-fold decrease of cell viability ($p<0.001$ and $p<0.01$, respectively) relative to the parental VHH. Higher cytotoxicity of αNCL-CDR3 VHH compared to αNCL-CDR1-L VHH ($p<0.01$) was also observed at this concentration. In this cell line, parental VHH resulted in a 40% decrease of viable cells, for the highest concentration tested (Figure 2.7D).

2.4 DISCUSSION

Since the discovery of HCabs in 1993, nanobodies have been a focus of cancer research, due to their small size, versatility and therapeutic potential. Nanobodies have

been developed against cell surface receptors, such as EGFR[128,129,131], HER2[169] or VEGF[139], as well as novel targets involved in tumor development and progression, as CEACAM6[134] or HGF[135]. Another emerging area in antibody engineering is the development of bispecific antibodies, with the ability to bind two different targets, aiming at improving tumor growth inhibition[143]. In the work presented in this chapter, nanobodies have been developed against nucleolin, whose overexpression at the surface of cancer and endothelial cells from tumor blood vessels, makes it a promising target for cancer therapy.

The most common strategies to develop an antibody or an antibody fragment against a specific target encompass: (i) immunization of the animal model used for antibody generation, followed by spleen cell harvesting and antibody recovery, and (ii) generation of a library and selection of binders by display technologies (most frequently, phage display). However, when binders have already been described for the target of interest, an alternative strategy that bypasses these time-consuming steps is the grafting of a known binding sequence onto the CDRs[170,171], as far as it is compatible with the size of the CDR. CDR1, and especially CDR3, are the most important domains on antigen binding[99,100]. In VHHs, CDR1 usually has a length of 5-9 residues, whereas CDR3 usually comprises 16 amino acids[172]. Therefore, this alternative strategy can only be used when previously described binding motifs are of peptidic nature, with a molecular size that fits the CDR loops.

In the present work, a grafting strategy based on the nucleolin-binding F3 peptide was pursued. The F3 peptide had been previously generated by phage-display[173] and further demonstrated promising *in vivo* tumor targeting capabilities[46–49]. This suggested that nanobodies derived from this sequence were likely to present high extent of binding capacity to nucleolin and be equally relevant for tumor targeting. Due to its long length (31 amino acids), grafting was performed using a 10-amino acid sequence that had been proven responsible for the major component of nucleolin binding[173]. No other studies have reported the use of this smaller sequence alone for grafting onto antibody formats.

In fact, grafting of the PQRRSARLSA sequence, corresponding to the nucleolin binding motif of the F3 peptide, either onto CDR1 or CDR3 has proven to generate nanobodies with the ability to bind nucleolin, as demonstrated with purified nucleolin or cancer and endothelial cells. Competitive inhibition assays with the F3 peptide confirmed the nanobody binding to the cells was nucleolin-mediated, particularly in the case of the cancer cell lines tested. The anti-nucleolin nanobodies presented the highest extent of binding to MDA-MB-435S cells, followed by MDA-MB-231 and HMEC-1 cells. This was consistent with the reported higher association of F3 peptide targeted-liposomes to MDA-MB-435S cells relative to the two other cell lines[46,167] and with recent data reporting 102000 and 57000 nucleolin molecules at the surface of MDA-MB-435S and MDA-MB-231, respectively (JN Moreira, personal communication). The binding studies, along with the cytotoxicity experiments have further supported that the modification onto CDR3 enabled a higher extent of activity relative to the exact same grafting, onto CDR1. This was in agreement with the reports showing that CDR3 usually plays a more important role in antigen binding, than other CDRs[99,100]. Binding of the anti-nucleolin nanobodies to 4T1 confirmed that these entities also bound to mouse nucleolin, which is line with the 81% homology of the protein between these two species[174]. This is somehow in contrast with the ability of D3 antibody to bind to human nucleolin, but not the one from mouse origin[175]. Binding to an epitope in a less conserved region of the protein could support the difference in binding, between the two species. The slightly lower binding of the anti-nucleolin nanobodies to 4T1 relative to MDA-MB-231 is in accordance with the difference in the number of surface nucleolin molecules (45000 and 57000, respectively; JN Moreira, personal communication).

Of notice is the fact that the reported activity did not depend on loops with increased flexibility, as enabled by SGGGS linkers inserted at the end of CDRs[165,166]. This is in contrast with the activity of HCabs (camelid antibodies with VHH domains instead of the common VH-VL binding domains), where the longer and more flexible CDR3 loop of HCabs, favors the access to clefts, characteristic of enzymes' active site

(usually not accessible to conventional antibodies)[176–178]. The results herein presented suggested that the epitope recognized by the developed anti-nucleolin nanobodies was easily accessed, not requiring a longer or more flexible loop.

As previously explained, the anti-nucleolin VHHs were developed from a parental anti-human TNF-α VHH. Interestingly, the ungrafted CDRs, within the constructs modified with the nucleolin-binding motifs, retained the binding capacity to the original human TNF-α. Expectedly, the extent of binding was decreased relative to the parental VHH with two anti-TNF-α binding regions. In this respect, its binding to MDA-MB-231 cells (and further decrease of cell viability, as well) was in accordance with the reported overexpression of tmTNF-α on these cells[161]. The absence of binding to mouse 4T1 cells was in agreement with the parental VHH lack of cross-reactivity with TNF-α mouse counterpart[179].

The anti-nucleolin nanobodies here developed also presented cytotoxicity against the cancer cell lines tested, as well as the HMEC-1 endothelial cells, in the micromolar range. When compared to the cytotoxic effects that had been reported for other nucleolin-binding agents, the anti-nucleolin nanobodies here generated presented similar effects to most of them. The AS1411 aptamer and the HB-19 and N6L pseudopeptides have been reported to decrease cell viability or colony formation in the micromolar range in a variety of cell lines, including cancer cell lines, such as MDA-MB-231 and MDA-MB-435[65,79,81]. This effect was, however, of a lower extent than the one observed with the anti-nucleolin scFv 4LB5, which presented IC_{50} values in the nanomolar range (3-58 nM)[87]. Such level of cytotoxicity enabled by the scFv could rely on the presence of two binding domains, VH and VL, which could contribute to a more potent cytotoxic effect. In this respect, strategies to increase the cytotoxicity of the anti-nucleolin VHHs could be used, either through engineering a VHHs in a multivalent format (as it will be described in Chapter 3) or grafting the F3 peptide-derived sequence onto more than one CDR.

The fact that the new generated nanobodies bound not only to nucleolin but also to TNF-α confirmed the successful generation of bispecific nanobodies from a single VHH. The developed strategy, which conferred different targeting capabilities to different CDRs, has not been reported yet and could be used to generate bispecific nanobodies against different target combinations. This new class of bispecific nanobodies retained a molecular weight smaller than regular bispecific antibodies, currently in clinical trials for the treatment of solid tumors, such as, RG7221 (targeting angiopoietin 2 and VEGF) or MM141 (targeting IGF1R and HER3)[142,143]. The referred advantage also applies upon comparison with bispecific antibody fragments, like AFM13 (targeting CD30 and CD16A), MM111 (targeting HER2 and HER3, fused to modified serum albumin) or ALX0761 (targeting IL17A and IL17F). These last three are being tested for the treatment of Hodgkin lymphoma, advanced gastric and esophageal cancer and inflammatory diseases, respectively[142,143,180].

Although the focus of this work has been on the development and characterization of anti-nucleolin VHHs in the context of cancer therapy, this antibody format also has applicability for diagnostic applications, such as imaging, as described for the bispecific nanobodies, and immunohistochemistry. Nanobodies have been show to often be more effective than full-length antibodies for immunohistochemistry applications, as they present better diffusion in fixed tissues[181,182].

When considering the VHHs as a platform for generating other entities, several strategies could be explored to further develop their effectiveness, from incorporation on the surface of nanoparticles, to conjugation to toxins and multimerization, as performed for other nanobodies[128,132,152,153].

Collectively, the results presented in this chapter validated the use of a F3 peptide-based grafting onto the CDRs of a nanobody to generate nucleolin-binding nanobodies, which bind cancer cells and angiogenic endothelial cells, and further enable cytotoxic effects on their own. In addition, the results supported the development of a bispecific construct from a single VHH, a strategy that could be applied to any other target, by

altering the CDR specificity. Such strategy could be particularly useful to improve penetration into solid tumors and therefore the pharmacodynamic outcome[183].

Chapter 3

Development and characterization of a nucleolin-targeting nanobody-Fc antibody

3.1 INTRODUCTION

The efficacy of an antibody in cancer therapy is determined by several factors, ranging from its biodistribution and access to the tumor, to its antitumor activity and underlying mechanism of action[119,184,185]. Advances on antibody engineering, namely at the level of antibody molecular size and serum half-life[119,186], have enabled improvements on its biodistribution profile[120,130,187].

The biodistribution of an antibody can be largely affected by its rate of blood clearance, which is mainly dependent on kidney filtration[188]. The extent of clearance associated with this component is significantly decreased for therapeutic agents, as (150 kDa) full-length IgGs, with a molecular weight above the renal filtration threshold (of approximately 50 kDa)[120]. The downside of a high molecular weight (100 kDa upward) relates with the impaired tumor penetration, limiting the access to the tumor periphery. Therefore, a molecular weight between 50 kDa and 100 kDa is a good balance aiming at improving the antibody bioavailability in the tumor[188]. Accordingly, this has been demonstrated in mouse models, where 80 kDa antibody formats presented higher tumor/blood ratio than full-length IgG (150 kDa), a scFv (28 kDa) or a diabody (55 kDa). In fact, scFv and diabody formats presented undetectable levels in the tumor and blood, 72 h after intravenous administration. In an independent experiment, using antibody formats against a different antigen, the 80 kDa construct presented a higher tumor accumulation than full-length IgG and a Fab'2 fragment (fusion of two Fab fragments, 110 kDa)[120].

The Fc domain of an antibody is the main responsible for its increased half-life in the blood, as it binds to FcRn, enabling antibody transport within and across cells and avoiding degradation[101]. In fact, 1 h after intravenous administration of three formats of anti-EGFR antibodies, without the Fc domain, as a 16 kDa single domain, a 126 kDa multimeric pentabody or a 80 kDa chimeric HCab, a high extent kidney accumulation

was observed, namely for the first two formats, along with low tumor accumulation. The presence of a Fc domain in the chimeric HCab, which led to a significant increase of blood half-life and tumor accumulation, while decreasing the rate of kidney clearance[130]. The presence of the Fc region may also impact the outcome of the antibody therapy, as it might enable immune responses, as antibody-dependent cell-mediated cytotoxicity (ADCC). This mechanism of action has supported the activity of trastuzumab, cetuximab or rituximab[112,113,116,117,189] and other surface targets on cancer cells have been explored to enable a similar effect [137,190,191].

Overall, the choice of an adequate format for cancer therapy is of extreme importance, as it impacts the pharmacokinetics and pharmacodynamics of the antibody.

As described in the previous chapter, nucleolin-binding nanobodies have been developed and presented cytotoxic effects against several cancer cell lines, as well as an angiogenic endothelial cell line. Taking into account that the small size of nanobodies strongly limits their therapeutic efficacy, the work presented in this chapter aimed at developing a nanobody-Fc fusion protein targeting nucleolin. This type of construct is expected to enable a protein of approximately 80 kDa, likely to favor tumor penetration, and capable of triggering an ADCC effect. This is particular relevant as that this kind of response has not been reported yet in the context of nucleolin targeting.

3.2 MATERIALS AND METHODS

3.2.1 Cell lines

MDA-MB-435S, MDA-MB-231, 4T1 and HMEC-1 cell lines were maintained as described in section 2.2.12.

HEK293T cell line (ATCC® CRL-3216™, USA) was cultured in Dulbecco's Modified Eagle's Medium (DMEM, Lonza, Switzerland), supplemented with 10% (v/v) heat-inactivated FBS (HyClone, USA), 2 mM of L-glutamine (Lonza, Switzerland), 1% (v/v) Pen/Strep/Fungiezone solution (HyClone, USA), and maintained at 37°C in a humidified atmosphere of 5% CO_2.

3.2.2 Development of an anti-nucleolin nanobody-Fc antibody

An anti-nucleolin nanobody-Fc antibody (αNCL-VHH-Fc) was generated by inserting the nanobody sequence of αNCL-CDR3 VHH in a pFuse-hIgG1-Fc2 plasmid (Figure 3.1; DNA and protein sequences are presented in Appendix, Figure 1). The pFuse-hIgG1-Fc2 vector contains not only the CH2 and CH3 domains, but also the hinge region, which confers flexibility to the antibody. In addition, this vector contains an interleukin 2 (IL2) signal sequence, which leads to the secretion of the expressed protein. The parental VHH, used in chapter 2 for the grafting of the F3 peptide-derived sequence, was also cloned in fusion to a Fc region (parental VHH-Fc).

To obtain these two nanobody-Fc antibodies, each nanobody sequence was first amplified by PCR, using Phusion DNA Polymerase (Thermo Scientific, USA; conditions and primers indicated in Appendix, Tables 1 and 3). PCR products were visualized on 1.5% (w/v) agarose gel and recovered as described in section 2.2.2. These PCR products were then inserted onto pFuse-hIgG1-Fc2 vector, using the enzymes NcoI and BglII, and performing ligation as previously described in section 2.2.2.

Colony screening, preparation of electrocompetent cells and sequencing were performed as described in sections 2.2.4, 2.2.5 and 2.2.9, but instead of ampicillin, the resistance marker of the pFuse-hIgG1-Fc2 vector, zeocin (25 µg/mL, Invivogen, France), was used.

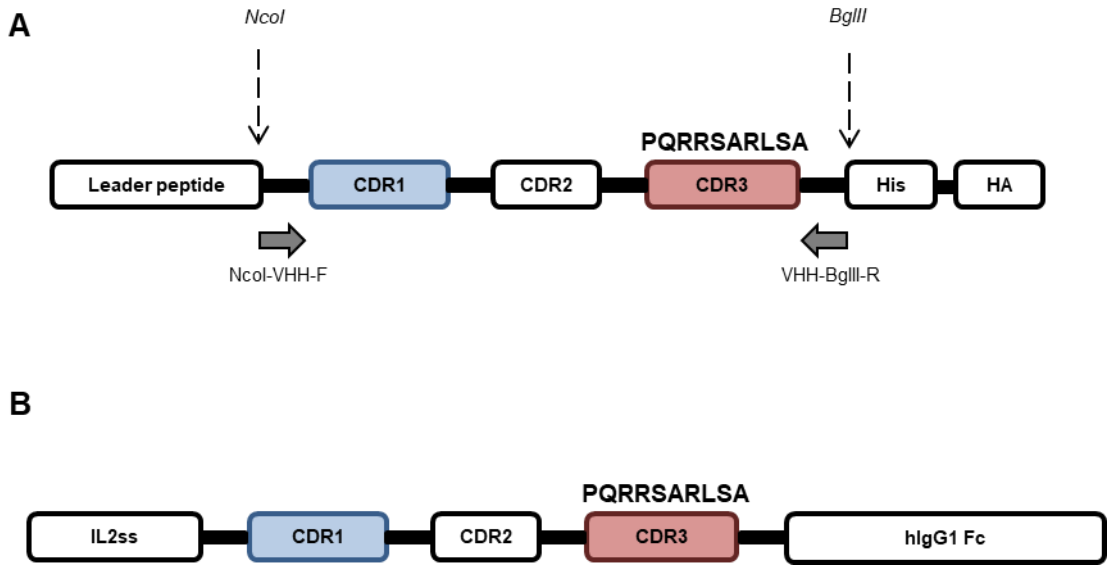

Figure 3.1. Schematic representation of the VHH/nanobody-Fc cloning. (A) Primers used in the PCR reactions and restriction sites of the enzymes used to generate the VHH fragment for cloning. (B) VHH fragment cloned onto the pFuse-hIgG1-Fc2 vector, containing the IL2 signaling sequence and the Fc region.

3.2.3 Expression and purification of nanobody-Fc fusion proteins

HEK293T cells were used as the expression system for the nanobody-Fc fusion proteins[192], using the calcium phosphate transfection method[193,194]. Briefly, 3 million cells were seeded in a 10-cm tissue culture dish and after 24 h, cells were transfected with 20 µg of DNA, for 6 h. Cell culture medium was then exchanged for fresh one, without serum. After 48-60 h, supernatant was recovered, sterile filtered (at 0.2 µm pore size), and diluted (1:1, v/v) in binding buffer (100 mM sodium phosphate, 150 mM sodium chloride, pH 7.2). Protein purification was performed by affinity chromatography using Pierce Chromatography Cartridges Protein A columns (Thermo Scientific, USA), attached to a peristaltic pump (GE Healthcare, UK), upon elution at 4°C with 0.1 M glycine, pH 2.0, at a flow rate of 1 mL/min. Half milliliter fractions were collected into

tubes containing 0.05 ml of neutralization buffer (1M Tris, pH 8.0) to immediately neutralize the pH and thus prevent protein degradation.

After confirmation of the presence of pure protein in Coomassie-stained SDS-PAGE gels (1 mm, 12% (w/v) polyacrylamide), protein desalting was performed using disposable PD-10 columns (GE Healthcare, UK). The protein was then concentrated (Vivaspin 500, 50 kDa cutoff, GE Healhcare, UK) and stored in 20 mM HEPES, 100 mM NaCl, 5% (v/v) glycerol, pH 8.0.

SDS-PAGE, Western Blot and coomassie staining were performed as described in sections 2.2.8 and 2.2.11, using 12% (w/v) polyacrilamide gels and goat anti-human IgG-HRP antibody (sc-2907, Santa Cruz Biotechnology, USA, diluted at 1:5000 in blocking buffer).

3.2.4 Nanobody-Fc cytotoxicity against cancer and endothelial cells

Different cell densities of cancer or endothelial cell lines were seeded in 96-well plates (5000 MDA-MB-435S or MDA-MB-231 cells, 3000 4T1 cells or 7500 HMEC-1 cells, per well). After 24 h, cell culture medium was exchanged for fresh one, and cells were incubated with serial dilutions of VHH proteins (from 31.25 to 1000 nM, each condition performed in duplicate), for a total of 72 h. Cell viability was then determined by the MTT assay, as described in section 2.2.14, using the following formula:

$$\%\ \text{cell viability} = \frac{\text{ODcontrol cells} - \text{ODcondition}}{\text{ODcontrol cells}} \text{x}100$$

3.2.5 PBMC isolation and culture

Human PBMCs were isolated from buffy coats of healthy donors obtained at Instituto Português do Sangue e da Transplantação, to be used as effector cells in the ADCC assays. Isolation was performed by a Ficoll-Paque PLUS density gradient (GE Healthcare, UK). A 1:1 buffy coat dilution in 1% (v/v) FBS in PBS (FBS-PBS) was placed on a Ficoll-Paque PLUS layer, and centrifugation was then performed (750 x g, 20 min, room temperature) to separate the different blood constituents and recover the PBMC fraction. This fraction was then washed until the pellet was clear (300 x g, 5 min, 4°C) and finally resuspended in FBS-PBS. PBMCs were then resuspended in RPMI-1640 medium (Lonza, Switzerland), supplemented with 10% (v/v) heat-inactivated FBS (HyClone, USA), 2 mM of L-glutamine (Lonza, Switzerland), 1% (v/v) Pen/Strep/Fungiezone solution (HyClone, USA) and placed at 37°C in a humidified atmosphere of 5% CO_2, overnight. After this recovering step, PBMCs were counted and frozen in freezing medium (10% (v/v) DMSO in FBS) and kept at -80°C. When needed, PBMCs were thawed and maintained overnight in the same supplemented-RPMI-1640, at 37°C in a humidified atmosphere of 5% CO_2, to decrease loss of effector capacity[195]. Only then, they were used in the ADCC assays.

3.2.6 ADCC effect of anti-nucleolin nanobody-Fc fusion protein against cancercells

To evaluate the ADCC potential of the anti-nucleolin nanobody-Fc fusion protein, MDA-MB-435S or 4T1 were used as target cells. ADCC was assessed using xCELLigence Real Time Cell Analyzer (Roche, Switzerland), described in Figure 3.2. Different target cell densities (7500 MDA-MB-435S cells or 5000 4T1 cells) were plated

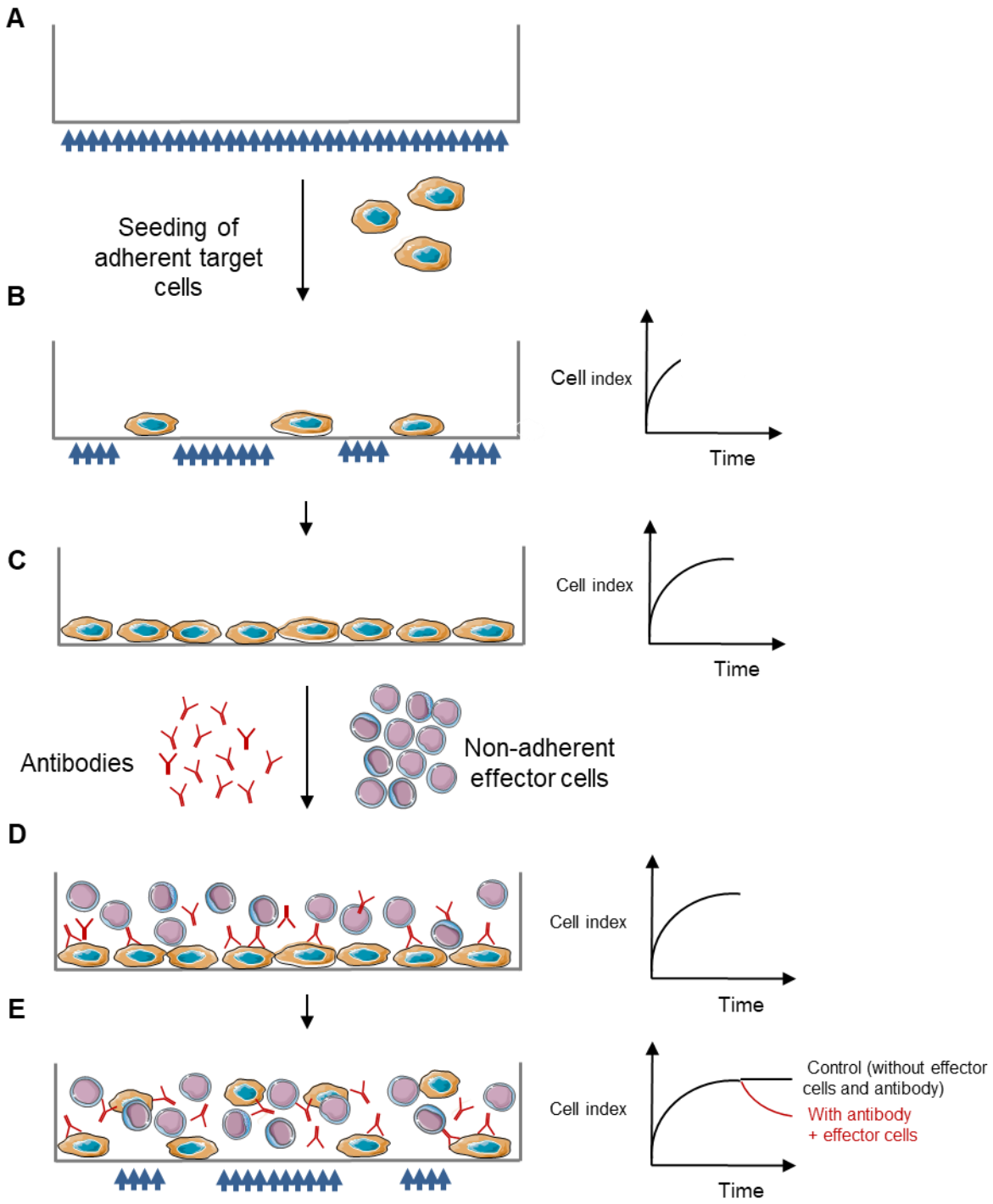

Figure 3.2. Diagram of the antibody-dependent cell-mediated cytotoxicity assessment using the xCELLigence system. Assessment of cell viability is based on cell adhesion, using plates with electrode-coated wells that generate an electric current (blue arrows, A) when a low voltage is applied. As target cells adhere and proliferate, impedance (opposition presented to the electric current) increases (B-C). Upon incubation with antibodies and effector cells of the immune system (which are non-adherent and therefore do not affect impedance) (D), target cell death leads to loss of adhesion and consequently to lower impedance (E). These impedance alterations are recorded in short intervals and plotted as cell index, which increases proportionally to adherent cell density.

on aRTCA 96-well plate for 24 h and then incubated with thawed PBMCs (at 10:1 or 5:1 ratio of effector cells to target cells) and/or nanobody-Fc antibody (at 25 or 125 nM). Cancer cells incubated only with effector cells or fusion protein were included as additional controls. Since ADCC is a Fc-dependent mechanism, an additional control consisted on target cells incubated with the VHH counterpart of the fusion proteins (αNCL-CDR3 VHH or parental VHH), as well as αNCL-CDR1 VHH or F3 peptide, with or without PBMCs. As the nanobody-Fc antibodies are dimeric, the VHH proteins and the F3 peptide were added in a concentration of either 50 or 250 nM.

Cell index was measured every 15 min for 96 h and the resulting curves were plotted and normalized to 1.0, matching the beginning of the incubation of PBMC with the different tested proteins and the cancer cells. Data were analyzed with RTCA Software Package, and cancer cell death, resulting from incubation with both antibody and PBMCs, was calculated from the area under the curve (AUC) values, as following:

$$\%\ \text{cell death} = \frac{\text{AUC}(\text{protein} + \text{PBMC}) - \text{AUC}(\text{protein}) - \text{AUC}(\text{PBMC})}{\text{AUC}(\text{untreated cells})} \text{x}100$$

To evaluate the ADCC effect, cell death values obtained with the nanobody-Fc fusion protein and its nanobody counterpart were compared.

3.2.7 Statistical analysis

Student's t-test was performed to analyze differences between the cytotoxicity of the nanobody-Fc antibodies. Repeated measures ANOVA followed by Post hoc analysis

with Tukey test was performed to assess differences in cell death upon incubation with PBMCs and each of the tested proteins, in the ADCC assay. Analyses were performed with a level of significance of 5%.

3.3 RESULTS

3.3.1 Expression and purification of anti-nucleolin nanobody-Fc antibody

Herein, a novel nanobody-Fc antibody, formed by an anti-nucleolin nanobody and a Fc fragment of human IgG1 was expressed (along with the corresponding parental VHH-Fc) in HEK293T cells and the purity further evaluated by Western Blot. In addition to the bands corresponding to denatured proteins, of approximately 40 kDa, two additional bands were detected (Figure 3.3A). These could correspond to degraded forms of the proteins, of approximately 35 and 25 kDa, due to the presence of proteases during the purification procedure. Nevertheless, purification followed by concentration using a Vivaspin with a 50 kDa cutoff, enabled a high-purity fraction containing the proteins with the highest molecular weight, corresponding to the nanobody-Fc antibodies (Figure 3.3B).

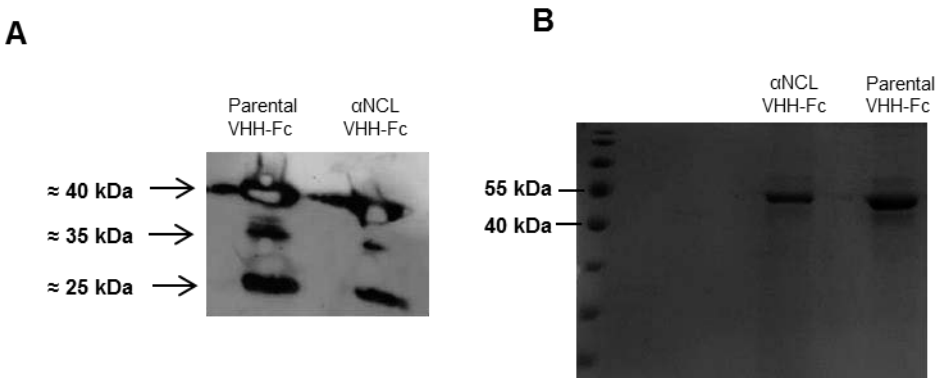

Figure 3.3. Expression and purification of anti-nucleolin or parental VHH-Fc antibody. (A) Expression of anti-nucleolin (αNCL-VHH-Fc) or parental (VHH-Fc) nanobody-Fc fusion proteins in the supernatant of HEK293T cells (48-60 h after transfection) was evaluated by SDS-PAGE followed by Western Blot. (B) Representative coomassie-stained SDS-PAGE gels of the purified fusion proteins, αNCL-VHH-Fc and parental VHH-Fc.

3.3.2 Cytotoxicity of anti-nucleolin nanobody-Fc antibody against cancer and endothelial cells

The anti-nucleolin nanobody-Fc antibody, αNCL-VHH-Fc, presented cytotoxic effects within the nanomolar range (Figure 3.4A-D). For all cell lines, a more pronounced decrease of cell viability was observed upon incubation with αNCL-VHH-Fc, relative to the parental antibody, without the nucleolin-binding component. This was especially relevant in MDA-MB-435S and 4T1 cell lines (less than 25% of viable cells at the highest concentration tested, Figures 3.4A-B) when compared with MDA-MB-231 and HMEC-1 (approximately 50% of viability at 1000 nM, Figures 3.4C-D). At the highest concentration tested, αNCL-VHH-Fc enabled a 1.7-, 1.5- or 1.4-fold decrease of viability of MDA-MB-435S, MDA-MB-231 or HMEC-1 cells, respectively, relative to the parental VHH-Fc. This protein did not present any cytotoxic effect against 4T1 cells, but decreased the viability

of MDA-MB-435S, MDA-MB-231 and HMEC-1 cells down to 53%, 64% and 68%, respectively.

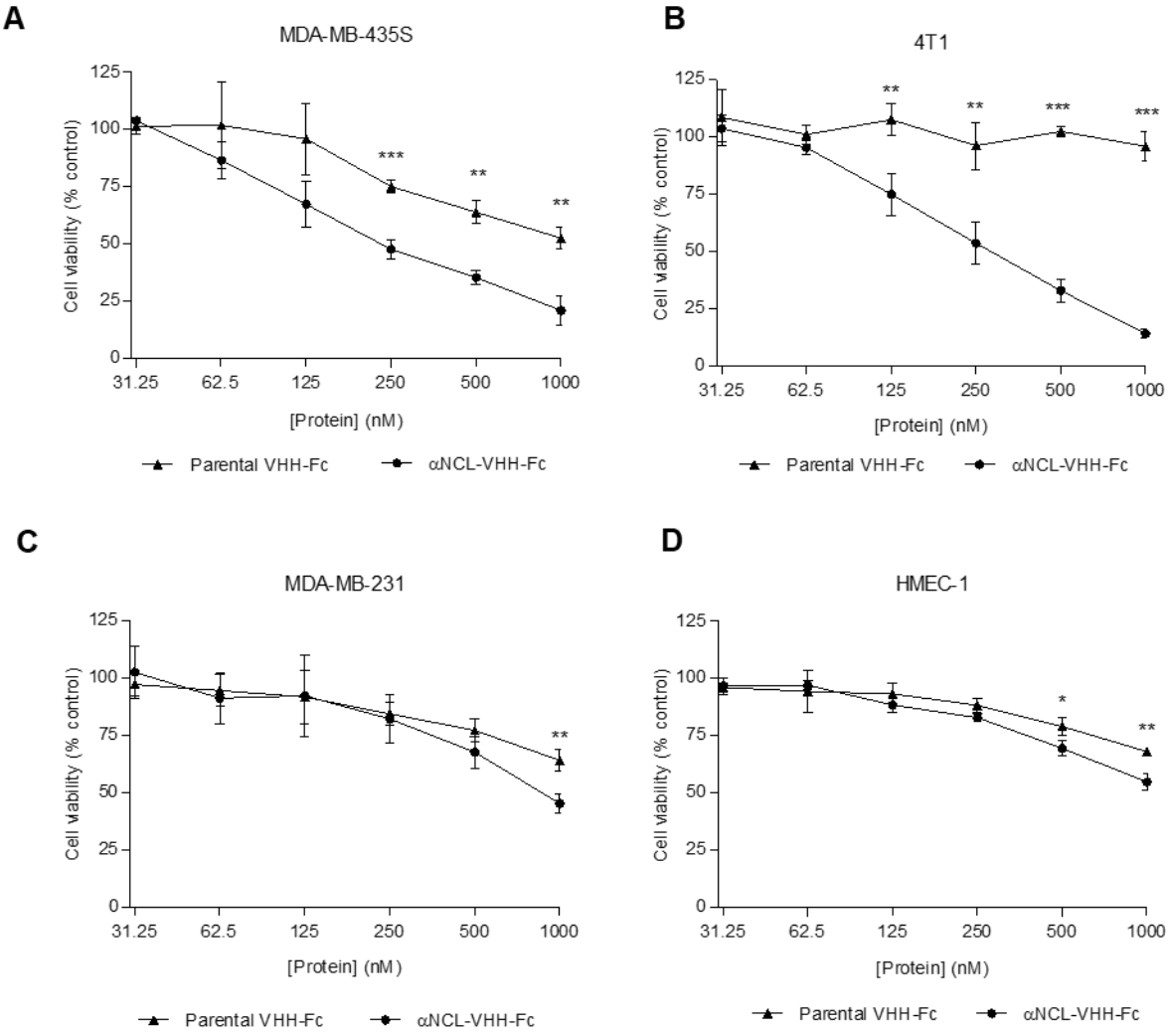

Figure 3.4. Cytotoxicity of anti-nucleolin nanobody-Fc against cancer or endothelial cells. Anti-nucleolin VHH-Fc antibody (αNCL-VHH-Fc) or control protein (parental VHH-Fc) were incubated with cells, either neoplastic as (A) MDA-MB-435S, (B) 4T1 and (C) MDA-MB-231 or the (D) endothelial HMEC-1 cells, at concentrations up to 1000 nM, for 72 h. In the end of the incubation, cytotoxicity was assessed by the MTT assay. Data represent the mean ± SD from three independent experiments, performed in duplicate. Differences in cytotoxicity between the tested proteins were evaluated by Student's t-test (*p<0.05, **p<0.01, ***p<0.001).

3.3.3 Antibody-dependent cell-mediated cytotoxicity of anti-nucleolin nanobody-Fc antibody against MDA-MB-435S

In MDA-MB-435S cells, 25 nM αNCL-VHH-Fc, in the presence of PBMCs, enabled higher cell death than equimolar parental VHH-Fc ($p<0.001$, Figure 3.5A). Important to point out that this difference was completely dissipated in the absence of PBMCs (Figure 3.5A). Moreover, the effect was partly dependent on the presence of the Fc region, as in the absence of the latter, the αNCL-CDR3 VHH protein triggered a lower level of cancer cell death in the presence of PBMCs ($p<0.01$, Figure 3.5B). The absence of ADCC activity of the parental VHH-Fc construct was further demonstrated, as it enabled similar levels of cell viability as its VHH counterpart, upon incubation with PBMCs. (Figure 3.5C). These results supported an overall nucleolin-dependent ADCC effect by the anti-nucleolin nanobody-Fc antibody. This effect suggested to be concentration-independent within the range of 25 - 125 nM (Figure 3.5D).

The increased cytotoxicity observed upon incubation of MDA-MB-435S with αNCL-CDR3 VHH and PBMCs, relative to incubation with αNCL-CDR3 VHH alone (Figure 3.5B), suggested that the anti-nucleolin ligands, in the presence of PBMCs, could have an Fc-independent effect. Therefore, the cytotoxicity of the anti-nucleolin VHHs αNCL-CDR1 VHH and αNCL-CDR3 VHH, as well as the nucleolin-binding F3 peptide, was evaluated in the presence of PBMCs. The parental VHH, without a nucleolin-binding component, was included as a control. αNCL-CDR1 and αNCL-CDR3 VHH and F3 peptide, enabled similar levels of cytotoxicity against MDA-MB-435S cells, in the presence of PBMCs. However, significant increased cell death was observed with αNCL-CDR3 VHH and F3 peptide, relative to the parental VHH, in the presence of PBMCs ($p<0.05$, Figure 3.6A-C). These results suggested a Fc domain-independent cytotoxicity of anti-nucleolin constructs, in the presence of PBMCs. αNCL-CDR1 VHH enabled a similar effect, although a statistically significant difference was not observed. This

A

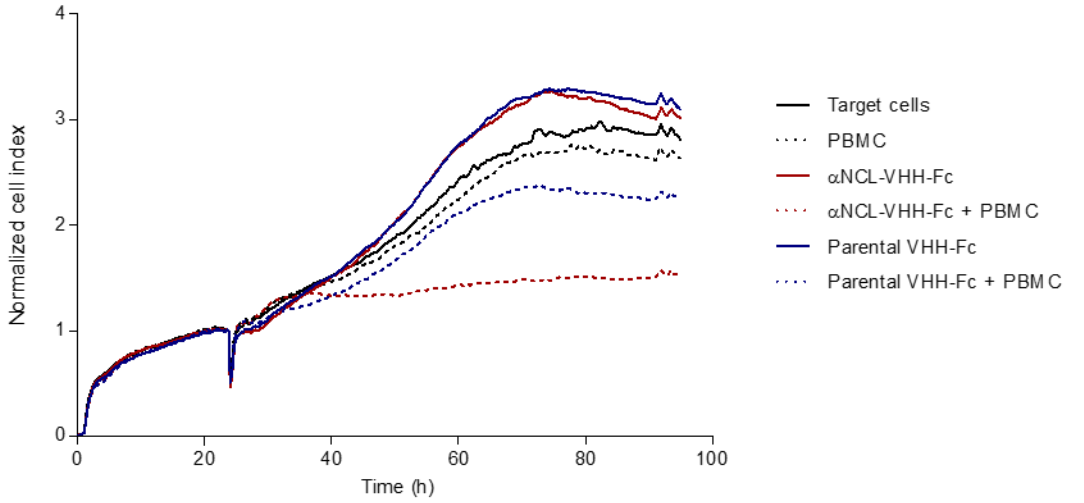
Normalized cell index
Time (h)
Target cells
PBMC
αNCL-VHH-Fc
αNCL-VHH-Fc + PBMC
Parental VHH-Fc
Parental VHH-Fc + PBMC

B

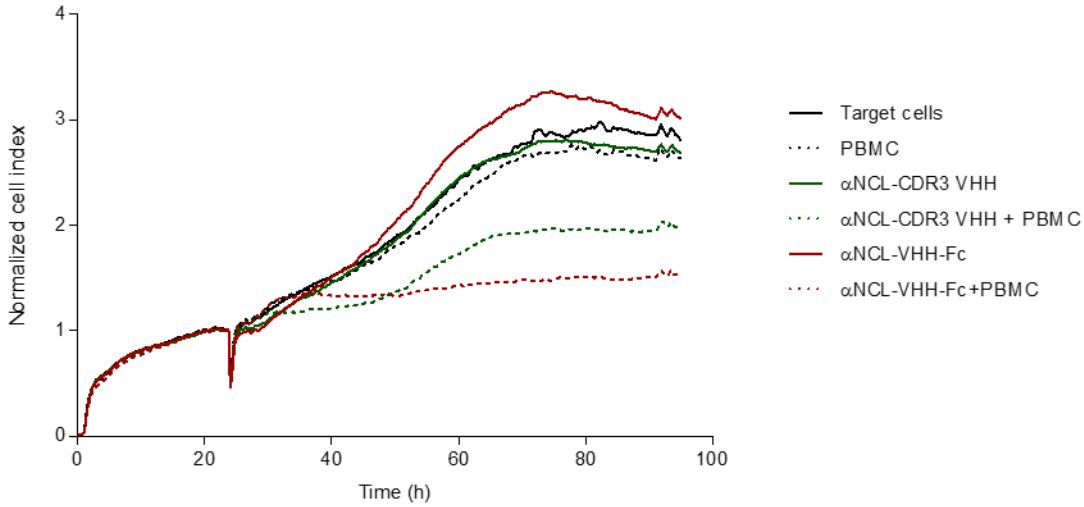
Normalized cell index
Time (h)
Target cells
PBMC
αNCL-CDR3 VHH
αNCL-CDR3 VHH + PBMC
αNCL-VHH-Fc
αNCL-VHH-Fc+PBMC

C

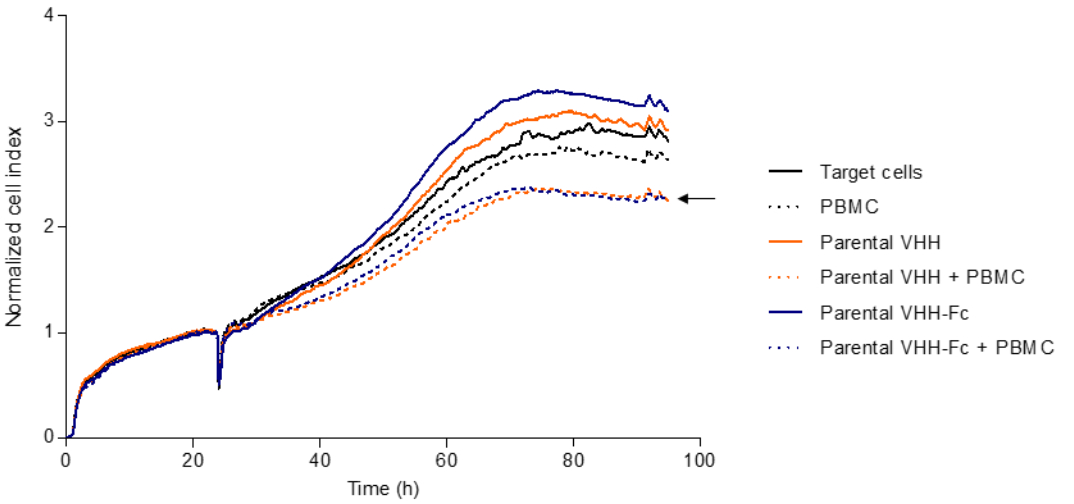
Normalized cell index
Time (h)
Target cells
PBMC
Parental VHH
Parental VHH + PBMC
Parental VHH-Fc
Parental VHH-Fc + PBMC

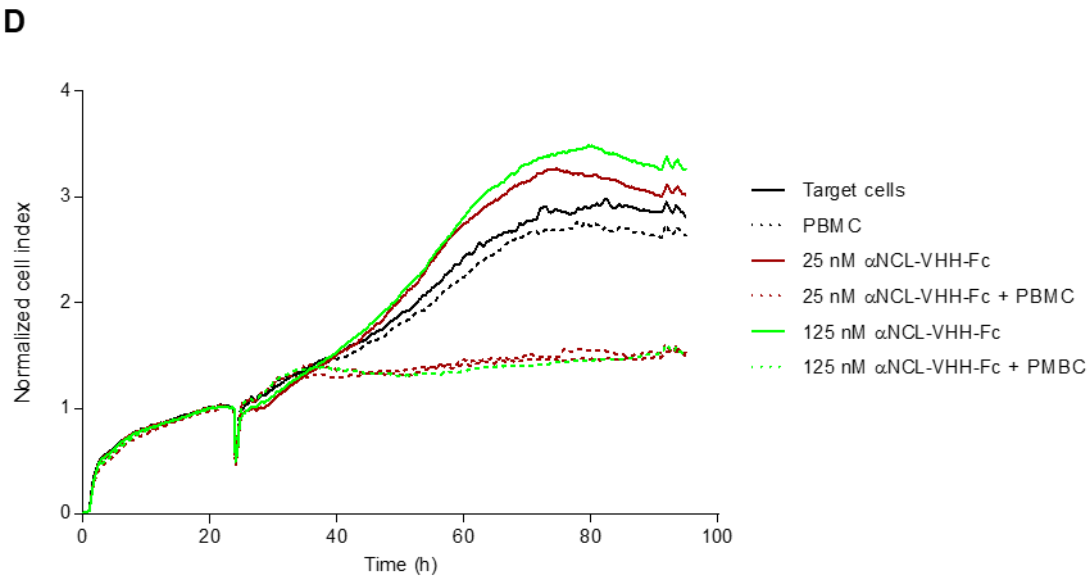

Figure 3.5. Antibody-dependent cell-mediated cytotoxicity of anti-nucleolin nanobody-Fc antibody against MDA-MB-435S cells. MDA-MB-435S cells, previously cultured in a RTCA plate for 24 h, were incubated with protein, without (solid lines) or with human PBMCs (at a target cells/PBMCs ratio of 1:10 or 1:5 ratio, dotted lines), for 72 h. Cell index, normalized to the beginning of the incubation, was measured every 15 min, using the xCELLigence system. ADCC effect of the anti-nucleolin nanobody-Fc antibody (red) was further supported upon assessing its activity *versus* (A) 25 nM parental VHH-Fc (blue), (B) 50 nM αNCL-CDR3 VHH (green), (C) 25 nM parental VHH-Fc (blue) *versus* 50 nM parental VHH (orange), and (D) 125 nM (light green) αNCL-VHH-Fc. Data are from a representative experiment, performed in duplicate.

suggested that grafting onto CDR1 was not as effective as onto CDR3, as already suggested by the binding and cytotoxicity results described in Chapter 2.

The extent of cell death for each anti-nucleolin ligand and control proteins as a function of individual PBMCs donors (Figures 3.7A-D), revealed similar profiles, except for parental VHH, for one of the PBMCs sets (Figure 3.7B). The extent of ADCC effect by the anti-nucleolin nanobody-Fc antibody in MDA-MB-435S varied with the PBMCs donors (Figure 3.7). Increase in PBCM-dependent cell death ranged from, approximately, 1.3- to 2-fold, relative to the parental VHH-Fc and a 1.3- to 1.7-fold increase relative to the VHH counterpart ($p<0.01$). Therefore, and regardless of the

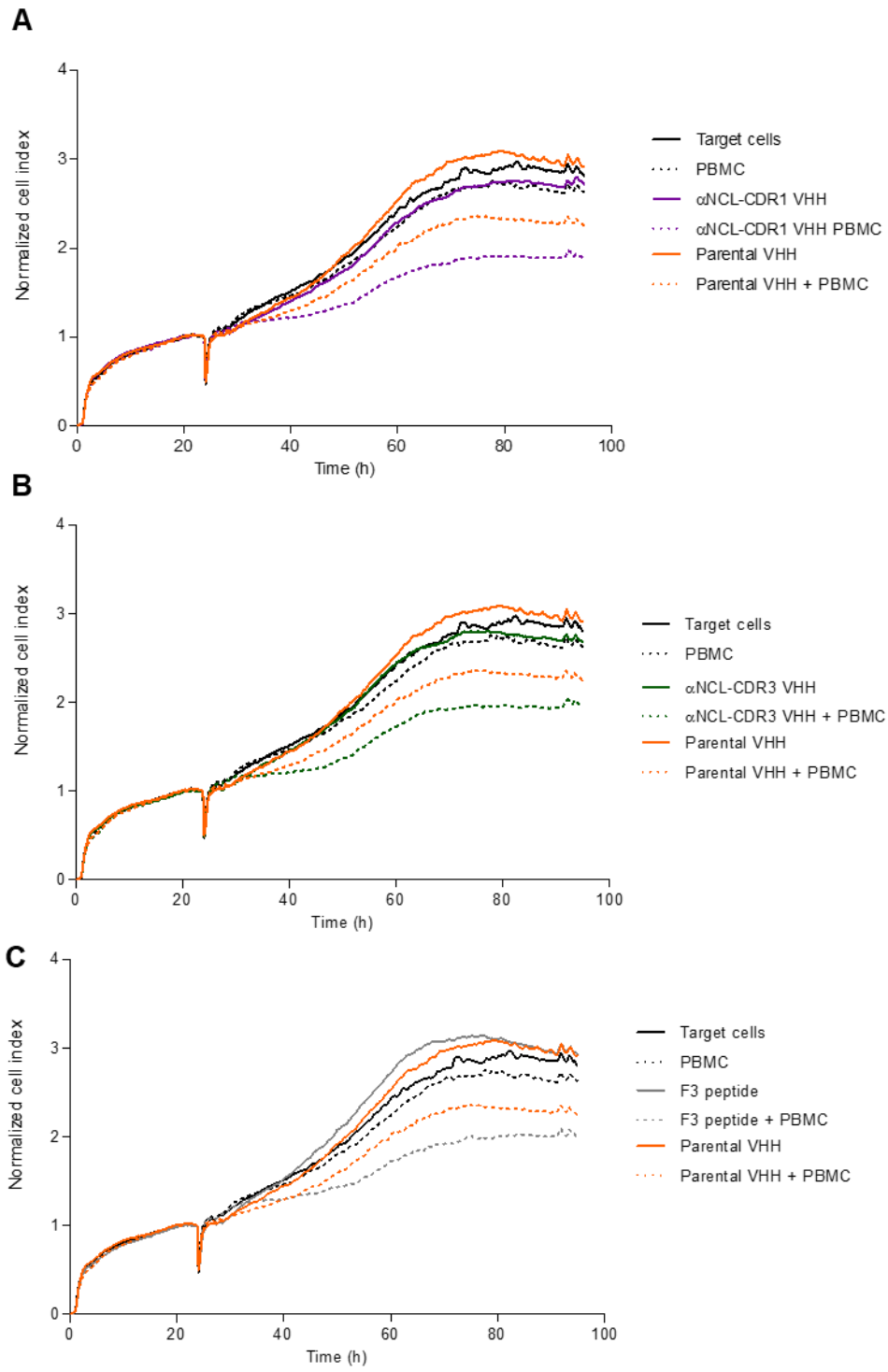

Figure 3.6. Cytotoxicity of anti-nucleolin nanobodies, without Fc region, in the presence of PBCMs, against MDA-MB-435S cells. MDA-MB-435S cells, previously cultured in a RTCA plate for 24 h, were incubated with protein, without (solid lines) or with human PBMCs (at a target cells/PBMCs ratio of 1:10 or 1:5 ratio, dotted lines), for 72 h. Cell index, normalized to the beginning of the incubation, was measured every 15 min, using the xCELLigence system. Cytotoxicity of anti-nucleolin nanobodies was assessed upon incubation of MDA-MB-435S cells with PBMCs and 50 nM of (A) αNCL-CDR1 VHH, (B) αNCL-CDR3 VHH, or (C) F3 peptide. Data are from a representative experiment, performed in duplicate.

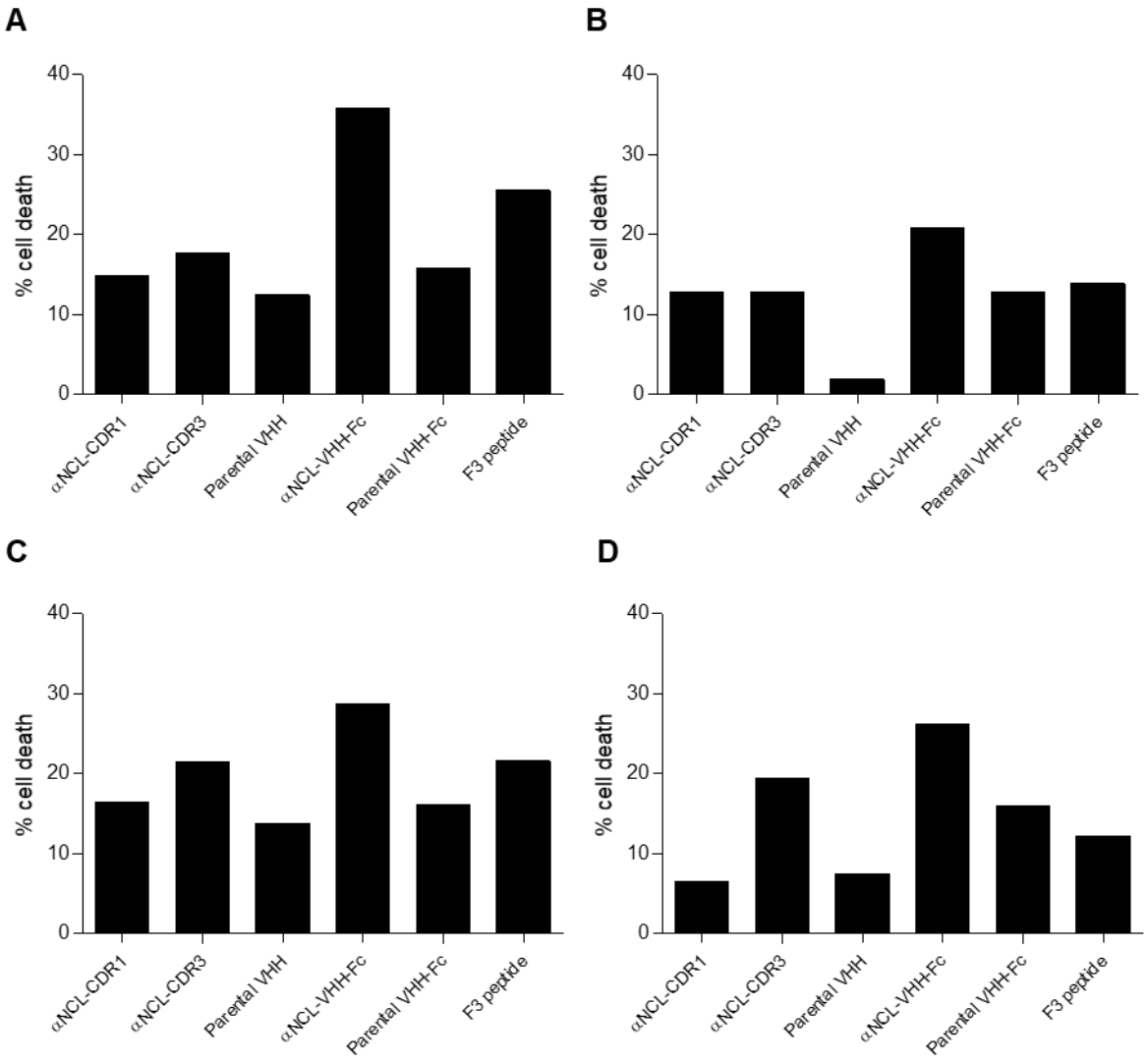

Figure 3.7. Cytotoxicity of nucleolin-binding proteins against MDA-MB-435S cells, upon incubation with human PBMCs harvested from different donors. Figures A-D represent the cytotoxicity assays, performed in duplicate, with PBCMs harvested from four donors, using the xCELLigence system. MDA-MB-435S, previously cultured in a RTCA plate for 24 h, were incubated with PBMCs (at a target cells/PBMCs ratio of 1:10 or 1:5 ratio) and 25 nM anti-nucleolin nanobody-Fc antibody (αNCL-VHH-Fc). Nucleolin-binding proteins without the Fc region (50 nM αNCL-CDR1 VHH, αNCL-CDR3 VHH or F3 peptide) or proteins without the nucleolin-binding component (50 nM parental VHH or 25 nM parental VHH-Fc) were included as controls. Cancer cell death was calculated from the area under the curve (AUC), as described in Material and Methods.

PBMC origin, these results supported a Fc-dependent and nucleolin-specific ADCC effect of αNCL-VHH-Fc against MDA-MB-435S cells.

3.3.4 Antibody-dependent cell-mediated cytotoxicity of anti-nucleolin nanobody-Fc antibody against 4T1 mouse cancer cells

In contrast with the activity observed with the MDA-MB-435 cells, incubation of 4T1 mouse cancer cells with either 25 nM or 125 nM of αNCL-VHH-Fc antibody, in the presence of PBMCs, did not result in a decreased cell viability, relative to the incubation with the αNCL-VHH-Fc antibody alone (Figure 3.8). These results strongly suggested that the antibody did not trigger an ADCC effect against these cells.

3.4 DISCUSSION

The efficacy of antibody therapy against solid tumors can be hampered, depending on the targeted tumor cell sub-populations, by their high molecular weight (of approximately 150 kDa), as it strongly limits their access to the inner tumor areas[119]. Antibody formats of approximately 80 kDa have increased access to these areas, without increased extent of kidney filtration[188]. In fact, this was the rationale that led to the fusion of a Fc domain of human IgG1 to the anti-nucleolin nanobody, αNCL-CDR3 VHH, previously described (Chapter 2). The higher extent of cytotoxicity enabled by the αNCL-CDR3 VHH relative to the CDR1-grafted counterpart, and regardless of the presence of the flanking linkers at each end of the grafted CDR, supported the choice of the former to generate the novel αNCL-CDR3 VHH-Fc antibody. This format is expected to enable improved tumor penetration relative to full-length IgGs, while maintaining a prolonged

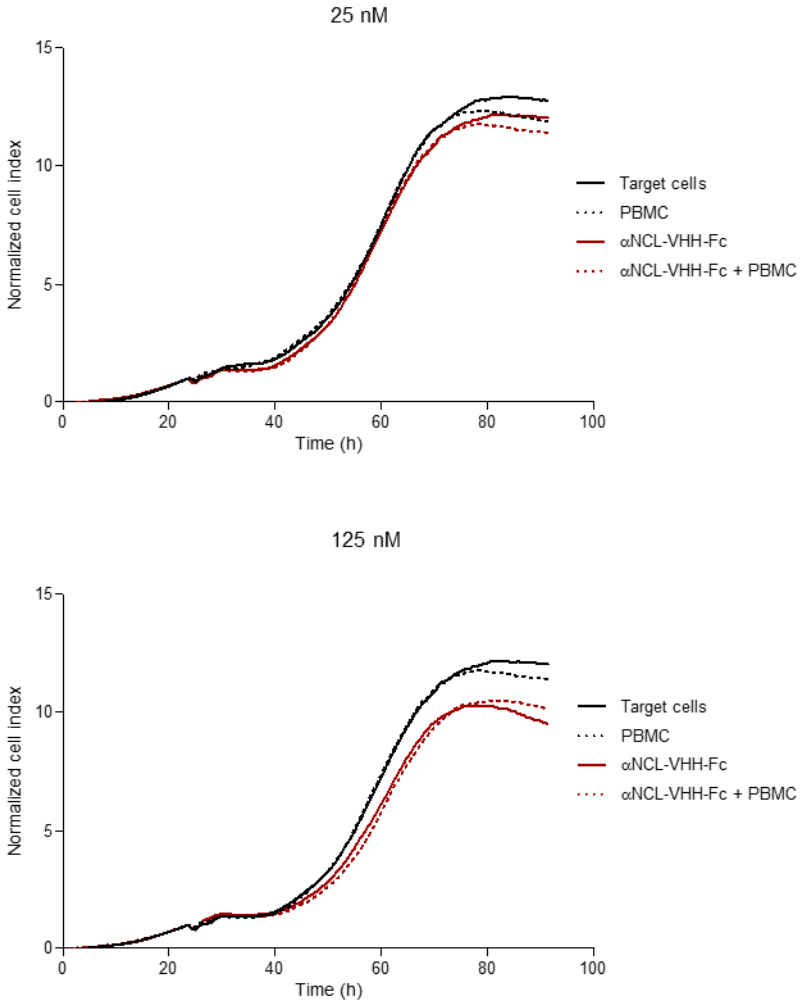

Figure 3.8. ADCC effect of nanobody-Fc antibody against 4T1 mouse cancer cells. 4T1 cells, previously cultured in a RTCA plate for 24 h, were incubated with the anti-nucleolin nanobody-Fc (αNCL-VHH-Fc, red) or control antibody (parental VHH-Fc, blue), at a concentration of 25 or 125 nM, without (solid lines) or with human PBMCs (at a target cells/PBMCs ratio of 1:10 or 1:5 ratio, dotted lines), for 72 h. Cell index, normalized to the beginning of the incubation, was measured every 15 min, using the xCELLigence system.

blood circulation time, due to the presence of the Fc region[120,188]. In addition, the human IgG1-derived Fc domain can potentially enable a strong ADCC effect[113,115,116,118]. This is

of particular importance towards antibody therapies with increased efficacy, being an area still unexplored in the context of nucleolin targeting[80–82,87].

The use of antibodies in a nanobody-Fc format might enable additional pharmacodynamics features, besides the potential for ADCC effects. In fact, VHH-Fc are dimeric proteins, thus increasing the binding avidity and, subsequently, the cytotoxic effects, relative to the nanobodies alone[196]. This could support the overall increased cytotoxicity (in the nanomolar range) enabled by the anti-nucleolin nanobody-Fc antibody (in the micromolar range), relative to its VHH counterpart. Although the increased extent of cytotoxicity of the former could be supported by the presence of two VHH monomers[196], other mechanisms are likely to contribute to this effect, as even twice the concentration of nanobody does not enable an effect as strong as the VHH-Fc counterpart. A similar observation has been reported for cetuximab and its Fab counterpart, with the former presenting higher cytotoxicity than the latter, at concentrations of 66 and 132 nM, respectively. However, a Fab2' fragment (bivalent) counterpart presented similar cytotoxicity to cetuximab, suggesting that the higher cytotoxicity enabled by the IgG and Fab2' antibodies, relative to Fab, derived from their ability to bind to two target receptors simultaneously[197]. It is interesting to notice that the level of cell death enabled by the anti-nucleolin VHH-Fc against MDA-MB-231 cells was, approximately, 80% lower than the one enabled by anti-nucleolin scFv, 4LB5[87]. Differences on the targeted epitope and format could account for the differences in activity. While the former binds to the N-terminal domain of nucleolin, through a sequence derived from the F3 peptide[23], the latter binds to the central domain[87].

Despite its lower cytotoxicity relative to the anti-nucleolin scFv 4LB5, the anti-nucleolin VHH-Fc antibody herein developed was able to trigger a nucleolin-dependent ADCC effect against MDA-MB-435S cells. The protein concentration initially used for this assay was 25 nM, within the range used for similar *in vitro assays* with antibodies currently used in the clinic and with proven ADCC activity, which commonly varies between 6 nM and 600 nM[118,198–202].

None of the human anti-nucleolin antibody formats developed so far, both human full-length IgG1 antibodies[89] and the human scFV 4LB5[87], have been associated with ADCC activity, notwithstanding CDC activity has been reported for the former[89]. This can be intriguing as the former format incorporates a Fc domain. An important characteristic that differentiates the antibody formats herein developed (targeting nucleolin N-terminal) from the ones previously reported is the targeted domain of nucleolin. Anti-nucleolin full-length antibodies previously developed target either the central domain or the C-terminal domain of nucleolin[89], whereas the scFv 4LB5 targets the central domain[87]. Interestingly, the capacity of an antibody to trigger ADCC and the extent of this response depends on the epitope to which the antibody binds[203–205]. The anti-nucleolin VHH-Fc antibody was generated from the N-terminal-binding F3 peptide[23], likely enabling binding to the target protein N-terminal, different from the binding domains of the anti-nucleolin proteins aforementioned. This difference could support the nucleolin-mediated ADCC effect associated with the anti-nucleolin VHH-Fc antibody herein developed.

Several molecules (including antibodies and chemotherapeutic drugs) are known to play a role in the recruitment of the immune system, in a Fc-independent manner (and thus, ADCC-independent mechanism)[206]. Therefore, in the ADCC assays, a control using the nanobody counterpart was included (without Fc domain). The fact that an anti-nucleolin VHH (grafted onto CDR3) and the F3 peptide were able to induce an increased PBMC-dependent MDA-MB-435S cell death, relative to the parental VHH, suggested that nucleolin targeting might modulate Fc-independent immune responses. This is an observation reported with antibodies, such as bevacizumab, trastuzumab and cetuximab, but also tyrosine kinase inhibitors, such as erlotinib[206]. Incubation of EGFR-targeting agents (with and without Fc domain) with different EGFR-overexpressing cells, led to increased MHCI and MHCII expression, resulting in increased CD4 T cell responses[207,208]. As nucleolin interacts with EGFR at the cell surface[36,38], clarifying whether the same type of mechanisms occur upon nucleolin targeting would be

important, to thoroughly characterize the mechanism of action of nucleolin-targeting entities.

Despite this ADCC effect of the anti-nucleolin VHH-Fc antibody, this type of response was not observed with 4T1 cancer cells, even upon increasing protein concentration, matching values for other antibodies reported to trigger an ADCC effect[209]. This lack of activity could rely on the lower expression of surface nucleolin in these cells, when compared with MDA-MB-435S (45000 and 102000 molecules/cell, respectively; JN Moreira, personal communication), as higher antigen density correlates with stronger ADCC responses[103,189,210,211].

The results presented in this chapter support an ADCC activity of anti-nucleolin nanobody-Fc antibody against some target cancer cells. This is, to the author's best knowledge, the first anti-nucleolin agent with ADCC activity. Due to the recognized importance of this kind of mechanism in cancer therapy, this new entity could pave the way for a new nucleolin-targeting therapeutic strategy.

Chapter 4

Conclusions and Future Perspectives

The development of antibodies for cancer therapy has been a major breakthrough that allowed a marked improvement in the patients' outcome for several types of malignancies[109]. The increasing understanding on the biology underlying tumor development, has enabled new research approaches to tackle this disease.

However, for some types of cancer this has been particularly difficult, as the case of triple-negative breast cancer. The fact that these tumors do not express any of the common breast cancer markers (ER, PR or HER2) has hampered the development of targeted therapies[212], in contrast to HER2-positive tumors. In this respect, the approval of the anti-HER2 monoclonal antibody, trastuzumab, enabled an improvement of therapeutic outcome in the treatment of HER2-overexpressing early-stage and metastatic breast cancer, as well as metastatic gastric cancer. Therefore, unraveling new relevant targets for subtypes of cancer that have not been contemplated so far with targeted treatments has been a major focus of research[4].

The notion of the tumor microenvironment as a central player in tumor progression, has been supporting the concept of therapeutic target in the tumor stroma[5], namely the tumor vasculature[8]. In this respect, nucleolin is a multifunctional protein (reviewed by Fonseca *et al.*[213]), with an expression pattern that makes it a promising therapeutic target: (i) it is expressed on the surface of cancer cells and angiogenic endothelial cells and (ii) is involved in several pathways that regulate tumor cell proliferation[87,214].

This work aimed at developing new anti-nucleolin antibody formats for anticancer therapy, including formats enabling antibody-dependent cell-mediated cytotoxicity (ADCC), a strategy so far unexplored in the context of nucleolin.

The results presented in this thesis support the following main conclusions:

(i) F3 peptide-based grafting onto the CDRs of a nanobody is a suitable strategy for generation of anti-nucleolin antibody formats, as confirmed by their binding to both purified nucleolin and cancer and endothelial cells, regardless of the grafted CDR (CDR1 or CDR3);

(ii) these nanobodies can have bispecific properties, as evidenced by the additional binding to TNF-α protein;

(iii) anti-nucleolin nanobodies presented cytotoxicity against cancer cell lines and an angiogenic endothelial cell line);

(iv) nanobodies grafted onto CDR3 evidenced higher binding and cytotoxicity than the corresponding counterparts grafted onto CDR1;

(v) increased CDR flexibility, conferred by the presence of linkers at each end of the grafted CDR, did not enable improved binding or cytotoxicity;

(vi) anti-nucleolin nanobody fusion to a Fc domain from human IgG1, originating a nanobody-Fc antibody format, enabled increased cytotoxicity and nucleolin-mediated ADCC against the MDA-MB-435S cancer cell line.

Overall, the construct developed in this project could pave the way to explore novel antitumor mechanisms of action, namely potentially affecting both cancer cells and tumor blood vessels. Notwithstanding studies addressing ADCC effects on endothelial cells remain scarce, there are reports suggesting that these effects can also be triggered against these cells[215]. Moreover, the demonstrated binding specific (towards nucleolin and TNF-α), supports the flexibility of the grafting strategy herein used, to develop the same kind of construct for virtually any target.

Future characterization of pharmacokinetics of the developed antibody formats, along with the effect on tumor growth and tumor vasculature will provide additional information on their therapeutic potential. As the anti-nucleolin antibody has a molecular weight of approximately 84 kDa and this has been proposed to be the most appropriate antibody size for long circulation times, while retaining tumor accumulation, this construct could impact tumor growth, while presenting low toxicity.

Evaluation of the *in vivo* contribution of ADCC for effective therapeutic outcomes remains a challenging task, as the human and mouse immune systems present relevant differences, namely regarding the affinity of Fc domain of antibodies towards Fc

receptors at the surface of the immune cells[216]. Some recently developed mouse models, aiming at better recapitulating the human immune system, may offer promising tools for this evaluation[217,218]. These models lack not only functional T and B cells, but also mature NK cells, resulting in improved engraftment of human cancer cells and allowing ADCC evaluation upon (intravenous) inoculation of human NK cells[217,218].

Notwithstanding anti-nucleolin proteins enabled the highest extent of cytotoxicity against 4T1 cancer cells, the absence of an ADCC effect against this cancer cell line was in contrast with the one observed with MDA-MB-435S cancer cells. This could rely on the lower levels of surface nucleolin in the latter (JN Moreira, personal communication), as ADCC responses are affected by antigen density at the target cells. It would be relevant to determine whether the absence the mentioned ADCC effect could be overcome with strategies such as potentiation of NK cell activity with IL-2 and IL-15[199,219,220].

Alternative strategies to boost ADCC-based immune responses could encompass, for example, altering the carbohydrates bound to the Fc (mainly by reduction of the fucose levels) or performing specific amino acid substitutions in the Fc sequence. Supporting the validity of these strategies, an anti-EGFR IgG1 antibody, with reduced fucose levels, presented improved *in vitro* ADCC capacity and increased survival in an *in vivo* model of colorectal cancer, relative to cetuximab, notwithstanding the similar *in vitro* antiproliferative effect presented by both antibodies[221]. Moreover, this glycoengineered antibody enabled ADCC responses upon incubation with NK cells from colorectal cancer patients, even when the NK cells had impaired direct toxicity[222] In addition, low fucose versions of rituximab decreased the dependency of the extent of ADCC response from Fc receptors polymorphisms (usually associated with reduced ADCC response)[223], or from antigen density on target cells[224]. These examples support the relevance of such strategies not only in triggering ADCC, but also in compensating for the weaker immune response that could be observed in some cancer patients[225].

In conclusion, this work has resulted in anti-nucleolin antibodies (nanobodies and nanobody-Fc formats) with cytotoxic activity against cancer and endothelial cells and in the first anti-nucleolin antibody with ADCC activity. These new entities could pave the way for a nucleolin-based therapy that takes advantage of this mechanism. The versatile application associated with antibody molecules, as for example, ligands for targeted nanoparticles or glyco-engineered antibodies, further expands the potential of the constructs developed herein.

Appendix

Figure 1

Parental VHH – DNA sequence

ATGAAAAAGACAGCTATCGCGATTGCAGTGGCACTGGCTGGTTTCGCTACCGT
leader peptide

GGCCCAGGTGCAGCTGCAGGAATCTGGCGGTGGCCTGGTTCAGCCGGGTGGCAG

TCTGCGCCTGAGCTGTGCCGCCTCTGGTCGTACCTTTAGCGATCATTCTGGTTATA
CDR1

CCTACACGATTGGCTGGTTTCGTCAGGCGCCGGGCAAAGAACGTGAATTCGTGGC

CCGCATCTATTGGAGCTCTGGTAACACCTATTACGCAGATAGTGTTAAAGGCCGTT

TCGCCATTAGCCGCGATATCGCAAAAAATACCGTGGATCTGACGATGAACAATCTG

GAACCGGAAGATACCGCCGTTTATTACTGTGCAGCGCGTGATGGCATTCCGACGT
CDR3

CTCGCAGTGTGGAAAGCTATAACTACTGGGGTCAGGGCACCCAGGTGACCGTTAG

TAGCGGCCAGGCCGGCCAGCACCATCACCATCACCATGGCGCATACCCGTACGAC
histidine tag

GTTCCGGACTACGCTTCTTAG
HA tag

Parental VHH – Protein sequence

M K K T A I A I A V A L A G F A T V A Q A A Q V Q L Q E S G G G L V Q P G G S L R

leader peptide

L S C A A S G R T F S D H S G Y T Y T I G W F R Q A P G K E R E F V A R I Y W S S

CDR1

G N T Y Y A D S V K G R F A I S R D I A K N T V D L T M N N L E P E D T A V Y Y C A

A R D G I P T S R S V E S Y N Y W G Q G T Q V T V S S G Q A G Q H H H H H H G A

CDR3 *histidine tag*

Y P Y D V P D Y A S Stop

HA tag

αNCL-CDR1 VHH – DNA sequence

ATGAAAAAGACAGCTATCGCGATTGCAGTGGCACTGGCTGGTTTCGCTACCGTGGCCC

leader peptide

AGGCGGCCCAGGTGCAGCTGCAGGAATCTGGCGGTGGCCTGGTTCAGCCGGGTGGCA

GTCTGCGCCTGAGCTGTGCCGCCTCTCCGCAGCGTCGTAGCGCGCGTCTGAGCGCGT

CDR1

GGTTTCGTCAGGCGCCGGGCAAAGAACGTGAATTCGTGGCCCGCATCTATTGGAGCTC

TGGTAACACCTATTACGCAGATAGTGTTAAAGGCCGTTTCGCCATTAGCCGCGATATCG

CAAAAAATACCGTGGATCTGACGATGAACAATCTGGAACCGGAAGATACCGCCGTTTAT

TACTGTGCAGCGCGTGATGGCATTCCGACGTCTCGCAGTGTGGAAAGCTATAACTACT

GGGGTCAGGGCACCCAGGTGACCGTTAGTAGCGGCCAGGCCGGCCAGCACCATCACC

histidine tag

ATCACCATGGCGCATACCCGTACGACGTTCCGGACTACGCTTCTTAG

HA tag

αNCL-CDR1 VHH – Protein sequence

M K K T A I A I A V A L A G F A T V A Q A A Q V Q L Q E S G G G L V Q P G G S L R L S C

leader peptide

A A S P Q R R S A R L S A W F R Q A P G K E R E F V A R I Y W S S G N T Y Y A D S V K

CDR1

G R F A I S R D I A K N T V D L T M N N L E P E D T A V Y Y C A A R D G I P T S R S V E

S Y N Y W G Q G T Q V T V S S G Q A G Q H H H H H H G A Y P Y D V P D Y A S

histidine tag *HA tag*

αNCL-CDR3 VHH – DNA sequence

ATGAAAAAGACAGCTATCGCGATTGCAGTGGCACTGGCTGGTTTCGCTACCGTGGCCC

leader peptide

AGGTGCAGCTGCAGGAATCTGGCGGTGGCCTGGTTCAGCCGGGTGGCAGTCTGCGCC

TGAGCTGTGCCGCCTCTGGTCGTACCTTTAGCGATCATTCTGGTTATACCTACACGATT

GGCTGGTTTCGTCAGGCGCCGGGCAAAGAACGTGAATTCGTGGCCCGCATCTATTGGA

GCTCTGGTAACACCTATTACGCAGATAGTGTTAAAGGCCGTTTCGCCATTAGCCGCGAT

ATCGCAAAAAATACCGTGGATCTGACGATGAACAATCTGGAACCGGAAGATACCGCCGT

TTATTACTGTGCAGCGCCGCAGCGTCGTAGCGCGCGTCTGAGCGCGTGGGGTCAGGG

CDR3

CACCCAGGTGACCGTTAGTAGCGGCCAGGCCGGCCAGCACCATCACCATCACCATGG

histidine tag

CGCATACCCGTACGACGTTCCGGACTACGCTTCTTAG

HA tag

αNCL-CDR3 VHH – Protein sequence

M K K T A I A I A V A L A G F A T V A Q A A Q V Q L Q E S G G G L V Q P G G S L R L S C
leader peptide

A A S G R T F S D H S G Y T Y T I G W F R Q A P G K E R E F V A R I Y W S S G N T Y Y

A D S V K G R F A I S R D I A K N T V D L T M N N L E P E D T A V Y Y C A A P Q R R S
CDR3

A R L S A W G Q G T Q V T V S S G Q A G Q H H H H H H G A Y P Y D V P D Y A S Stop
histidine tag *HA tag*

αNCL-CDR1-L VHH – DNA sequence

ATGAAAAAGACAGCTATCGCGATTGCAGTGGCACTGGCTGGTTTCGCTACCGTGGCCC
leader peptide

AGGCGGCCCAGGTGCAGCTGCAGGAATCTGGCGGTGGCCTGGTTCAGCCGGGTGGCA

GTCTGCGCCTGAGCTGTGCCGCCTCTAGCGGCGGCGGCAGCCCGCAGCGTCGTAGC
CDR1

GCGCGTCTGAGCGCGAGCGGCGGCGGCAGCTGGTTTCGTCAGGCGCCGGGCAAAGA

ACGTGAATTCGTGGCCCGCATCTATTGGAGCTCTGGTAACACCTATTACGCAGATAGTG

TTAAAGGCCGTTTCGCCATTAGCCGCGATATCGCAAAAAATACCGTGGATCTGACGATG

AACAATCTGGAACCGGAAGATACCGCCGTTTATTACTGTGCAGCGCGTGATGGCATTCC

GACGTCTCGCAGTGTGGAAAGCTATAACTACTGGGGTCAGGGCACCCAGGTGACCGTT

AGTAGCGGCCAGGCCGGCCAGCACCATCACCATCACCATGGCGCATACCCGTACGAC
histidine tag *HA tag*

GTTCCGGACTACGCTTCTTAG

αNCL-CDR1-L VHH – Protein sequence

M K K T A I A I A V A L A G F A T V A Q A A Q V Q L Q E S G G G L V Q P G G S L R L S C
leader peptide

A A S S G G G S P Q R R S A R L S A S G G G S W F R Q A P G K E R E F V A R I Y W S
CDR1

S G N T Y Y A D S V K G R F A I S R D I A K N T V D L T M N N L E P E D T A V Y Y C A A

R D G I P T S R S V E S Y N Y W G Q G T Q V T V S S G Q A G Q H H H H H H G A Y P Y
histidine tag

D V P D Y A S
HA tag

αNCL-CDR3-L VHH – DNA sequence

ATGAAAAAGACAGCTATCGCGATTGCAGTGGCACTGGCTGGTTTCGCTACCGTGGCCC
leader peptide

AGGTGCAGCTGCAGGAATCTGGCGGTGGCCTGGTTCAGCCGGGTGGCAGTCTGCGCC

TGAGCTGTGCCGCCTCTGGTCGTACCTTTAGCGATCATTCTGGTTATACCTACACGATT

GGCTGGTTTCGTCAGGCGCCGGGCAAAGAACGTGAATTCGTGGCCCGCATCTATTGGA

GCTCTGGTAACACCTATTACGCAGATAGTGTTAAAGGCCGTTTCGCCATTAGCCGCGAT

ATCGCAAAAAATACCGTGGATCTGACGATGAACAATCTGGAACCGGAAGATACCGCCGT

TTATTACTGTGCAGCGAGCGGCGGCGGCAGCCCGCAGCGTCGTAGCGCGCGTCTGAG
CDR3

CGCGAGCGGCGGCGGCAGCTGGGGTCAGGGCACCCAGGTGACCGTTAGTAGCGGCC

AGGCCGGCCAGCACCATCACCATCACCATGGCGCATACCCGTACGACGTTCCGGACTA
histidine tag *HA tag*

CGCTTCTTAG

αNCL-CDR3-L VHH – DNA sequence

MKKTAIAIAVALAGFATVAQAAQVQLQESGGGLVQPGGSLRLSC

leader peptide

AASGRTFSDHSGYTYTIGWFRQAPGKEREFVARIYWSSGNTYY

ADSVKGRFAISRDIAKNTVDLTMNNLEPEDTAVYYCAA SGGGS

PQRRSARLSASGGGS WGQGTQVTVSSGQAGQ HHHHHH GAYP

CDR3 *histidine tag*

YDVPDYAS Stop

HA tag

αNCL-VHH-Fc – DNA sequence

ATGTACAGGATGCAACTCCTGTCTTGCATTGCACTAAGTCTTGCACTTGTCACGAATTC

IL2 ss

GATATCGGCCATGGAA**CAGGTGCAGCTGCAGGAATCTGGCGGTGGCCTGGTTCAGCC**

GGGTGGCAGTCTGCGCCTGAGCTGTGCCGCCTCTGGTCGTACCTTTAGCGATCATTCT

GGTTATACCTACACGATTGGCTGGTTTCGTCAGGCGCCGGGCAAAGAACGTGAATTC

anti-nucleolinVHH

GTGGCCCGCATCTATTGGAGCTCTGGTAACACCTATTACGCAGATAGTGTTAAAGGC

CGTTTCGCCATTAGCCGCGATATCGCAAAAAATACCGTGGATCTGACGATGAACAAT

CTGGAACCGGAAGATACCGCCGTTTATTACTGTGCAGCGAGCGGCGGCGGCCCGCA

GCGTCGTAGCGCGCGTCTGAGCGCGTGGGGTCAGGGCACCCAGGTGACCGTTAGTA

GCGACAAAACTCACACATGCCCACCGTGCCCAGCACCTGAACTCCTGGGGGGACCGT

IgG1 Fc

CAGTCTTCCTCTTCCCCCCAAAACCCAAGGACACCCTCATGATCTCCCGGACCCCTGA

GGTCACATGCGTGGTGGTGGACGTGAGCCACGAAGACCCTGAGGTCAAGTTCAACTGG

TACGTGGACGGCGTGGAGGTGCATAATGCCAAGACAAAGCCGCGGGAGGAGCAGTAC

AACAGCACGTACCGTGTGGTCAGCGTCCTCACCGTCCTGCACCAGGACTGGCTGAATG

GCAAGGAGTACAAGTGCAAGGTCTCCAACAAAGCCCTCCCAGCCCCCATCGAGAAAAC

CATCTCCAAAGCCAAAGGGCAGCCCCGAGAACCACAGGTGTACACCCTGCCCCCATCC

CGGGAGGAGATGACCAAGAACCAGGTCAGCCTGACCTGCCTGGTCAAAGGCTTCTATC

CCAGCGACATCGCCGTGGAGTGGGAGAGCAATGGGCAGCCGGAGAACAACTACAAGA

CCACGCCTCCCGTGCTGGACTCCGACGGCTCCTTCTTCCTCTACAGCAAGCTCACCGT

GGACAAGAGCAGGTGGCAGCAGGGGAACGTCTTCTCATGCTCCGTGATGCACGAGGC

TCTGCACAACCACTACACGCAGAAGAGCCTCTCCCTGTCTCCGGGTAAATGA

αNCL-VHH-Fc – Protein sequence

M Y R M Q L L S C I A L S L A L V T N S I S A M E **Q V Q L Q E S G G G L V Q P G G S L**

IL2 ss

R L S C A A S G R T F S D H S G Y T Y T I G W F R Q A P G K E R E F V A R I Y W S S G

anti-nucleolinVHH

N T Y Y A D S V K G R F A I S R D I A K N T V D L T M N N L E P E D T A V Y Y C A A P

Q R R S A R L S A W G Q G T Q V T V S S D K T H T C P P C P A P E L L G G P S V F L F

P P K P K D T L M I S R T P E V T C V V V D V S H E D P E V K F N W Y V D G V E V H N

IgG1 Fc

A K T K P R E E Q Y N S T Y R V V S V L T V L H Q D W L N G K E Y K C K V S N K A L P

A P I E K T I S K A K G Q P R E P Q V Y T L P P S R E E M T K N Q V S L T C L V K G F Y

P S D I A V E W E S N G Q P E N N Y K T T P P V L D S D G S F F L Y S K L T V D K S R

W Q Q G N V F S C S V M H E A L H N H Y T Q K S L S L S P G K Stop

Table 1 . PCR conditions for CDR grafting

Temperature	Time	Number of cycles
98 °C	30 s	1
98 °C	10 s	35
58 °C	30 s	
72 °C	30 s	
72 °C	10 min	1

Table 2 . PCR conditions for colony screening

Temperature	Time	Number of cycles
95 °C	5 min	1
95 °C	30 s	30
58 °C	30 s	
72 °C	30 s	
72 °C	10 min	1

Table 3 . List of primers

CDR1-F	5’ AGCTGTGCCGCCTCTCCGCAGCGTCGTAGCGCGCGTCTGAGCGCGT GGTTTCGTCAGGCG
CDR1-R	5’ CGCGCTCAGACGCGCGCTACGACGCTGCGGAGAGGCGGCACAGCT
CDR1L-F	5’ AGCTGTGCCGCCTCTAGCGGCGGCGGCAGCCCGCAGCGTCGTAGCG CGCGTCTGAGCGCGAGCGGCGGCGGCAGCTGGTTTCGTCAGGCG
CDR1L-R	5’ CGCGCTCAGACGCGCGCTACGACGCTGCGGGCTGCCGCCGCCGCTA GAGGCGGCACAGCT
CDR3-F	5’ TATTACTGTGCAGCGCCGCAGCGTCGTAGCGCGCGTCTGAGCGCGTG GGGTCAGGGCACC
CDR3-R	5’ CGCGCTCAGACGCGCGCTACGACGCTGCGGCGCTGCACAGTAATA
CDR3L-F	5’ TATTACTGTGCAGCGCCGCAGCGTCGTAGCGCGCGTCTGAGCGCGTG GGGTCAGGGCACC
CDR3L-R	5’ CGCGCTCAGACGCGCGCTACGACGCTGCGGCGCTGCACAGTAATA
HindII-LP-F	5’ AAGCTTATGAAAAAGACAGCTATCGCGATTGCAGTGGCACTGGCTGGT TTCGCTACCGTGGCCCAGGCGGCCCA
HA-BglII-R	5’ AATGGAAGATCTTTATTAGCTCGCGTAATCAGGCACGTCGTAG
NcoI-VHH-F	5’ AAACCATGGAACAGGTGCAGCTGCAG
VHH-BglII-R	5’ ATAAGATCTGCTACTAACGGTCACCC

References

1. Torre, L. A. *et al.* Global Cancer Statistics, 2012. *CA A Cancer J. Clin.* **65,** 87–108 (2015).

2. Nounou, M. I. *et al.* Breast Cancer: Conventional Diagnosis and Treatment Modalities and Recent Patents and Technologies. *Breast Cancer Basic Clin. Res.* **9,** 17–34 (2015).

3. Schmadeka, R., Harmon, B. E. & Singh, M. Triple-negative breast carcinoma: Current and emerging concepts. *Am. J. Clin. Pathol.* **141,** 462–477 (2014).

4. Tomao, F. *et al.* Triple-negative breast cancer: New perspectives for targeted therapies. *Onco. Targets. Ther.* **8,** 177–193 (2015).

5. Hanahan, D. & Weinberg, R. A. Hallmarks of cancer: the next generation. *Cell* **144,** 646–674 (2011).

6. Hanahan, D. & Coussens, L. M. Accessories to the Crime: Functions of Cells Recruited to the Tumor Microenvironment. *Cancer Cell* **21,** 309–322 (2012).

7. Yuan, Y., Jiang, Y.-C., Sun, C.-K. & Chen, Q.-M. Role of the tumor microenvironment in tumor progression and the clinical applications. *Oncol. Rep.* **35,** 2499–2515 (2016).

8. Albini, A., Tosetti, F., Li, V. W., M., D. & Li, W. W. Cancer prevention by targeting angiogenesis. *Nat. Rev. Clin. Oncol.* **9,** 498–50 (2012).

9. Fukumura, D. & Jain, R. K. Tumor microvasculature and microenvironment-Targets for antiangiogenesis and normalization. *Microvasc. Res.* **141,** 520–529 (2008).

10. Bergers, G. & Benjamin, L. E. Tumorigenesis and the angiogenic switch. *Nat. Rev. Cancer* **3,** 401–410 (2003).

11. Ariffin, A. B., Forde, P. F., Jahangeer, S., Soden, D. M. & Hinchion, J. Releasing pressure in tumors: What do we know so far and where do we go from here a review. *Cancer Res.* **74,** 2655–2662 (2014).

12. Harlozinska, A. Progress in Molecular Mechanisms of Tumor Metastasis and Angiogenesis. *Anticancer Res.* **3334,** 3327–3333 (2005).

13. Ebos, J. M. L. & Kerbel, R. S. Antiangiogenic therapy: impact on invasion,

disease progression, and metastasis. *Nat. Rev. Clin. Oncol.* **8,** 210–221 (2011).

14. Liu, T. *et al.* Combination gene therapy using VEGF-shRNA and fusion suicide gene yCDglyTK inhibits gastric carcinoma growth. *Exp. Mol. Pathol.* **91,** 745–752 (2011).

15. Huang, S. *et al.* Tumor-Targeting and Smart Nanoparticles for Combination Therapy of Angiogenesis and Apoptosis. *ACS Nano* **7,** 2860–2871 (2013).

16. Orrick, L. R., Olson, M. J. & Busch, H. Comparison of Nucleolar Proteins of Normal Rat Liver and Novikoff Hepatoma Ascites Cells by Two-Dimensional Polyacrylamide Gel Electrophoresis. *Proc. Natl. Acad. Sci. U. S. A.* **70,** 1316–1320 (1973).

17. Bugler, B., Caizergues-Ferrer, M., Bouche, G., Bourbon, H. & Amalric, F. Detection and localization of a class of proteins immunologically related to a 100-kDa nucleolar protein. *Eur. J. Biochem.* **128,** 475–480 (1982).

18. Roussel, P. & Hernandez-Verdun, D. Identification of Ag-NOR proteins, Markers of Proliferation Related to Ribosomal Gene Activity. *Exp. Cell Res.* **214,** 465–472 (1994).

19. Ginisty, H., Sicard, H., Roger, B. & Bouvet, P. Structure and functions of nucleolin. *J. Cell Sci.* **112,** 761–72 (1999).

20. Srivastava, M. & Pollard, H. B. Molecular dissection of nucleolin's role in growth and cell proliferation: new insights. *FASEB J.* **13,** 1911–1922 (1999).

21. Tajrishi, M. M., Tuteja, R. & Tuteja, N. Nucleolin: The most abundant multifunctional phosphoprotein of nucleolus. *Commun. Integr. Biol.* **4,** 267–275 (2011).

22. Hovanessian, A. G. *et al.* The cell-surface-expressed nucleolin is associated with the actin cytoskeleton. *Exp. Cell Res.* **261,** 312–28 (2000).

23. Christian, S. *et al.* Nucleolin expressed at the cell surface is a marker of endothelial cells in angiogenic blood vessels. *J. Cell Biol.* **163,** 871–878 (2003).

24. Fonseca, N. A. *et al.* Nucleolin overexpression in breast cancer cell sub-populations with different stem-like phenotype enables targeted intracellular delivery of synergistic drug combination. *Biomaterials* **69,** 76–88 (2015).

25. Visvader, J. E. & Lindeman, G. J. Cancer stem cells: Current status and evolving complexities. *Cell Stem Cell* **10,** 717–728 (2012).

26. Pattabiraman, D. R. & Weinberg, R. A. Tackling the cancer stem cells - what challenges do they pose? *Nat. Rev. Drug Discov.* **13,** 497–512 (2014).

27. Hovanessian, A. G. *et al.* Surface expressed nucleolin is constantly induced in tumor cells to mediate calcium-dependent ligand internalization. *PLoS One* **5,** e15787 (2010).

28. Stepanova, V. *et al.* Nuclear translocation of urokinase-type plasminogen activator. *Blood* **112,** 100–110 (2008).

29. Said, E. A. *et al.* The anti-HIV cytokine midkine binds the cell surface-expressed nucleolin as a low affinity receptor. *J. Biol. Chem.* **277,** 37492–37502 (2002).

30. Said, E. A. *et al.* Pleiotrophin inhibits HIV infection by binding the cell surface-expressed nucleolin. *FEBS J.* **272,** 4646–4659 (2005).

31. Legrand, D. *et al.* Surface nucleolin participates in both the binding and endocytosis of lactoferrin in target cells. *Eur. J. Biochem.* **271,** 303–317 (2004).

32. Zhuo, W. *et al.* Endostatin inhibits tumour lymphangiogenesis and lymphatic metastasis via cell surface nucleolin on lymphangiogenic endothelial cells. *J. Pathol.* **222,** 249–260 (2010).

33. Take, M. *et al.* Identification of Nucleolin as a Binding Protein for Midkine (MK) and Heparin-Binding Growth Associated Molecule (HB-GAM). *J. Biochem.* **116,** 1063–1068 (1994).

34. Shi, H. *et al.* Nucleolin is a receptor that mediates antiangiogenic and antitumor activity of endostatin. *Blood* **110,** 2899–2906 (2007).

35. Di Segni, A., Farin, K. & Pinkas-Kramarski, R. Identification of nucleolin as new ErbB receptors-interacting protein. *PLoS One* **3,** e2310 (2008).

36. Farin, K. *et al.* Oncogenic synergism between ErbB1, nucleolin, and mutant Ras. *Cancer Res.* **71,** 2140–2151 (2011).

37. Schokoroy, S., Juster, D., Kloog, Y. & Pinkas-Kramarski, R. Disrupting the Oncogenic Synergism between Nucleolin and Ras Results in Cell Growth

Inhibition and Cell Death. *PLoS One* **8,** e75269 (2013).

38. Goldshmit, Y., Trangle, S. S., Kloog, Y. & Pinkas-Kramarski, R. Interfering with the interaction between ErbB1, nucleolin and Ras as a potential treatment for glioblastoma. *Oncotarget* **5,** 8602–13 (2014).

39. Wise, J. F. *et al.* Nucleolin inhibits Fas ligand binding and suppresses Fas-mediated apoptosis in vivo via a surface nucleolin-Fas complex. *Blood* **121,** 4729–4739 (2013).

40. Tate, A. *et al.* Met-Independent Hepatocyte Growth Factor-mediated regulation of cell adhesion in human prostate cancer cells. *BMC Cancer* **6,** (2006).

41. Chen, S.-C. *et al.* Hepatoma-derived growth factor/nucleolin axis as a novel oncogenic pathway in liver carcinogenesis. *Oncotarget* **6,** 16253–16270 (2015).

42. Yang, X. *et al.* Cell surface nucleolin is crucial in the activation of the CXCL12/CXCR4 signaling pathway. *Tumor Biol.* **35,** 333–338 (2014).

43. Lv, S. *et al.* Cell Surface Protein C23 Affects EGF-EGFR Induced Activation of ERK and PI3K-AKT Pathways. *J. Mol. Neurosci.* **55,** 519–524 (2014).

44. Dai, C. *et al.* Nuclear Protein C23 on the Cell Surface Plays an Important Role in Activation of CXCR4 Signaling in Glioblastoma. *Mol. Neurobiol.* **52,** 1521–1526 (2014).

45. Koutsioumpa, M. *et al.* Interplay between avb3 integrin and nucleolin regulates human endothelial and glioma cell migration. *J. Biol. Chem.* **288,** 343–354 (2013).

46. Moura, V. *et al.* Targeted and intracellular triggered delivery of therapeutics to cancer cells and the tumor microenvironment: impact on the treatment of breast cancer. *Breast Cancer Res. Treat.* **133,** 61–73 (2012).

47. Winer, I., Wang, S. & Lee, Y. K. F3-Targeted Cisplatin-Hydrogel Nanoparticles as an Effective Therapeutic That Targets Both Murine and Human Ovarian Tumor Endothelial Cells In vivo. *Cancer Res.* **70,** 8674–8683 (2010).

48. Reddy, G. R. *et al.* Vascular Targeted Nanoparticles for Imaging and Treatment of Brain Tumors argeted Nanoparticles for Imaging and T. *Clin. Cancer Res.* **12,** 6677–6686 (2006).

49. Drecoll, E. *et al.* Treatment of Peritoneal Carcinomatosis by Targeted Delivery of the Radio-Labeled Tumor Homing Peptide Bi-DTPA- [F3] 2 into the Nucleus of Tumor Cells. **4,** e5715 (2009).

50. Fonseca, N. A., Gomes-Da-Silva, L. C., Moura, V., Simões, S. & Moreira, J. N. Simultaneous active intracellular delivery of doxorubicin and C6-ceramide shifts the additive/antagonistic drug interaction of non-encapsulated combination. *J. Control. Release* **196,** 122–131 (2014).

51. Gomes-Da-Silva, L. C., Ramalho, J. S., Pedroso De Lima, M. C., Simões, S. & Moreira, J. N. Impact of anti-PLK1 siRNA-containing F3-targeted liposomes on the viability of both cancer and endothelial cells. *Eur. J. Pharm. Biopharm.* **85,** 356–364 (2013).

52. Shin, M. C. *et al.* Tandem-multimeric F3-gelonin fusion toxins for enhanced anti-cancer activity for prostate cancer treatment. *Int. J. Pharm.* **524,** 101–110 (2017).

53. Li, L. *et al.* Nucleolin-targeting liposomes guided by aptamer AS1411 for the delivery of siRNA for the treatment of malignant melanomas. *Biomaterials* **35,** 3840–3850 (2014).

54. Guo, J. *et al.* Aptamer-functionalized PEG-PLGA nanoparticles for enhanced anti-glioma drug delivery. *Biomaterials* **32,** 8010–8020 (2011).

55. Li, Z. *et al.* Aptamer-Capped Multifunctional Mesoporous Strontium Hydroxyapatite Nanovehicle for Cancer-Cell-Responsive Drug Delivery and Imaging. *Biomacromolecules* **13,** 4257–4263 (2012).

56. Song, C. *et al.* Nucleolin Targeting AS1411 Modified Protein Nanoparticle for Antitumor Drugs Delivery. *Mol. Pharm.* **10,** 3555–3563 (2013).

57. Latorre, A. *et al.* DNA and aptamer stabilized gold nanoparticles for targeted delivery of anticancer therapeutics. *Nanoscale* **6,** 7436–7442 (2014).

58. Ai, J., Xu, Y., Lou, B., Li, D. & Wang, E. Multifunctional AS1411-functionalized fluorescent gold nanoparticles for targeted cancer cell imaging and efficient photodynamic therapy. *Talanta* **118,** 54–60 (2014).

59. Gao, H. *et al.* Precise glioma targeting of and penetration by aptamer and

peptide dual-functioned nanoparticles. *Biomaterials* **33,** 5115–5123 (2012).

60. Li, X., Zhu, X. & Qiu, L. Constructing aptamer anchored nanovesicles for enhanced tumor penetration and cellular uptake of water soluble chemotherapeutics. *Acta Biomater.* **35,** 269–279 (2016).

61. Luo, Z. *et al.* Precise glioblastoma targeting by AS1411 aptamer-functionalized poly (l-γ-glutamylglutamine)–paclitaxel nanoconjugates. *J. Colloid Interface Sci.* **490,** 783–796 (2017).

62. Soundararajan, S., Chen, W., Spicer, E. K., Courtenay-Luck, N. & Fernandes, D. J. The nucleolin targeting aptamer AS1411 destabilizes Bcl-2 messenger RNA in human breast cancer cells. *Cancer Res.* **68,** 2358–2365 (2008).

63. Pichiorri, F. *et al.* In vivo NCL targeting affects breast cancer aggressiveness through miRNA regulation. *J. Exp. Med. Med.* **210,** 951–68 (2013).

64. Girvan, A. C. *et al.* AGRO100 inhibits activation of nuclear factor-kB (NF-kB) by forming a complex with NF-kB essential modulator (NEMO) and nucleolin. *Mol. Cancer Ther.* **5,** 1790–1799 (2006).

65. Bates, P. J., Laber, D. A., Miller, D. M., Thomas, S. D. & Trent, J. O. Discovery and development of the G-rich oligonucleotide AS1411 as a novel treatment for cancer. *Exp. Mol. Pathol.* **86,** 151–64 (2009).

66. Bates, P. J. *et al.* G-quadruplex oligonucleotide AS1411 as a cancer-targeting agent: Uses and mechanisms. *Biochim. Biophys. Acta* **1861,** 1414–1428 (2017).

67. Aravind, A. *et al.* AS1411 aptamer tagged PLGA-lecithin-PEG nanoparticles for tumor cell targeting and drug delivery. *Biotechnol. Bioeng.* **109,** 2920–2931 (2012).

68. Zhang, J. *et al.* Nucleolin targeting AS1411 aptamer modified pH-sensitive micelles for enhanced delivery and antitumor efficacy of paclitaxel. *Nano Res.* **8,** 201–218 (2015).

69. Liao, Z. X. *et al.* An AS1411 aptamer-conjugated liposomal system containing a bubble-generating agent for tumor-specific chemotherapy that overcomes multidrug resistance. *J. Control. Release* **208,** 42–51 (2015).

70. Zhuang, Y. *et al.* Aptamer-Functionalized and Backbone Redox-Responsive

Hyperbranched Polymer for Targeted Drug Delivery in Cancer Therapy. *Biomacromolecules* **17,** 2050–2062 (2016).

71. Alibolandi, M., Ramezani, M., Abnous, K. & Hadizadeh, F. AS1411 Aptamer-Decorated Biodegradable Polyethylene Glycol-Poly(lactic-co-glycolic acid) Nanopolymersomes for the Targeted Delivery of Gemcitabine to Non-Small Cell Lung Cancer in Vitro. *J. Pharm. Sci.* **105,** 1741–1750 (2016).

72. Chen, Z. *et al.* Aptamer-mediated delivery of docetaxel to prostate cancer through polymeric nanoparticles for enhancement of antitumor efficacy. *Eur. J. Pharm. Biopharm.* **107,** 130–141 (2016).

73. Tao, W. *et al.* Polydopamine-based surface modification of novel nanoparticle-aptamer bioconjugates for in vivo breast cancer targeting and enhanced therapeutic effects. *Theranostics* **6,** 470–484 (2016).

74. Xu, G. *et al.* Robust aptamer-polydopamine-functionalized M-PLGA-TPGS nanoparticles for targeted delivery of docetaxel and enhanced cervical cancer therapy. *Int. J. Cancer* **11,** 2953–2965 (2016).

75. Alibolandi, M. *et al.* Smart AS1411-aptamer conjugated pegylated PAMAM dendrimer for the superior delivery of camptothecin to colon adenocarcinoma in vitro and in vivo. *Int. J. Pharm.* **519,** 352–364 (2017).

76. Wang, Y. *et al.* Nucleolin-targeted Extracellular Vesicles as a Versatile Platform for Biologics Delivery to Breast Cancer. *Theranostics* **7,** 1360–1372 (2017).

77. Mosafer, J., Abnous, K., Tafaghodi, M., Mokhtarzadeh, A. & Ramezani, M. In vitro and in vivo evaluation of anti-nucleolin-targeted magnetic PLGA nanoparticles loaded with doxorubicin as a theranostic agent for enhanced targeted cancer imaging and therapy. *Eur. J. Pharm. Biopharm.* **113,** 60–74 (2017).

78. Callebaut, C. *et al.* Inhibition of HIV infection by pseudopeptides blocking viral envelope glycoprotein-mediated membrane fusion and cell death. *Virology* **218,** 181–192 (1996).

79. Destouches, D. *et al.* Suppression of tumor growth and angiogenesis by a specific antagonist of the cell-surface expressed nucleolin. *PLoS One* **3,** e2518 (2008).

80. El Khoury, D. *et al.* Targeting surface nucleolin with a multivalent pseudopeptide delays development of spontaneous melanoma in RET transgenic mice. *BMC Cancer* **10,** 325 (2010).

81. Destouches, D. *et al.* A simple approach to cancer therapy afforded by multivalent pseudopeptides that target cell-surface nucleoproteins. *Cancer Res.* **71,** 3296–3305 (2011).

82. Krust, B., El Khoury, D., Nondier, I., Soundaramourty, C. & Hovanessian, A. G. Targeting surface nucleolin with multivalent HB-19 and related Nucant pseudopeptides results in distinct inhibitory mechanisms depending on the malignant tumor cell type. *BMC Cancer* **11,** 333 (2011).

83. Benedetti, E. *et al.* Nucleolin antagonist triggers autophagic cell death in human glioblastoma primary cells and decreased in vivo tumor growth in orthotopic brain tumor model. *Oncotarget* **6,** 42091–42104 (2015).

84. Birmpas, C., Briand, J. P., Courty, J. & Katsoris, P. Nucleolin mediates the antiangiogenesis effect of the pseudopeptide N6L. *BMC Cell Biol.* **13,** 32 (2012).

85. Gilles, M.-E. *et al.* Nucleolin targeting impairs the progression of pancreatic cancer and promotes the normalization of tumor vasculature. *Cancer Res.* (2016). doi:10.1158/0008-5472

86. Fogal, V., Sugahara, K. N., Ruoslahti, E. & Christian, S. Cell surface nucleolin antagonist causes endothelial cell apoptosis and normalization of tumor vasculature. *Angiogenesis* **12,** 91–100 (2009).

87. Palmieri, D. *et al.* Human anti-nucleolin recombinant immunoagent for cancer therapy. *Proc. Natl. Acad. Sci. U. S. A.* **112,** 9418–23 (2015).

88. Avino, C. D. *et al.* A novel fully human anti-NCL immunoRNase for triple-negative breast cancer therapy. *Oncotarget* **5,** (2016).

89. Natalie Sutkowski, Daniel Fernandes, Brian Hoel, S. R. Human monoclonal antibodies to human nucleolin. *U.S. Pat. 20160215050* (2016).

90. Krust, B., El Khoury, D., Soundaramourty, C., Nondier, I. & Hovanessian, A. G. Suppression of tumorigenicity of rhabdoid tumor derived G401 cells by the multivalent HB-19 pseudopeptide that targets surface nucleolin. *Biochimie* **93,**

426–433 (2011).

91. Dunn, G. P. *et al.* The Immunobiology of Cancer Immunosurveillance and Immunoediting. *Immunity* **21,** 137–148 (2004).

92. Vanneman, M. & Dranoff, G. Combining immunotherapy and targeted therapies in cancer treatment. *Nat Rev Cancer* **12,** 237–251 (2012).

93. Kazemi, T., Younesi, V., Jadidi-Niaragh, F. & Yousefi, M. Immunotherapeutic approaches for cancer therapy: An updated review. *Artif. Cells, Nanomedicine, Biotechnol.* 1–11 (2015). doi:10.3109/21691401.2015.1019669

94. Makkouk, A. & Weiner, G. J. Cancer immunotherapy and breaking immune tolerance: New approaches to an old challenge. *Cancer Res.* **75,** 5–10 (2015).

95. Hodi, S., O'Day, S., McDermott, D., Weber, R. & Sosman, J. Improved Survival with Ipilimumab in Patients with Metastatic Melanoma. *N. Engl. J. Med.* **363,** 711–723 (2010).

96. Pardoll, D. M. The blockade of immune checkpoints in cancer immunotherapy. *Nat. Rev. Cancer* **12,** 252–64 (2012).

97. Robert, C. *et al.* Pembrolizumab versus Ipilimumab in Advanced Melanoma. *N. Engl. J. Med.* **372,** 2521–2532 (2015).

98. Adams, G. P. & Weiner, L. M. Monoclonal antibody therapy of cancer. *Nat. Biotechnol.* **23,** 1147–1157 (2005).

99. Pares, S. & Mouz, N. The crystal structure of a llama heavy chain variable domain. *Nat. Struct. Biol.* **3,** 752–757 (1996).

100. Muyldermans, S. & Lauwereys, M. Unique single- domain antigen binding fragments derived from naturally occurring camel heavy-chain. *J. Mol. Recognit.* 131–140 (1999). doi:10.1002/(SICI)1099-1352(199903/04)12

101. Aires da Silva, F., Corte-Real, S. & Goncalves, J. Recombinant Antibodies as Therapeutic Agents. *Drug Dev.* **22,** 301–314 (2008).

102. Vidarsson, G., Dekkers, G. & Rispens, T. IgG subclasses and allotypes: From structure to effector functions. *Front. Immunol.* **5,** 1–17 (2014).

103. Velders, M. P. *et al.* The impact of antigen density and antibody affinity on

antibody-dependent cellular cytotoxicity: relevance for immunotherapy of carcinomas. *Br. J. Cancer* **78,** 478–483 (1998).

104. Tang, Y. *et al.* Regulation of antibody-dependent cellular cytotoxicity by IgG intrinsic and apparent affinity for target antigen. *J. Immunol.* **179,** 2815–2823 (2007).

105. Gancz, D. & Fishelson, Z. Cancer resistance to complement-dependent cytotoxicity (CDC): Problem-oriented research and development. *Mol. Immunol.* **46,** 2794–2800 (2009).

106. Li, M. *et al.* Promotion of cell proliferation and inhibition of ADCC by cancerous immunoglobulin expressed in cancer cell lines. *Cell. Mol. Immunol.* **9,** 54–61 (2012).

107. Weiner, L. M., Surana, R. & Wang, S. Monoclonal antibodies: versatile platforms for cancer immunotherapy. *Nat. Rev. Immunol.* **10,** 317–27 (2010).

108. Golay, J. & Introna, M. Mechanism of action of therapeutic monoclonal antibodies: Promises and pitfalls of in vitro and in vivo assays. *Arch. Biochem. Biophys.* **526,** 146–153 (2012).

109. Scott, A. M., Wolchok, J. D. & Old, L. J. Antibody therapy of cancer. *Nat. Rev. Cancer* **12,** 278–287 (2012).

110. Carter, P. Improving the efficacy of antibody-based cancer therapies. *Nat. Rev. Cancer* **1,** 118–129 (2001).

111. Lieberman, J. The ABCs of granule-mediated cytotoxicity: new weapons in the arsenal. *Nat. Rev. Immunol.* **3,** 361–370 (2003).

112. Cartron, G. *et al.* Therapeutic activity of humanized anti-CD20 monoclonal antibody and polymorphism in IgG Fc receptor FcγrIIIa gene. *Blood* **99,** 754–758 (2002).

113. Paiva, M. *et al.* FcγRIIa polymorphism and clinical response to rituximab in non-Hodgkin lymphoma patients. *Cancer Genet. Cytogenet.* **183,** 35–40 (2008).

114. Bibeau, F. *et al.* Impact of Fc RIIa-Fc RIIIa Polymorphisms and KRAS Mutations on the Clinical Outcome of Patients With Metastatic Colorectal Cancer Treated With Cetuximab Plus Irinotecan. *J. Clin. Oncol.* **27,** 1122–1129 (2009).

115. Musolino, A. *et al.* Immunoglobulin g fragment c receptor polymorphisms and clinical efficacy of trastuzumab-based therapy in patients with HER-2/neu-positive metastatic breast cancer. *J. Clin. Oncol.* **26,** 1789–1796 (2008).

116. Tamura, K. *et al.* FcgR2A and 3A polymorphisms predict clinical outcome of trastuzumab in both neoadjuvant and metastatic settings in patients with HER2-positive breast cancer. *Ann. Oncol.* **22,** 1302–1307 (2011).

117. Gennari, R. *et al.* Pilot Study of the Mechanism of Action of Preoperative Trastuzumab in Patients with Primary Operable Breast Tumors Overexpressing HER2 Pilot Study of the Mechanism of Action of Preoperative Trastuzumab in Patients with Primary Operable Breast Tumors Overe. *Clin. Cancer Res.* **10,** 5650–5655 (2004).

118. Taylor, R. J. *et al.* Ex vivo antibody-dependent cellular cytotoxicity inducibility predicts efficacy of cetuximab. *Cancer Immunol Res* **3,** 567–574 (2015).

119. Beckman, R. a, Weiner, L. M. & Davis, H. M. Antibody constructs in cancer therapy: protein engineering strategies to improve exposure in solid tumors. *Cancer* **109,** 170–179 (2007).

120. Holliger, P. & Hudson, P. J. Engineered antibody fragments and the rise of single domains. *Nat. Biotechnol.* **23,** 1126–1136 (2008).

121. Hamers-Casterman, C. *et al.* Naturally occurring antibodies devoid of light chains. *Nature* **363,** 446–448 (1993).

122. Muyldermans, S. Single domain camel antibodies: current status. *J. Biotechnol.* **74,** 277–302 (2001).

123. Riechmann, L. & Muyldermans, S. Single domain antibodies: comparison of camel VH and camelised human VH domains. *J. Immunol. Methodsmunological methods* **231,** 25–38 (1999).

124. Flajnik, M. F., Deschacht, N. & Muyldermans, S. A case of convergence: Why did a simple alternative to canonical antibodies arise in Sharks and Camels? *PLoS Biol.* **9,** (2011).

125. Perchiacca, J. M. & Tessier, P. M. Engineering Aggregation-Resistant Antibodies. *Annu. Rev. Chem. Biomol. Eng.* **3,** 263–286 (2012).

126. Vincke, C. *et al.* General strategy to humanize a camelid single-domain antibody and identification of a universal humanized nanobody scaffold. *J. Biol. Chem.* **284,** 3273–3284 (2009).

127. Steeland, S., Vandenbroucke, R. E. & Libert, C. Nanobodies as therapeutics: Big opportunities for small antibodies. *Drug Discov. Today* **0,** (2016).

128. Roovers, R. C. *et al.* Efficient inhibition of EGFR signalling and of tumour growth by antagonistic anti-EGFR Nanobodies. *Cancer Immunol. Immunother.* **56,** 303–317 (2007).

129. Tijink, B. M. *et al.* Improved tumor targeting of anti-epidermal growth factor receptor Nanobodies through albumin binding: taking advantage of modular Nanobody technology. *Mol. Cancer Ther.* **7,** 2288–2297 (2008).

130. Bell, A. *et al.* Differential tumor-targeting abilities of three single-domain antibody formats. *Cancer Lett.* **289,** 81–90 (2010).

131. Roovers, R. C. *et al.* A biparatopic anti-EGFR nanobody efficiently inhibits solid tumour growth. *Int. J. Cancer* **129,** 2013–2024 (2011).

132. Oliveira, S. *et al.* Downregulation of EGFR by a novel multivalent nanobody-liposome platform. *J. Control. Release* **145,** 165–175 (2010).

133. van der Meel, R. *et al.* Tumor-targeted Nanobullets: Anti-EGFR nanobody-liposomes loaded with anti-IGF-1R kinase inhibitor for cancer treatment. *J. Control. Release* 1–9 (2011). doi:10.1016/j.jconrel.2011.12.027

134. Cheng, T. M. *et al.* Single domain antibody against carcinoembryonic antigen-related cell adhesion molecule 6 (CEACAM6) inhibits proliferation, migration, invasion and angiogenesis of pancreatic cancer cells. *Eur. J. Cancer* **50,** 713–721 (2014).

135. Vosjan, M. J. W. D. *et al.* Nanobodies Targeting the Hepatocyte Growth Factor: Potential New Drugs for Molecular Cancer Therapy. *Mol. Cancer Ther.* **11,** 1017–1025 (2012).

136. Maussang, D. *et al.* Llama-derived single variable domains (nanobodies) directed against chemokine receptor CXCR7 reduce head and neck cancer cell growth in vivo. *J. Biol. Chem.* **288,** 29562–29572 (2013).

137. Tang, Z. *et al.* A human single-domain antibody elicits potent antitumor activity by targeting an epitope in mesothelin close to the cancer cell surface. *Mol Cancer Ther* **12,** 416–426 (2013).

138. Farajpour, Z., Rahbarizadeh, F., Kazemi, B. & Ahmadvand, D. A nanobody directed to a functional epitope on VEGF, as a novel strategy for cancer treatment. *Biochem. Biophys. Res. Commun.* **446,** 132–136 (2014).

139. Kazemi-Lomedasht, F. *et al.* Inhibition of angiogenesis in human endothelial cell using VEGF specific nanobody. *Mol. Immunol.* **65,** 58–67 (2015).

140. Behdani, M. *et al.* Generation and characterization of a functional Nanobody against the vascular endothelial growth factor receptor-2; angiogenesis cell receptor. *Mol. Immunol.* **50,** 35–41 (2012).

141. Ahmadvand, D., Rasaee, M. J., Rahbarizadeh, F., Kontermann, R. E. & Sheikholislami, F. Cell selection and characterization of a novel human endothelial cell specific nanobody. *Mol. Immunol.* **46,** 1814–1823 (2009).

142. Kontermann, R. E. & Brinkmann, U. Bispecific antibodies. *Drug Discov Today* **20,** 838–847 (2015).

143. Fan, G., Wang, Z., Hao, M. & Li, J. Bispecific antibodies and their applications. *J. Hematol. Oncol.* **8,** 1–14 (2015).

144. Castoldi, R. *et al.* A novel bispecific EGFR/Met antibody blocks tumor-promoting phenotypic effects induced by resistance to EGFR inhibition and has potent antitumor activity. *Oncogene* **32,** 5593–601 (2013).

145. Lee, D. *et al. Simultaneous blockade of VEGF and Dll4 by HD105, a bispecific antibody, inhibits tumor progression and angiogenesis. mAbs* **862,** (2016).

146. Kienast, Y. *et al.* Ang-2-VEGF-A crossmab, a novel bispecific human IgG1 antibody Blocking VEGF-A and Ang-2 functions simultaneously, mediates potent antitumor, antiangiogenic, and antimetastatic efficacy. *Clin. Cancer Res.* **19,** 6730–6740 (2013).

147. Xu, M. *et al.* A Novel Bispecific Diabody Targeting both Vascular Endothelial Growth Factor Receptor 2 and Epidermal Growth Factor Receptor for Enhanced Antitumor Activity. *Biotechnol. Prog.* **32,** 294–302 (2016).

148. McDonagh, C. F. *et al.* Antitumor Activity of a Novel Bispecific Antibody That Targets the ErbB2/ErbB3 Oncogenic Unit and Inhibits Heregulin-Induced Activation of ErbB3. *Mol. Cancer Ther.* **11,** 582–593 (2012).

149. Muyldermans, S. Nanobodies: natural single-domain antibodies. *Annu. Rev. Biochem.* **82,** 775–797 (2013).

150. Kijanka, M., Dorresteijn, B., Oliveira, S. & van Bergen en Henegouwen, P. M. P. Nanobody-based cancer therapy of solid tumors. *Nanomedicine* **10,** 161–174 (2015).

151. Oliveira, S., Heukers, R., Sornkom, J., Kok, R. J. & Van Bergen En Henegouwen, P. M. P. Targeting tumors with nanobodies for cancer imaging and therapy. *J. Control. Release* **172,** 607–617 (2013).

152. Behdani, M. *et al.* Development of VEGFR2-specific Nanobody Pseudomonas exotoxin A conjugated to provide efficient inhibition of tumor cell growth. *N. Biotechnol.* **30,** 205–209 (2013).

153. Van Driel, P. B. A. A. *et al.* EGFR targeted nanobody-photosensitizer conjugates for photodynamic therapy in a pre-clinical model of head and neck cancer. *J. Control. Release* **229,** 93–105 (2016).

154. Hansel, T. T., Kropshofer, H., Singer, T., Mitchell, J. A. & George, A. J. The safety and side effects of monoclonal antibodies. *Nat. Rev. Drug Discov.* **9,** 325–338 (2010).

155. Zhao, J. *et al.* Thermal-activated nanocarriers for the manipulation of cellular uptake and photothermal therapy on command. *Chem. Commun.* (2016). doi:10.1039/C6CC01162D

156. Wu, C. Der *et al.* Nucleolin antisense oligodeoxynucleotides induce apoptosis and may be used as a potential drug for nasopharyngeal carcinoma therapy. *Oncol. Rep.* **27,** 94–100 (2012).

157. Sedger, L. M. & McDermott, M. F. TNF and TNF-receptors: From mediators of cell death and inflammation to therapeutic giants - past, present and future. *Cytokine Growth Factor Rev.* **25,** 453–472 (2014).

158. Aggarwal, B. B. Signalling pathways of the TNF superfamily: a double-edged

sword. *Nat. Rev. Immunol.* **3,** 745–56 (2003).

159. Zhang, H. *et al.* Transmembrane TNF-alpha mediates ‘forward’ and ‘reverse’ signaling, inducing cell death or survival via the NF-kappaB pathway in Raji Burkitt lymphoma cells. *J. Leukoc. Biol.* **84,** 789–797 (2008).

160. Yan, D. *et al.* Expression of TNFa leader sequence renders MCF-7 tumor cells resistant to the cytotoxicity of soluble TNFa. *Breast Cancer Res. Treat.* **116,** 91–102 (2009).

161. Yu, M. *et al.* Targeting transmembrane TNF-a suppresses breast cancer growth. *Cancer Res.* **73,** 4061–4074 (2013).

162. Silence, K., Lauwereys, M. & Haard, H. De. Single domain antibodies directed against tumour necrosis factor-alpha and uses therefor. *U.S. Pat. 2004041862* (2004).

163. Morais, M. *et al.* Biodistribution of a 67Ga-labeled anti-TNF VHH single-domain antibody containing a bacterial albumin-binding domain (Zag). *Nucl. Med. Biol.* **41,** 1–5 (2014).

164. Mosmann, T. Rapid colorimetric assay for cellular growth and survival: Application to proliferation and cytotoxicity assays. *J. Immunol. Methods* **65,** 55–63 (1983).

165. Fellouse, F. a, Wiesmann, C. & Sidhu, S. S. Synthetic antibodies from a four-amino-acid code: a dominant role for tyrosine in antigen recognition. *Proc. Natl. Acad. Sci. U. S. A.* **101,** 12467–12472 (2004).

166. Birtalan, S., Fisher, R. D. & Sidhu, S. S. The functional capacity of the natural amino acids for molecular recognition. *Mol. Biosyst.* **6,** 1186–1194 (2010).

167. Gomes-Da-Silva, L. C. *et al.* Toward a siRNA-containing nanoparticle targeted to breast cancer cells and the tumor microenvironment. *Int. J. Pharm.* **434,** 9–19 (2012).

168. Marchiò, S. *et al.* Aminopeptidase A is a functional target in angiogenic blood vessels. *Cancer Cell* **5,** 151–162 (2004).

169. D’Huyvetter, M. *et al.* Targeted radionuclide therapy with A 177Lu-labeled anti-HER2 nanobody. *Theranostics* **4,** 708–720 (2014).

170. Barbas, C. F., Languino, L. R. & Smith, J. W. High-affinity self-reactive human antibodies by design and selection: targeting the integrin ligand binding site. *Proc. Natl. Acad. Sci. U. S. A.* **90,** 10003–10007 (1993).

171. Man, Y. K. S. *et al.* Structural Guided Scaffold Phage Display Libraries as a Source of Bio-Therapeutics. *PLoS One* **8,** e70452 (2013).

172. Muyldermans, S. *et al.* Camelid immunoglobulins and nanobody technology. *Vet. Immunol. Immunopathol.* **128,** 178–183 (2009).

173. Porkka, K., Laakkonen, P., Hoffman, J. a, Bernasconi, M. & Ruoslahti, E. A fragment of the HMGN2 protein homes to the nuclei of tumor cells and tumor endothelial cells in vivo. *Proc. Natl. Acad. Sci. U. S. A.* **99,** 7444–7449 (2002).

174. Srivastava, M., Fleming, P. J., Pollard, H. B. & Burns, A. L. Cloning and sequencing of the human nucleolin cDNA. *FEBS Lett.* **250,** 99–105 (1989).

175. Deng, J. S., Ballou, B. & Hofmeister, J. K. Internalization of anti-nucleolin antibody into viable HEp-2 cells. *Mol. Biol. Rep.* **23,** 191–195 (1996).

176. Lauwereys, M. *et al.* Potent enzyme inhibitors derived from dromedary heavy-chain antibodies. *EMBO J.* **17,** 3512–3520 (1998).

177. Muyldermans, S., Cambillau, C. & Wyns, L. Recognition of antigens by single-domain antibody fragments: The superfluous luxury of paired domains. *Trends Biochem. Sci.* **26,** 230–235 (2001).

178. De Genst, E. *et al.* Molecular basis for the preferential cleft recognition by dromedary heavy-chain antibodies. *Proc. Natl. Acad. Sci. U. S. A.* **103,** 4586–91 (2006).

179. Coppieters, K. *et al.* Formatted anti–tumor necrosis factor α VHH proteins derived from camelids show superior potency and targeting to inflamed joints in a murine model of collagen-induced arthritis.pdf. *Arthritis Rheum.* **54,** 1856–1866 (2006).

180. Grandjenette, C., Dicato, M. & Diederich, M. Bispecific antibodies: An innovative arsenal to hunt, grab and destroy cancer cells. *Curr. Pharm. Biotechnol.* **16,** 670–683 (2015).

181. Perruchini, C. *et al.* Llama VHH antibody fragments against GFAP: Better

diffusion in fixed tissues than classical monoclonal antibodies. *Acta Neuropathol.* **118,** 685–695 (2009).

182. Lafaye, P., Achour, I., England, P., Duyckaerts, C. & Rougeon, F. Single-domain antibodies recognize selectively small oligomeric forms of amyloid beta , prevent Abeta-induced neurotoxicity and inhibit fibril formation. *Mol. Immunol.* **46,** 695–704 (2009).

183. De Vos, J., Devoogdt, N., Lahoutte, T. & Muyldermans, S. Camelid single-domain antibody-fragment engineering for (pre)clinical in vivo molecular imaging applications: adjusting the bullet to its target. *Expert Opin. Biol. Ther.* **13,** 1149–60 (2013).

184. Muchekehu, R. *et al.* The Effect of Molecular Weight , PK , and Valency on Tumor Biodistribution and Efficacy of. *Transl. Oncol.* **6,** 562–572 (2013).

185. Glassman, P. M., Balthasar, J. P. & Lilly, S. E. Mechanistic considerations for the use of monoclonal antibodies for cancer therapy. *Cancer Biol. Med.* **15,** 20–33 (2014).

186. Tabrizi, M., Bornstein, G. G. & Suria, H. Biodistribution mechanisms of therapeutic monoclonal antibodies in health and disease. *AAPS J.* **12,** 33–43 (2010).

187. Stork, R., Campigna, E., Robert, B., Müller, D. & Kontermann, R. E. Biodistribution of a bispecific single-chain diabody and its half-life extended derivatives. *J. Biol. Chem.* **284,** 25612–25619 (2009).

188. Cuesta, Á. M., Sainz-Pastor, N., Bonet, J., Oliva, B. & Álvarez-Vallina, L. Multivalent antibodies: When design surpasses evolution. *Trends Biotechnol.* **28,** 355–362 (2010).

189. López-Albaitero, A. *et al.* Role of polymorphic Fc gamma receptor IIIa and EGFR expression level in cetuximab mediated, NK cell dependent in vitro cytotoxicity of head and neck squamous cell carcinoma cells. *Cancer Immunol Immunother* **58,** 1853–1864 (2009).

190. Lin, J. *et al.* The antitumor activity of the human FOLR1-specific monoclonal antibody, farletuzumab, in an ovarian cancer mouse model is mediated by antibody-dependent cellular cytotoxicity. *Cancer Biol. Ther.* **14,** 1032–1038

(2013).

191. Silence, K. *et al.* ARGX-110, a highly potent antibody targeting CD70, eliminates tumors via both enhanced ADCC and immune checkpoint blockade. *MAbs* **6,** 523–532 (2014).

192. Li, J. *et al.* A comparative study of different vector designs for the mammalian expression of recombinant IgG antibodies. *J. Immunol. Methods* **318,** 113–124 (2007).

193. Graham, F. & Van der Eb, J. A New Technique for the Assay of Infectivity of Adenovirus 5 DNA. *Virology* **52,** 456–467 (1973).

194. Jordan, M., Schallhorn, A. & Wurm, F. M. Transfecting mammalian cells: Optimization of critical parameters affecting calcium-phosphate precipitate formation. *Nucleic Acids Res.* **24,** 596–601 (1996).

195. Mata, M. M., Mahmood, F., Sowell, R. T. & Baum, L. L. Effects of cryopreservation on effector cells for antibody dependent cell-mediated cytotoxicity (ADCC) and natural killer (NK) cell activity in 51Cr-release and CD107a assays. *J. Immunol. Methods* **406,** 1–9 (2014).

196. Crépin, R. *et al.* Development of human single-chain antibodies to the transferrin receptor that effectively antagonize the growth of leukemias and lymphomas. *Cancer Res.* **70,** 5497–5506 (2010).

197. Perez-Torres, M., Guix, M., Gonzalez, A. & Arteaga, C. L. Epidermal Growth Factor Receptor (EGFR) antibody down-regulates mutant receptors and inhibits tumors expressing EGFR mutations. *J. Biol. Chem.* **281,** 40183–40192 (2006).

198. Levy, E. M. *et al.* Cetuximab-mediated cellular cytotoxicity is inhibited by HLA-E membrane expression in colon cancer cells. *Innate Immun* **15,** 91–100 (2009).

199. Roberti, M. P. *et al.* IL-15 and IL-2 increase Cetuximab-mediated cellular cytotoxicity against triple negative breast cancer cell lines expressing EGFR. *Breast Cancer Res. Treat.* **130,** 465–475 (2011).

200. Hara, M. *et al.* Interleukin-2 potentiation of cetuximab antitumor activity for epidermal growth factor receptor-overexpressing gastric cancer xenografts through antibody-dependent cellular cytotoxicity. *Cancer Sci.* **99,** 1471–1478

(2008).

201. Yoshida, R. *et al.* Mechanism of resistance to trastuzumab and molecular sensitization via ADCC activation by exogenous expression of HER2-extracellular domain in human cancer cells. *Cancer Immunol. Immunother.* **61,** 1905–1916 (2012).

202. Collins, D. M. *et al.* Trastuzumab induces antibody-dependent cell-mediated cytotoxicity (ADCC) in HER-2-non-amplified breast cancer cell lines. *Ann. Oncol.* **23,** 1788–1795 (2012).

203. Nakano, K. *et al.* Anti-glypican 3 antibodies cause ADCC against human hepatocellular carcinoma cells. *Biochem. Biophys. Res. Commun.* **378,** 279–284 (2009).

204. Oshima, T. *et al.* Nectin-2 is a potential target for antibody therapy of breast and ovarian cancers. *Mol. Cancer* **12,** 60 (2013).

205. Bredow, B. Von *et al.* Virus Neutralization by HIV-1 Env-Specific Monoclonal Antibodies. *J. Virol.* **90,** 6127–6139 (2016).

206. Galluzzi, L., Senovilla, L., Zitvogel, L. & Kroemer, G. The secret ally: immunostimulation by anticancer drugs. *Nat. Rev. Drug Discov.* **11,** 215–233 (2012).

207. Pollack, B. P., Sapkota, B. & Cartee, T. V. Epidermal growth factor receptor inhibition augments the expression of MHC class I and II genes. *Clin. Cancer Res.* **17,** 4400–4413 (2011).

208. Kumai, T. *et al.* EGFR inhibitors augment antitumour helper T-cell responses of HER family-specific immunotherapy. *Br. J. Cancer* **109,** 2155–66 (2013).

209. Morse, M. A. *et al.* Synergism from combined immunologic and pharmacologic inhibition of HER2 in vivo. *Int. J. Cancer* **126,** 2893–2903 (2010).

210. Kawaguchi, Y. *et al.* Cetuximab induce antibody-dependent cellular cytotoxicity against EGFR-expressing esophageal squamous cell carcinoma. *Int. J. Cancer* **120,** 781–787 (2007).

211. Scaltriti, M. *et al.* Lapatinib, a HER2 tyrosine kinase inhibitor, induces stabilization and accumulation of HER2 and potentiates trastuzumab-dependent

cell cytotoxicity. *Oncogene* **28,** 803–14 (2009).

212. Rodler, E., Korde, L. & Gralow, J. Current treatment options in triple negative breast cancer. *Breast Dis.* **32,** 99–122 (2010).

213. Fonseca, N. A., Cruz, A. F., Moura, V., Simões, S. & Moreira, J. N. The cancer stem cell phenotype as a determinant factor of the heterotypic nature of breast tumors. *Crit. Rev. Oncol. Hematol.* **113,** 111–121 (2017).

214. Damien Destouches, M. S., Courty, J. & Destouches, D. Nanoparticles Functionalized with Ligands of Cell Surface Nucleolin for Cancer Therapy and Diagnosis. *J. Nanomed. Nanotechnol.* **6,** 1–9 (2015).

215. Sgonc, R. *et al.* Endothelial cell apoptosis in systemic sclerosis is induced by antibody-dependent cell-mediated cytotoxicity via CD95. *Arthritis Rheum.* **43,** 2550–2562 (2000).

216. Nimmerjahn, F. & Ravetch, J. V. Fcγ receptors as regulators of immune responses. *Nat. Rev. Immunol.* **8,** 34–47 (2008).

217. Shultz, L. D., Ishikawa, F. & Greiner, D. L. Humanized mice in translational biomedical research. *Nat. Rev. Immunol.* **7,** 118–30 (2007).

218. Zhou, Q., Facciponte, J., Jin, M., Shen, Q. & Lin, Q. Humanized NOD-SCID IL2rg-/- mice as a preclinical model for cancer research and its potential use for individualized cancer therapies. *Cancer Lett.* **344,** 13–19 (2014).

219. Robak, T. & Robak, E. New anti-CD20 monoclonal antibodies for the treatment of B-cell lymphoid malignancies. *BioDrugs* **25,** 13–25 (2011).

220. Roberti, M. P. *et al.* IL-2- or IL-15-activated NK cells enhance Cetuximab-mediated activity against triple-negative breast cancer in xenografts and in breast cancer patients. *Breast Cancer Res. Treat.* **136,** 659–671 (2012).

221. Gerdes, C. A. *et al.* GA201 (RG7160): A novel, humanized, glycoengineered anti - EGFR antibody with enhanced ADCC and superior in vivo efficacy compared with cetuximab. *Clin. Cancer Res.* **19,** 1126–1138 (2013).

222. Oppenheim, D. E. *et al.* Glyco-engineered anti-EGFR mAb elicits ADCC by NK cells from colorectal cancer patients irrespective of chemotherapy. *Br. J. Cancer* **110,** 1221–7 (2014).

223. Niwa, R. *et al.* Enhancement of the antibody-dependent cellular cytotoxicity of low-fucose IgG1 Is independent of FcgammaRIIIa functional polymorphism. *Clin. Cancer Res.* **10,** 6248–6255 (2004).

224. Niwa, R. *et al.* Enhanced Natural Killer Cell Binding and Activation by Low-Fucose IgG1 Antibody Results in Potent Antibody-Dependent Cellular Cytotoxicity Induction at Lower Antigen Density. *Clin. Cancer Res.* **11,** 2327–2336 (2005).

225. Suzuki, E. *et al.* A nonfucosylated anti-HER2 antibody augments antibody-dependent cellular cytotoxicity in breast cancer patients. *Clin. Cancer Res.* **13,** 1875–1882 (2007).